

MASTER OF SCIENCE THESIS

Fatigue Crack Growth in Solid Round Metallic Bars with a Shoulder Fillet

D.J. Pasma

Faculty of Aerospace Engineering · Delft University of Technology

Fatigue Crack Growth in Solid Round Metallic Bars with a Shoulder Fillet

MASTER OF SCIENCE THESIS

For obtaining the degree of Master of Science in Aerospace Engineering
at Delft University of Technology

D.J. Pasman

27 March 2015

The work in this thesis was supported by Atkins B.V. Their cooperation is gratefully acknowledged.



Copyright © D.J. Pasman
All rights reserved.



DELFT UNIVERSITY OF TECHNOLOGY
FACULTY OF AEROSPACE ENGINEERING
DEPARTMENT OF AEROSPACE STRUCTURES AND MATERIALS

The undersigned hereby certify that they have read and recommend to the Faculty of Aerospace Engineering for acceptance a thesis entitled "**Fatigue Crack Growth in Solid Round Metallic Bars with a Shoulder Fillet**" by **D.J. Pasman** in partial fulfillment of the requirements for the degree of **Master of Science**.

Dated: 27 March 2015

Supervisors:

Dr.ir. R.C. Alderliesten

Ir. M. van der Wees, Atkins B.V.

Committee members:

Dr. S. Teixeira De Freitas

Dr.ir. R. de Breuker

Summary

Solid round bars with a shoulder fillet are frequently used in engineering structures because it facilitates a smooth transition in thickness. However, the presence of shoulder fillets is currently neglected in the prediction of Fatigue Crack Growth (FCG) in engineering practice. Since stress concentrating locations like a shoulder fillet can have a significant effect on the FCG behaviour, neglecting the presence of a shoulder fillet may introduce unacceptable inaccuracies in the current FCG predictions done in solid round bars with a shoulder fillet.

Experimental research was done on characterizing the effect of shoulder fillets on the FCG behaviour in solid round bars loaded in tension. The problem was approached from two points of view: the conventional stress intensity approach and a novel energy approach. Proven methodologies were used for the stress intensity approach, the energy approach had a more exploratory character.

The first goal of the research was to investigate the influence of a shoulder fillet on the FCG behaviour in solid round bars loaded in tension. The influence of a shoulder fillet was quantified by the development of a Stress Intensity Factor (SIF) solution based on the results of FCG experiments. The developed SIF solution was implemented in an FCG prediction model for solid round bars with a shoulder fillet loaded in tension.

The SIF range ΔK is conventionally used as similarity parameter to predict FCG. An issue with this similarity parameter that has received a lot of attention in the past decades is the effect of the stress ratio. Empirically derived equations are proposed in literature to take the effect of the stress ratio into account for FCG predictions. Recent literature suggests that this effect of the stress ratio is a reflection of the inadequacy of the SIF range ΔK to uniquely describe the applied load cycle; it was suggested that these stress ratio correction equations mostly compensate for the fact that cyclic stress has been used in a methodology where cyclic energy should have been used instead.

The second goal of the research was to investigate how the energy used for a fatigue crack to grow in a complete load cycle relates to the FCG rate. A prediction methodology was developed based on the energy released in a complete fatigue cycle rather than at maximum and/or minimum load as is the case in the conventional stress intensity approach. It was found that the average cyclic Strain Energy Release Rate (SERR) $G_{avg,cyc}$ could be used as

similarity parameter in the developed methodology. The methodology was used to develop an FCG prediction model for solid round bars with a shoulder fillet loaded in tension.

As a result of the research project, it was concluded that the developed FCG prediction model, which makes use of the developed SIF solution, is able to predict FCG for different shoulder fillet geometries at one stress ratio; it was less accurate at other stress ratios. It is recommended to do further research to validate the developed SIF solution.

Next to that, it was concluded that the proposed prediction methodology with the average cyclic SERR $G_{avg,cyc}$ as similarity parameter was able to predict FCG independently of the applied stress ratio and shoulder fillet geometry. Points of further research are identified to continue the development of the average cyclic SERR $G_{avg,cyc}$ as similarity parameter for the prediction of FCG in general.

Acknowledgements

This thesis could not have been completed without the help, advise and guidance I received from many sides.

First of all I would like to thank my supervisors, René Alderliesten and Michiel van der Wees, for all their advice, feedback and valuable discussions we had about my work.

I would like to thank Atkins for the opportunity they gave me to carry out the research in cooperation with them. I am grateful that I could work on a research project that was initiated from a problem that is encountered in current engineering practice. I was given a lot of freedom by Atkins and never felt restricted to carry out the research the way I preferred.

The experimental part of the research would not have been possible without the support of the faculty of Aerospace Engineering of the TU Delft. I would like to thank DEMO, and in particular Ed Roessen, for the production of the specimens that were designed for this research. Furthermore, it would not have been possible to carry out the fatigue experiments without the help and assistance of the staff of the Delft Aerospace Structures and Materials Laboratory ([DASML](#)), in particular: Berthil Grashof, Bob de Vogel, Gertjan Mulder, Misja Huizinga and Frans Oostrum. My thanks go to them for teaching me how to set up and use the fatigue machine and the guidance I got during the inspection of the fracture surfaces using the available microscopes.

Finally, I want to thank all my colleagues, friends and family. Thank you for all the support, discussions about my work and -sometimes- necessary distraction I received during the months I carried out the research. Without all the help and support I received throughout the research I would not have come to this result.

Dirk-Jan Pasman
Delft, March 2015

“Although nature commences with reason and ends in experience it is necessary for us to do the opposite, that is to commence with experience and from this to proceed to investigate the reason.”

— *Leonardo Da Vinci*

Table of Contents

Summary	vii
Acknowledgements	ix
Glossary	xvii
List of Acronyms	xvii
List of Symbols	xviii
1 Introduction	1
2 Literature Review	3
2.1 Fatigue crack growth in metallic materials	3
2.1.1 The similarity principle based on the stress intensity factor for fatigue crack growth	5
2.1.2 Crack growth regions and prediction of fatigue crack growth	6
2.1.3 The effect of the stress ratio and plasticity induced crack closure	8
2.2 Fatigue crack growth in solid round bars	11
2.2.1 Stress intensity factor solutions for solid round bars	12
2.2.2 Experimental method to determine stress intensity factors	14
2.2.3 Prediction of fatigue crack growth in round bars	16
2.3 Fatigue crack growth in solid round bars with a circumferential stress concentration	18
2.3.1 Fatigue crack growth in solid round bars with a shoulder fillet	21
2.4 Energy considerations for fatigue crack growth	22
2.5 Synthesis	23
3 Research Approach and Theory	25
3.1 Problem Description and Scope of Research	25
3.2 Stress Intensity Approach	27
3.3 Energy Approach	29
3.4 Overall Research Approach	30

4	Experiments	31
4.1	Design of Experiments	31
4.1.1	Specimen Design	32
4.1.2	Location of the initial crack	33
4.1.3	Load spectrum design	33
4.1.4	Test matrix	35
4.1.5	Experimental Set-Up and Procedure	35
4.2	Pre-study using FE and AFGROW	36
4.2.1	The AFGROW simulations	38
4.2.2	The FE model	38
4.2.3	Results of the Pre-study	40
5	Results	43
5.1	Test Results	43
5.2	Digitizing the Fracture Surface	45
5.3	Crack Growth Rate Data	47
5.4	Development of a Stress Intensity Factor Solution	51
5.5	Influence of the Stress Ratio	56
5.6	Crack shape development	57
5.7	Energy Data	60
5.8	Relation Between the Fatigue Crack Growth Rate and Energy	64
6	The Prediction of Fatigue Crack Growth	71
6.1	Stress intensity based FCG prediction model	72
6.2	Energy based prediction model	73
6.3	Comparison Between Predictions and Experiments	74
6.3.1	Predictions with the stress intensity based model	74
6.3.2	Predictions with the energy based model	80
7	Discussion	83
7.1	Stress intensity approach	83
7.2	Energy approach	84
7.3	General research approach	85
8	Conclusions and Recommendations	89
8.1	Conclusions	89
8.2	Recommendations	90
	References	91

A Specimen Drawings	95
A.1 Straight specimen, $K_t = 1$	96
A.2 Specimen with fillet radius of 11.6 mm, $K_t = 1.5$	97
A.3 Specimen with fillet radius of 4.0 mm, $K_t = 2.0$	98
A.4 Specimen with fillet radius of 1.3 mm, $K_t = 3.0$	99
A.5 Specimen with fillet radius of 0.6 mm, $K_t = 4.1$	100
B Material Certificate Aluminium 7075-T651	101
C All Test Results	103
C.1 Straight specimens, $K_t = 1$	103
C.1.1 Specimen 1B, R=0.5	103
C.1.2 Specimen 1Z, R=0.5	105
C.2 Specimens with shoulder fillet, $K_t = 1.5$	108
C.2.1 Specimen 1B116, R=0.05	108
C.2.2 Specimen 2B116, R=0.5	111
C.3 Specimens with shoulder fillet, $K_t = 2$	113
C.3.1 Specimen 1B40, R=0.05	113
C.3.2 Specimen 2B40, R=0.5	116
C.4 Specimens with shoulder fillet, $K_t = 3$	118
C.4.1 Specimen 1Z13, R=0.05	118
C.4.2 Specimen 2Z13, R=0.5	121
C.5 Specimens with shoulder fillet, $K_t = 4.1$	123
C.5.1 Specimen 1Z06, R=0.05	123
C.5.2 Specimen 2Z06, R=0.5	124

Glossary

List of Acronyms

FCG Fatigue Crack Growth

AE Aerospace Engineering

SERR Strain Energy Release Rate

SIF Stress Intensity Factor

SCF Stress Concentration Factor

CA Constant Amplitude

FE Finite Element

OM Optical Microscope

EDM Electrical Discharge Machining

DASML Delft Aerospace Structures and Materials Laboratory

RBE Rigid Body Element

SEM Scanning Electron Microscope

RMSE Root Mean Squared Error

List of Symbols

Abbreviations

Hz	Hertz
J	Joules
kN	Kilonewton
mJ	Millijoules
mm	Millimetre
MPa	Megapascal

Greek Symbols

β	Geometry factor [-]
β_{corr}	Geometry correction factor for the presence of a shoulder fillet [-]
Λ	Normalized crack area $\frac{A}{\pi(\frac{D}{2})^2}$ [-]
λ	Normalized crack length $\frac{a}{D}$ [-]
Δ	Indicates the <i>range</i> of a quantity

Latin Symbols

A	Crack Area [mm ²]
a	Crack Length/Depth [mm]
C	Material constant for the Paris equation [-]
c_1	Parameter that defines the shape of the crack front [-]
D	Diameter of the bar at the location of the crack [mm]
d	Resulting axial displacement (of the clamps) [mm]
$D1$	Smallest diameter of the round bar [mm]
$D2$	Largest diameter of the round bar [mm]
F	Parameter that indicates the ratio between the supplied strain energy at a certain cracked area A and the supplied strain energy when no crack is present [-]
G	Strain Energy Release Rate [$\frac{J}{mm^2}$]
G_{avg}	Average Strain Energy Release Rate [$\frac{mJ}{mm^5}$]
H	Correction equation which is defined as the derivative of F with respect to the crack area A : $\frac{dF}{dA}$ [$\frac{1}{mm^2}$]
K	Stress Intensity Factor [MPa \sqrt{mm}]
K_t	Stress Concentration Factor [-]
m	Material constant for the Paris equation [-]
N	Number of load cycles [-]
P	Applied load to the specimen [kN]
r	Shoulder fillet radius [mm]
S	Stress [MPa]

U Strain Energy [J]

Subscripts

<i>avg</i>	Average
<i>a</i>	Amplitude
<i>corr</i>	Correction
<i>cyc</i>	Cyclic
<i>eff</i>	Effective
<i>f</i>	Failure
<i>III</i>	Opening mode III
<i>II</i>	Opening mode II
<i>in</i>	Delivered to the specimen during loading
<i>I</i>	Opening mode I
<i>max</i>	Maximum
<i>min</i>	Minimum
<i>m</i>	Mean
<i>out</i>	Delivered back by the specimen during unloading
<i>s</i>	Critical
<i>s</i>	Shifted
<i>th</i>	Threshold
<i>tot</i>	Total

Chapter 1

Introduction

That fatigue cracks can initiate, grow and cause catastrophic failure under the repeated loading of a metallic structure below its static strength is a widely recognized phenomenon in engineering practice [1]. The initiation and growth of fatigue cracks under repeated loading is taken into account during the structural design of a metallic structure. It is only possible to allow that fatigue cracks will grow in a structure, if an accurate prediction of the crack growth under the expected repeated loading can be done. An accurate Fatigue Crack Growth (FCG) prediction is essential to be able to determine appropriate inspection intervals of the structure to detect fatigue cracks before they grow to a critical size and to repair the structure accordingly.

The initial problem that created the need for a research project is the possible inaccuracy of current FCG predictions in solid metallic round bars with a thickness step in current engineering practice. Currently, in frequently used FCG prediction models that are used in engineering practice, the possible influence that a thickness step has on the FCG behaviour is neglected. The research focussed on solid round metallic bars under Constant Amplitude (CA) tension loading having a specific notch type as thickness step: a shoulder fillet, which is illustrated with its characteristic dimensions $D1$, $D2$ and r with a crack with length a in figure 1.1.

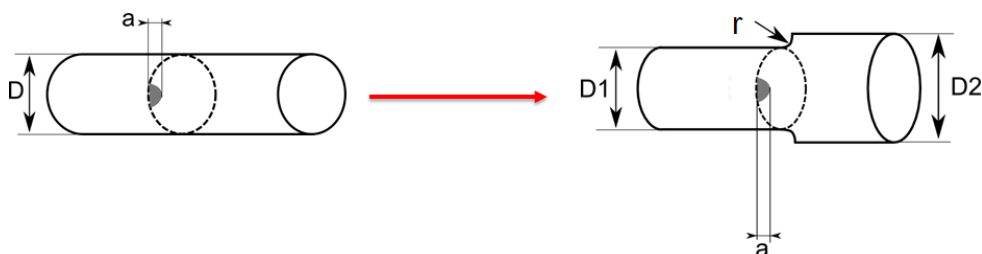


Figure 1.1: Fatigue crack present in a smooth solid round bar (left) and in a solid round bar with a shoulder fillet (right).

The problem of FCG through a solid round bar with a shoulder fillet was approached from two point of views: the conventional stress intensity approach and a novel energy based approach. The first goal of the research was to investigate the effect of a shoulder fillet on the FCG behaviour and to develop a FCG prediction model using the conventional stress intensity approach accordingly. The second goal was to develop a novel FCG prediction methodology on the basis of the energy released in a complete load cycle rather than the conventional stress intensity approach. Experimental work has been done on characterizing FCG in a solid round bar with a shoulder fillet and for both approaches, the predictions done with both developed prediction models were compared with the test results.

This thesis is structured as follows, in chapter 2, literature on FCG in metallic materials, and especially in solid round bars, is reviewed. On the basis of this literature review, a research approach is outlined in chapter 3. Chapter 4 discusses the experiments that were designed and executed for the research. The results of the experiments are presented in chapter 5. The developed prediction models, one on the basis of the conventional stress intensity approach and one on the basis of the energy approach, are discussed in chapter 6. Chapter 7 discusses the results of the research project. The conclusions and recommendations are presented in chapter 8.

Chapter 2

Literature Review

In this chapter, the current state of the art in the field of Fatigue Crack Growth (FCG) in metallic materials and in solid round metallic bars in particular, is reviewed. This literature review was done to get an accurate and up-to-date overview of the research field in which this research project was conducted.

First, current practice on how FCG in metallic materials is characterized and predicted under Constant Amplitude (CA) fatigue loading is discussed in section 2.1. Next, literature on FCG in solid round metallic round bars is reviewed in section 2.2. After that, literature on the influence of a circumferential stress concentration on the FCG behaviour in solid round metallic bars is reviewed in section 2.3. Lastly, recent literature on a cyclic energy concept, rather than the cyclic stress intensity concept to characterize fatigue crack growth is discussed in section 2.4.

2.1 Fatigue crack growth in metallic materials

The fatigue life of a structure is usually divided in two different phases: the initiation period and the crack growth period. Differentiation between the two periods is important because several surface conditions do have effect on the initiation period, but have a small or negligible effect on the crack growth period [1]. The research project was limited to the crack growth period of the fatigue phenomenon.

To describe the severity of the stress distribution around a crack tip, the concept of the Stress Intensity Factor (SIF) is widely used and the accepted current practice; the development was done through early work of Irwin [2]. The components of the stress around the crack tip can be expressed using a polar coordinate system as defined in figure 2.1. The stress components are a function of the distance from the crack r , angle θ , remote stress S and crack length a . For a mode I crack (as illustrated in figure 2.2) in an infinite sheet under tension, the stress components can be expressed as in equation 2.1. This equation is only valid considering its analytical limit for a relatively short distance of a point to the crack tip, i.e. a short distance compared to the crack length: $r \ll a$.

$$\sigma_{i,j} = \frac{S\sqrt{\pi a}}{\sqrt{2\pi r}} f_{i,j}(\theta) \quad (2.1)$$

Where:

$$S\sqrt{\pi a} = K \quad (2.2)$$

The function $f_{i,j}(\theta)$ determines the *shape* of the stress distribution around the crack tip, K represents the *severity* of the stress around the crack tip and $\frac{1}{\sqrt{2\pi r}}$ indicates how the stress components decrease away from the crack tip with the distance r . Equation 2.2 defines the stress intensity factor K , which is the characteristic parameter for the stress intensity around the crack tip.

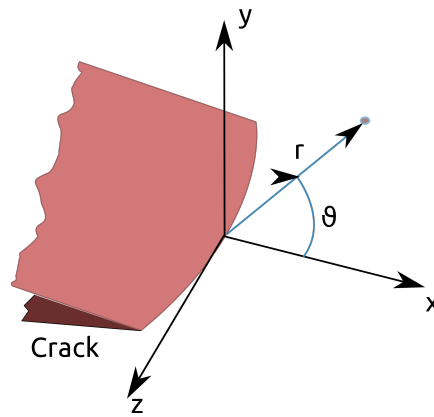


Figure 2.1: Polar coordinate system around the crack tip.

For a mode I crack, as illustrated in figure 2.2, the stress intensity factor K_I can be expressed as function of the remote stress and crack length as defined in equation 2.3. The subscript I refers to the opening mode of the crack.

$$K_I = \beta S\sqrt{\pi a} \quad (2.3)$$

In equation 2.3, S is the remote stress, a is the crack length and β is a dimensionless factor depending on the geometry of the crack problem; β is equal to 1 for a mode I crack in an infinite sheet loaded in tension as shown in the definition of the stresses around the crack tip in equation 2.2.

In principle, fatigue crack growth in mode II and III as illustrated in figure 2.2 is possible, but experience has shown that that small fatigue cracks which nucleate under cyclic shear stress in mode II or mode III quickly transform to fatigue crack growing in mode I, this is thus the most relevant mode for fatigue cracks [1]. In the rest of this thesis, only crack opening mode I is considered and the stress intensity factor K is used as the stress intensity factor for a crack in opening mode I, K_I .

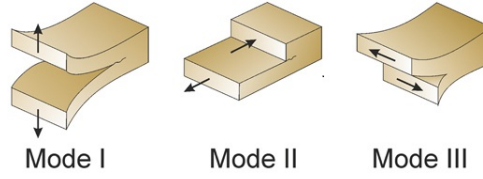


Figure 2.2: The three crack opening modes.

2.1.1 The similarity principle based on the stress intensity factor for fatigue crack growth

The concept of the SIF K is applied to FCG data and is used to predict FCG using a similarity principle. In an early paper of Paris et al.[3] it was recognized that similar FCG rates occur under a different applied stress amplitude (but same ratio between the minimum and maximum stress), although at different values of the crack length a itself. This observation led to the development of the *similarity principle* for FCG based on the SIF K .

Fatigue loads are defined as cyclic loads between a maximum stress S_{max} and a minimum stress S_{min} as illustrated in figure 2.3. The mean stress is indicated with S_m , the stress amplitude with S_a and the stress range with $\Delta S = S_{max} - S_{min}$.

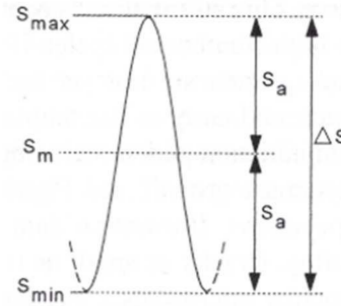


Figure 2.3: Definition of the stress levels in a load cycle.

Cyclic loads introduce a cyclic stress intensity at the crack tip. This cyclic stress intensity will vary between K_{max} and K_{min} corresponding with the applied stress cycle between the maximum stress S_{max} and minimum stress S_{min} . This stress intensity range, ΔK , is defined in equation 2.4 and equation 2.5.

$$\Delta K = K_{max} - K_{min} = \beta S_{max} \sqrt{\pi a} - \beta S_{min} \sqrt{\pi a} \quad (2.4)$$

Or:

$$\Delta K = \beta \Delta S \sqrt{\pi a} \quad (2.5)$$

The stress ratio R , which also applies to the corresponding stress intensities, is defined as the ratio between the minimum and maximum stress in equation 2.6.

$$R = \frac{S_{min}}{S_{max}} = \frac{K_{min}}{K_{max}} \quad (2.6)$$

According to the similarity principle, it appears to be correct to assume that the FCG rate, which is defined as the crack extension length in a load cycle $\frac{da}{dN}$, is a function of ΔK and R :

$$\frac{da}{dN} = f(\Delta K, R) \quad (2.7)$$

The similarity principle can be used to predict fatigue crack growth in another specimen or structural component, it says [1]:

”Similar cyclic conditions (ΔK and R) applied to fatigue cracks in different specimens or structures of the same material should have similar consequences, i.e. similar crack extensions per cycle, thus the same $\frac{da}{dN}$ ”

Although that this similarity principle is a physically sound concept, it remains always a basic problem if the physical FCG conditions are similar (enough) in experiments and real-life structures. This *similarity* is required to be able to do accurate predictions in actual structures based on FCG data obtained with experiments.

An important and widely observed phenomenon is the often in literature called ‘thickness-effect’ on FCG. Fatigue cracks in thick plates and thin plates under similar ΔK and R conditions will not grow with the same FCG rate because of a phenomenon called *plasticity induced crack closure*. A larger plastic zone around the crack tip in thinner plates compared to thicker ones is caused by a different *state of stress* at the crack tip: in thicker plates the lateral contraction at the crack tip will be largely restrained and *plane strain* conditions apply, where in thinner plates the lateral contraction cannot effectively be constrained and the crack tip will largely be in *plane stress*. Different FCG rates should be expected in cracks under similar ΔK and R conditions but a different state of stress due to *plasticity induced crack closure*, a phenomenon discussed in section 2.1.3. In general, larger plastic zone sizes occur under plane stress conditions making the effect of plasticity induced crack closure larger which results in lower crack growth rates than under plane strain conditions, where smaller plastic zones sizes occur. To apply the above stated *similarity principle* successfully, the state of stress of the crack tip in crack growth experiments and real-life structures should also be comparable to be able to do valid and accurate predictions.

2.1.2 Crack growth regions and prediction of fatigue crack growth

When the FCG rate of a growing fatigue crack is plotted against the stress intensity range ΔK at the crack tip, typically three different regions can be identified as illustrated in figure 2.4. The curve as illustrated in figure 2.4, illustrates typical FCG behaviour of a metallic material, note that both axes of the graph are on logarithmic scale.



Figure 2.4: The three different crack growth regions on a log-log scale plot.

The first region, region I, is called the *threshold region* and this is the area where (very) low FCG rates are observed. The SIF range from which fatigue cracks start to grow, the threshold SIF range, is indicated with ΔK_{th} . The second region, region II, is called the *Paris region* and can be described with the well-known Paris equation. According to Paris [4], the relation between $\frac{da}{dN}$ and ΔK can be described by a power-law (as indicated by the straight line on a log-log scale plot) given in equation 2.8. Region III is the *stable tearing* region with relative higher FCG rates, failure occurs when K_{max} equals the *critical stress intensity* K_c . Often, the *plane strain* fracture toughness K_{Ic} is used here since this is the lower bound of the critical stress intensity factor K_c and is considered as a material property [1].

$$\frac{da}{dN} = C \Delta K^m \tag{2.8}$$

In equation 2.8, C and m are the Paris equation parameters which are considered as material constants but are also dependent on the stress ratio R which will be discussed in section 2.1.3.

With knowledge of the stress intensity factor range ΔK at the tip of a fatigue crack, representing the *crack driving force*, and the characteristic $\frac{da}{dN}$ curve of the considered material as illustrated in figure 2.4, representing the *crack growth resistance of the material*, crack growth predictions can be done. In general, crack growth predictions under CA loading are done as illustrated in figure 2.19.

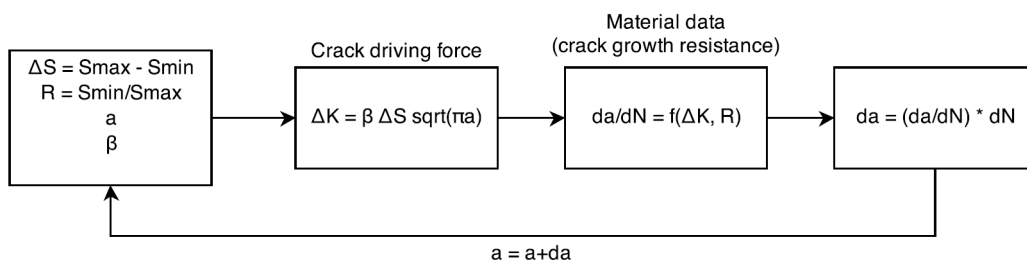


Figure 2.5: Prediction of fatigue crack growth under constant amplitude loading.

Over the past decades, there are numerous crack growth equations like equation 2.8 proposed to take the lower and upper asymptotic behaviour, in region I and III, into account in a single equation. Some proposed equations, like the NASGRO equation, take the effect of the stress ratio R also into account; the effect of the stress ratio R on the crack growth behaviour is discussed in section 2.1.3. With an equation like the NASGRO equation, taking the asymptotes and the stress ratio effect into account, the relation between $\frac{da}{dN}$ and ΔK is considered as material property and can be used in FCG predictions. Note that all of these proposed equations have no physical background and are proposed to agree with observed test results.

SIF solutions for specific crack problems are expressed in literature as values of the geometrical factor β . The solution of the dimensionless geometrical factor β in the definition of the stress intensity factor range ΔK for a certain fatigue crack configuration is a prerequisite to be able to do FCG predictions. For simple fatigue crack configurations, exact SIF solutions are derived analytically and can be found in various handbooks, of which the *Stress Analysis of Cracks Handbooks* by Tada et al. [5] is frequently used in engineering practice. For more complex configurations, solutions are derived using Finite Element (FE) techniques or experimental methods.

2.1.3 The effect of the stress ratio and plasticity induced crack closure

The crack growth curve as illustrated in figure 2.4 is only valid at one applied stress ratio R . How the applied stress ratio R typically effects the FCG rate curve is illustrated and compared with the curve for $R = 0$ in figure 2.6.

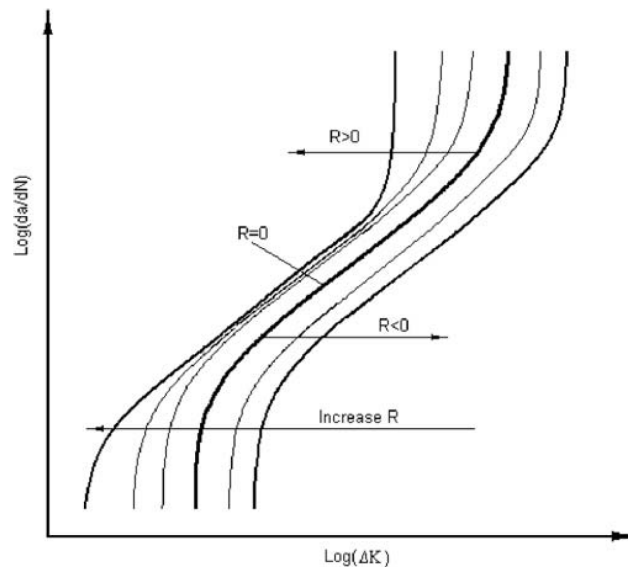


Figure 2.6: The effect of the R-ratio on the crack growth rate curve [6].

As can be seen in figure 2.6, the stress ratio R has a significant effect on the crack growth rate. The SIF range ΔK only is apparently not able to characterize the FCG rate at different stress ratios. To be able to predict FCG at different stress ratios, research has been done to find an expression which takes the stress ratio effect into account and to condense

the FCG rate curves at different stress ratios to a single and unique curve for a given material.

Elber was one of the first to observe that a fatigue crack closed before the tension stress became zero during unloading a fatigue crack growth specimen [7]. This had a great impact on fatigue crack growth predictions and this effect referred to in literature as *plasticity induced crack closure*. Since the concept of the SIF is only valid for an open crack, it was found that when only the portion of the stress range when the crack is open ΔS_{eff} as illustrated in figure 2.7 is taken into account in the definition of the SIF, the stress ratio effect seems to disappear in the FCG curve. It was concluded by Elber that the stress at which the crack opens S_{op} , only depends on the applied stress ratio R and empirical relationships have been derived in literature for different materials to take this phenomenon into account.

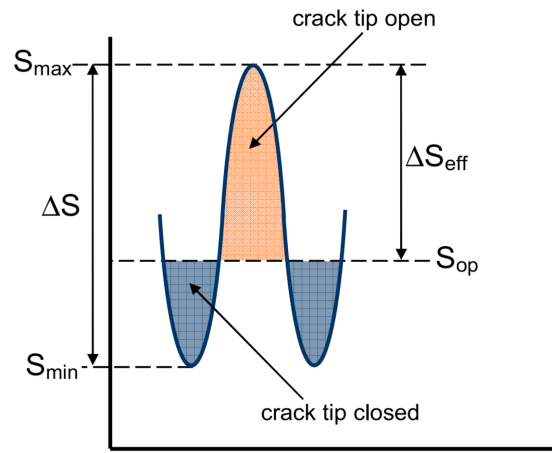


Figure 2.7: Illustration of the range in which the crack is open during a stress cycle [1].

When the *plasticity induced crack closure* concept is applied to the SIF range ΔK , an *effective SIF* range ΔK_{eff} is defined as the SIF range during the *effective* stress cycle ΔS_{eff} as given in equation 2.9.

$$\Delta K_{eff} = \beta \Delta S_{eff} \sqrt{\pi a} \quad (2.9)$$

The ratio between the *effective* range of the stress (intensity) and the *total* range of the stress (intensity) was found to be dependent on the stress ratio R as defined in equation 2.10.

$$\frac{\Delta K_{eff}}{\Delta K} = \frac{\Delta S_{eff}}{\Delta S} = U(R) \quad (2.10)$$

Where $U(R)$ was empirically determined by Elber for the aluminium alloy 2024-T3 within a range of R-values of 0.1 to 0.7 [7]:

$$U(R) = 0.5 + 0.4R \quad (2.11)$$

Various empirical equations for $U(R)$ like equation 2.11 have been derived for different materials and stress ratio ranges. The use of ΔK_{eff} condenses the crack growth rate data of a material into one unique curve as illustrated in figure 2.7, which makes it possible to do FCG predictions independently of the applied stress ratio R .

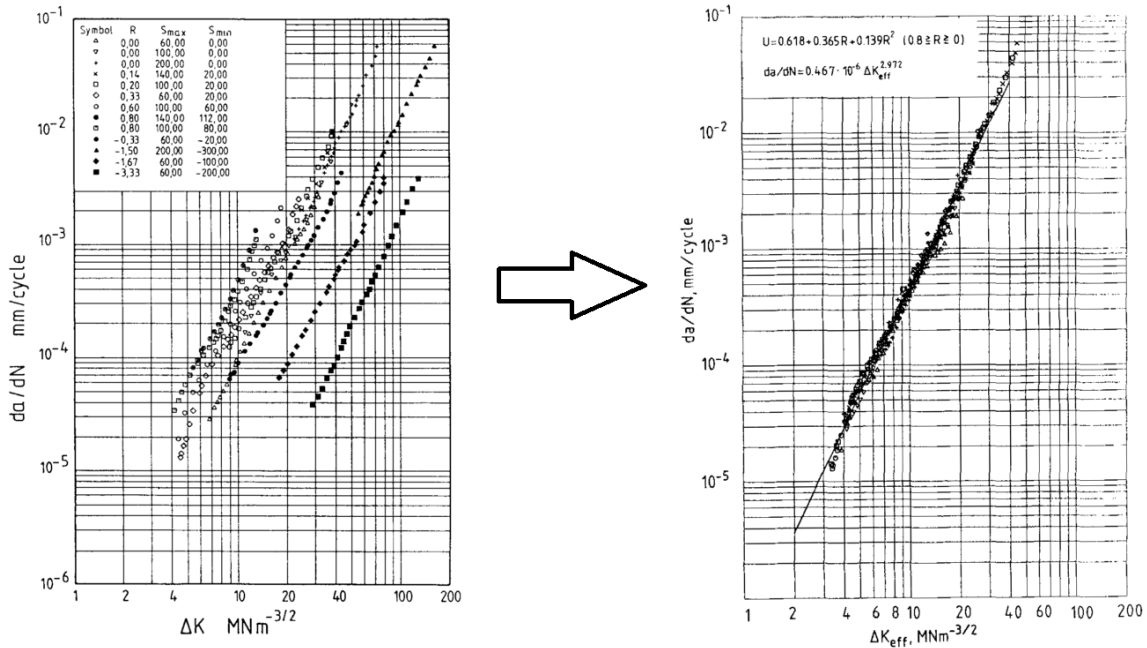


Figure 2.8: An example of the application of the effective stress intensity factor range ΔK to crack growth data [8]. Left, the crack growth data as function of the stress intensity factor range ΔK for different stress ratios fall all on a unique curve when the data is plotted as function of ΔK_{eff} on the right.

As can be seen in figure 2.8, $\frac{da}{dN}$ is directly related to ΔK_{eff} for multiple stress ratios and this implies that $\frac{da}{dN}$ is dependent on ΔK_{eff} only. The similarity principle for fatigue crack growth can now be stated as [1]: *a similar ΔK_{eff} in a cycle occurring in different specimen or structures should give the same $\frac{da}{dN}$ in that cycle.* Crack growth predictions under constant amplitude loading using this similarity principle can be done as illustrated in figure 2.9.

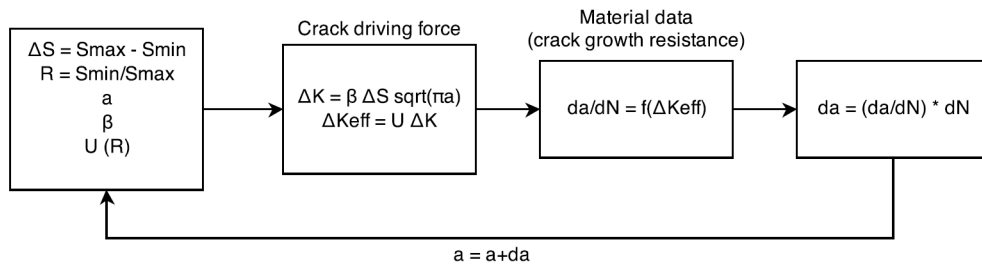


Figure 2.9: Prediction of fatigue crack growth under constant amplitude loading.

Some FCG equations, like the *NASGRO* equation, relate $\frac{da}{dN}$ to ΔK for a certain range of stress ratios without the explicit use of the *effective* stress intensity factor range. The material dependent parameters in those equations are determined using extensive regression analysis on a wide range of FCG data at different stress ratios, obtaining a closed-form equation valid for a range of stress ratios.

In section 2.4, it is questioned by a paper of Alderliesten if the empirical derived correction equations $U(R)$ in literature for the stress intensity range ΔK actually correct for plasticity induced crack closure only. It is shown that when considering cyclic energy instead of cyclic stress, a large part of these corrections can be explained by the fact that the cyclic stress ΔS only is not able to describe the applied load cycle correctly.

2.2 Fatigue crack growth in solid round bars

There are different kind of fatigue cracks possible in a structure: a through crack, which is through the entire thickness of the structure and part-through cracks, which can be corner cracks or surface cracks as illustrated in figure 2.10

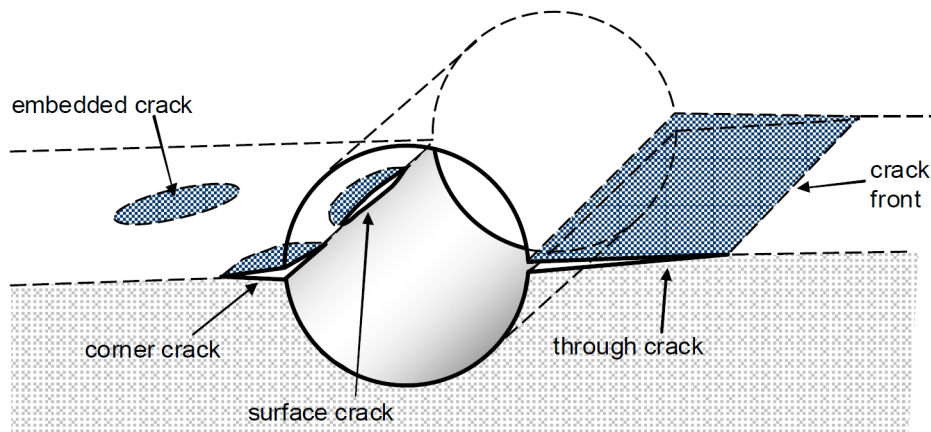


Figure 2.10: Different type of cracks in structures [1]

When a fatigue crack is present in a solid round bar, this is a typical surface crack as illustrated in figure 2.11. The prediction of the growth of a part-through crack is a more complex problem because the SIF K will vary along the crack front. This implies that the FCG rate $\frac{da}{dN}$ will also vary along the crack front.

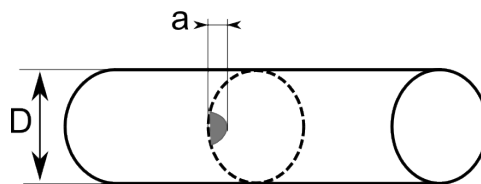


Figure 2.11: A surface crack in a solid round bar

A typical phenomenon observed in the fatigue growth of surface cracks is that the crack front near the material surface is lagging behind the rest of the crack front as illustrated in figure 2.12. This can be explained by the fact that at the outer material surface, the crack front is in a *plane stress* state which causes larger plastic zone sizes which results in lower crack growth rates because of more plasticity induced crack closure. The crack front, which is

deeper into the material is in a *plane strain* state which results in a smaller plastic zone size and thus higher crack growth rates due to less plasticity induced crack closure. However, in the prediction of FCG of surface cracks, the deviations in the shape of the crack front caused by this effect are usually ignored.

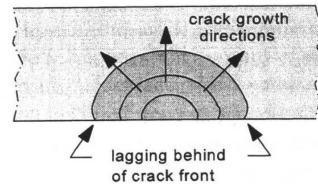


Figure 2.12: A surface crack in a plate showing that the crack at the surface lags behind [1].

The main focus in literature on FCG in solid round bars is on the determination of SIF solutions (in the form of a β factor) to be able to do FCG predictions. The different type of SIF solutions found in literature are shortly reviewed in section 2.2.1. Next to that, an experimental method to determine SIF solutions is discussed in section 2.2.2. At last, different methods found in literature to predict FCG in solid round bars is discussed in section 2.2.3.

2.2.1 Stress intensity factor solutions for solid round bars

The SIF of a surface crack in a round bar depends on the relative crack depth, crack shape (aspect ratio) and the position along the crack front. In general, the SIF solutions found and derived in literature can be divided into one-, two- and three-parameter solutions of β . In a recent paper by Toribio et al.[9], a large amount of different stress intensity factor solutions of fatigue cracks in solid round bars subjected to tension loading found by several authors are analysed and compared.

One-parameter SIF solutions are only valid for a certain crack shape and one location on the crack front, which is often the deepest point of the crack. The SIF solution is only dependent on the relative crack depth of the crack $\frac{a}{D}$. A standard SIF solution for a surface crack in a solid round bar which is used by FCG prediction software like NASGRO and AFGROW is derived by Forman et al.[10]. For this solution, it is assumed that the crack front shape is circular and always intersects perpendicular with the free surface of the bar during the whole period that the crack grows through the bar as illustrated in figure 2.13.

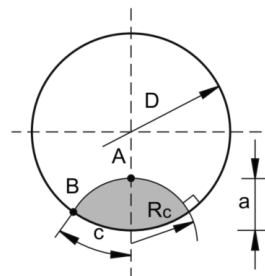


Figure 2.13: Crack shape assumed in the solution of Forman et al. [10]

Two-parameter **SIF** solutions are dependent on the crack shape (aspect ratio) and relative crack depth for a single point on the crack front, which is often either the surface point or the deepest point of the crack. For example, Carpinteri obtained **SIF** solutions using numerical techniques for *semi-elliptical* shaped crack fronts at point *A* and point *C* on the crack front as illustrated in figure 2.14 [11]. The **SIF** solution for either point *A* or *C* is dependent on the relative crack depth $\frac{a}{D}$ and crack aspect ratio $\frac{a}{b}$.

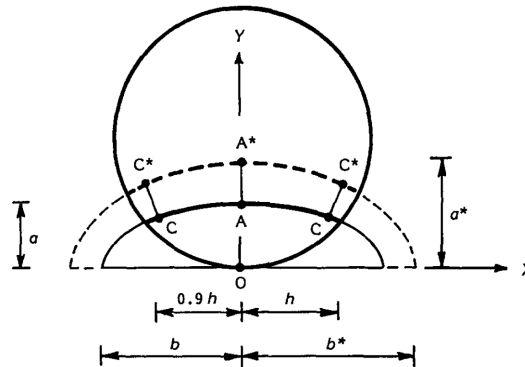


Figure 2.14: Semi-elliptical crack shape assumption and incremental crack front propagation by Carpinteri [11]

Three-parameter **SIF** solutions are dependent on the location along the crack front, relative crack depth and crack shape (aspect ratio) of the crack. A recent **SIF** solution was derived by Shin and Cai using numerical and experimental techniques [12]. The solution assumes a semi-elliptical shaped crack and is dependent on the relative position along the crack front $\frac{x}{h}$, the relative crack depth $\frac{a}{D}$ and on the crack shape aspect ratio $\frac{a}{b}$ as illustrated in figure 2.15.

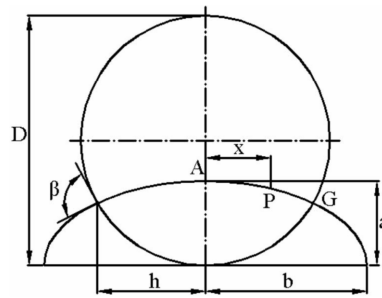


Figure 2.15: Semi-elliptical crack shape assumption by Shin and Cai. [12].

The **SIF** solutions in literature obtained with numerical techniques are always derived for a discrete amount of the dependent parameters (crack depth, crack aspect ratio and location). With the different combinations of the dependent parameters, this gives often a large data set of **SIF** values (or β factors) that are determined. To obtain practical expressions that can be used in the prediction of **FCG**, the discrete amount of **SIF** results derived are often used in a polynomial fitting technique to obtain closed-form expressions for the **SIF** solution.

Often, the **SIF** is not determined exactly where the crack intersects the outer surface of

the bar, as can be seen at with the 2-parameter solution of Carpinteri in figure 2.14: the surface point C where the SIF is determined is not present at the intersection of the crack with the outer surface of the bar. The meaning of the SIF breaks down at the surface point because of the complex singularity state there [13]. FCG is most often predicted at more inner points along the crack front and with fitting techniques through those inner points a complete crack front is reconstructed.

2.2.2 Experimental method to determine stress intensity factors

In this section, a method to experimentally determine SIF s from FCG experiments is reviewed. In this technique, with the use of FCG rates observed in FCG experiments and *baseline* FCG data of the same material, SIF s can be derived. The process is illustrated in figure 2.16 for a corner crack and was successfully applied in an investigation of Shin [14]. This method is also called the *backtracking technique* or the *James-Anderson method*, because the method was originally developed by James and Anderson [15]. The method is used to experimentally derive SIF solutions by several researchers in different studies for different types of part-through fatigue cracks [16] [17] [18].

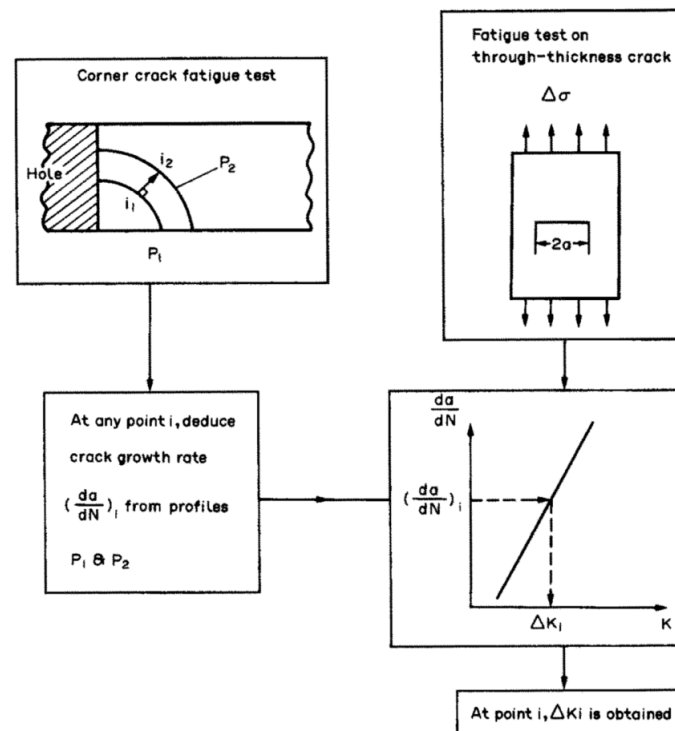


Figure 2.16: Experimental method to derive stress intensity factors from a part-through fatigue crack [14]

To be able to derive FCG rates along the crack front from surface cracks, crack fronts have to be reconstructed from the fracture surface since the (complete) crack is not visible from the outer surface of the specimen as with through cracks. *Fractography* can be used to inspect the fracture surface and reconstruct crack fronts. This can be done by making use of

marker loads in the load spectrum which will leave observable darker bands on the fracture surface when inspected using microscopic techniques. Different studies have been done to the implementation of marker loads in FCG experiments and were able to successfully reconstruct fatigue crack growth paths of part-through cracks [19] [20] [21]. For example, in the study by Schijve [21], a spectrum which is illustrated in figure 2.17 was used in FCG experiments on thick plates with countersunk holes made from aluminium 7075-T6 and 2024-T3. The marker load cycles were implemented as relatively small overloads of 15 MPa in comparison to the baseline loads; the minimum load of the marker load cycles were equal to the minimum load of the baseline cycles. Furthermore, the marker load cycle frequency was 1 Hz, where the baseline loads were applied at 10, 15 and 20 Hz. The marker loads were applied in three blocks of 10 overload cycles with 50 baseline cycles in between to make sure it is clearly observable using a Scanning Electron Microscope (SEM). The application of the spectrum illustrated in figure 2.17, made it possible to reconstruct the shape of the crack front using the SEM. The three marker load blocks can be observed as three bands on the fracture surface in the SEM illustrated in figure 2.18.

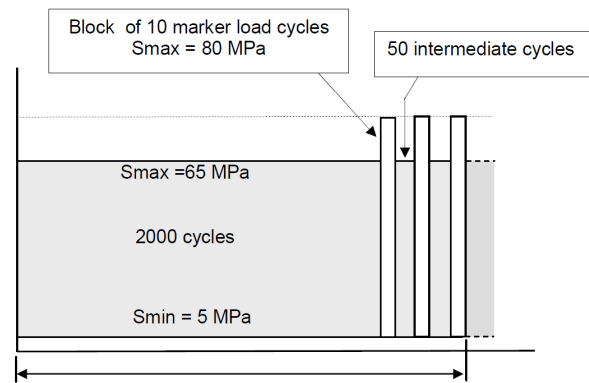


Figure 2.17: Marker load spectrum used in a study by Schijve. [21]

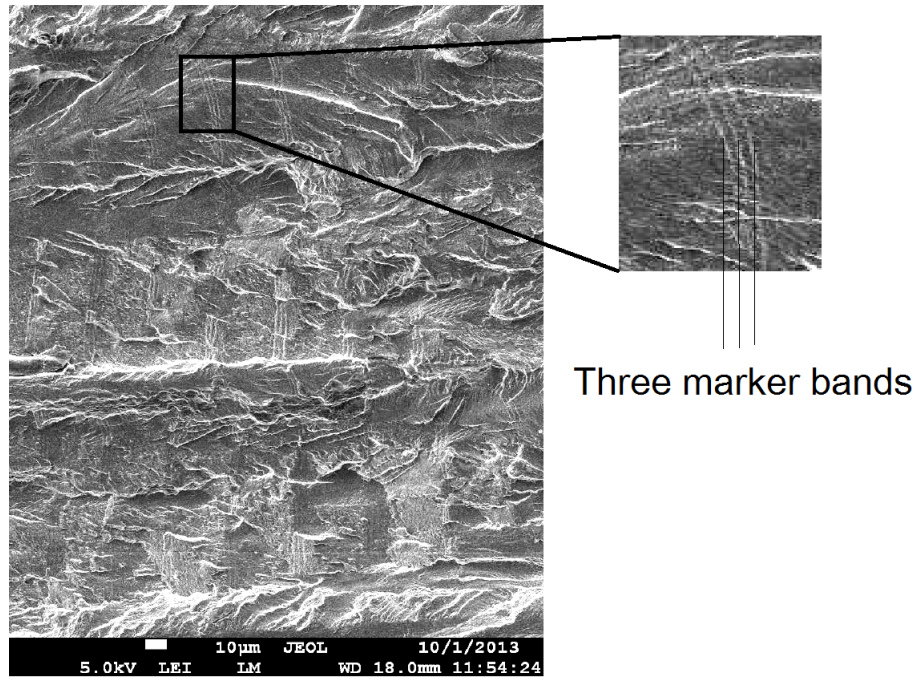


Figure 2.18: Picture of the fracture surface made with the SEM clearly shows the three marker load blocks close to each other. [21]

2.2.3 Prediction of fatigue crack growth in round bars

Roughly, the prediction of FCG in a solid round metallic bar is done with three different approaches in literature. Which one to use in engineering practice, is a trade-off between the required accuracy and complexity of the prediction. The three different approaches found will be discussed here. In widely used FCG prediction software like NASGRO and AFGROW, the first and most simple approach is used for fatigue cracks in solid round bars and is accepted current practice in industry:

1. Prediction of crack growth at the deepest point of the crack

In this approach, a closed-form one-parameter SIF solution for the deepest point of the crack is used (point A in figure 2.13). This SIF solution is only dependent on the relative crack depth $\frac{a}{D}$. This makes the FCG prediction relatively simple because the prediction is only done for the deepest point of the crack, making it practically the same as a FCG prediction as done for through the thickness cracks. Roughly, such a FCG prediction is done for CA loading as illustrated in figure 2.19.

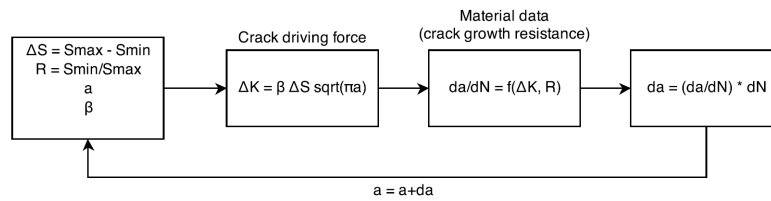


Figure 2.19: Prediction of fatigue crack growth under constant amplitude loading.

2. Prediction of crack growth at multiple points along the crack front

In this approach, a closed-form **SIF** solution is used to obtain the β factors at a discrete amount of locations along the crack front, consequently local growth is calculated for each of those points using the procedure illustrated in figure 2.19. A curve-fit through the new positions of the crack front is done to be able to calculate calculate new β factors using the **SIF** solution. For example, in a study of Carpinteri[11], the local growth of point *A* and *C* is calculated as illustrated in figure 2.14. A two-parameter **SIF** solution was used for both point *A* and *C*, depending on the relative crack depth $\frac{a}{D}$ and crack aspect ratio $\frac{a}{b}$. It is assumed that the crack can always be described as *semi-elliptical*, and after the local growth in point *A* and *C* is calculated a semi-elliptical crack front is fitted through the new points after which new β factors with the **SIF** solutions and local growth can be calculated for point *A* and *C*.

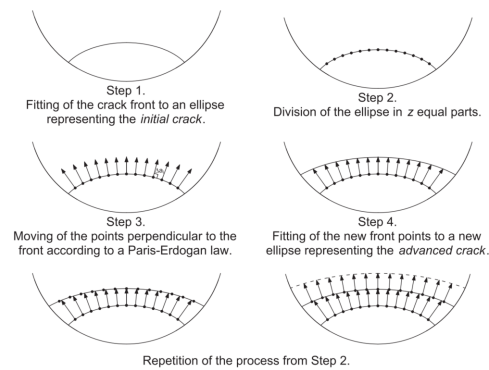


Figure 2.20: Incremental crack front propagation procedure by Torbio [22]

Another example of this method is shown in the work of Torbio [22] on the fatigue crack path of a growing fatigue crack through a round bar under cyclic tension loading. The same principle is used but at multiple points along the crack front. The three-parameter **SIF** solution determined in the study of Chin and Cai [12] is used in the numerical procedure. The incremental procedure to predict the crack growth is similar to the one used by Carpinteri and is shown in figure 2.20.

3. Fully automated crack growth simulations using finite element techniques

In this approach of predicting **FCG**, the crack is modelled with **FE** using special crack tip elements simulating the behaviour of a real-life crack. The **FCG** simulation is also incremental and the **SIF** values along a discrete amount of points along the crack front is subtracted from the **FE** model after which local growth of those points is calculated using a **FCG** equation. After this, the crack is advanced in the **FE** model and new **SIF** values can be calculated

along the crack front for the new crack configuration. This specific method is applied in several studies of Lin and Smith [23] [24] [25]. The largest difference with the previous two methods is that no crack shape assumption is done as in the previous two approaches in order to obtain β values with a SIF solution of points along the crack front. The K values are calculated numerically at a discrete amount of points along the crack border with FE techniques and subsequently local crack growth is calculated with a FCG equation. With automatic re-meshing techniques this procedure is repeated and no fitting through the newly predicted crack front points is not necessary since the K values are calculated instantaneously during the analysis.

2.3 Fatigue crack growth in solid round bars with a circumferential stress concentration

That fatigue cracks emanate most often from stress concentrating locations in engineering structures is a well-known phenomenon [1]. Solid round metallic structures are widely used and often have circumferential notches where stress will concentrate when loaded. Some often encountered circumferential notches in solid round structures are illustrated in figure 2.21. Since this type of structures are widely used in engineering environments, the growth of fatigue cracks in solid round bars with a circumferential notch have been subject of several studies over the past years. Literature on this subject will be briefly reviewed in this section.

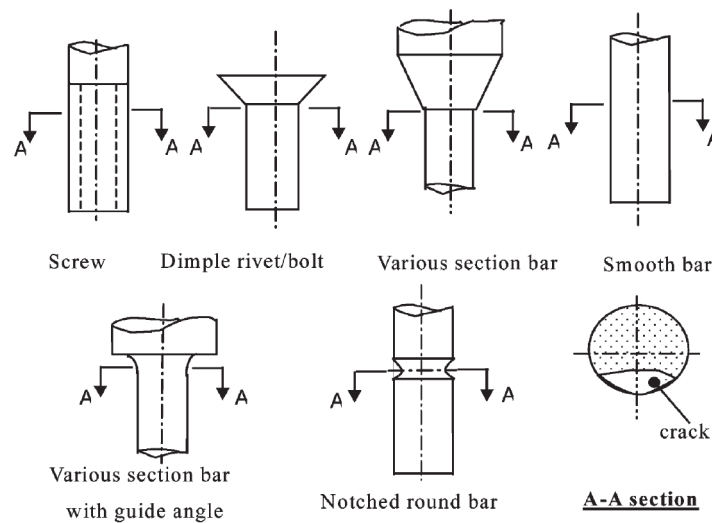


Figure 2.21: Fatigue crack emanating from different circumferential notch shapes in solid round bars [26].

Over the past decades, studies have been done to the effect of one specific circumferential notch geometry (and thus one specific corresponding Stress Concentration Factor (SCF)) on the FCG behaviour in a solid round metallic bar loaded in cyclic tension [27] [28] [29] [30] [31]. The general trend found in all of these studies is that fatigue cracks in a round bar with a circumferential stress concentration grows faster than in a smooth solid round bar without circumferential stress concentration: the fatigue crack growth life is lower. Next to that, it is observed that the crack shape develops in a different way through a solid round bar with a circumferential stress concentration than without as illustrated in figure 2.22. It

can be observed that the crack tends to grow faster along the outer surface of the bar when a circumferential notch is present, which can be explained by the fact that the circumferential notch raises the stress along the outer surface of the bar.

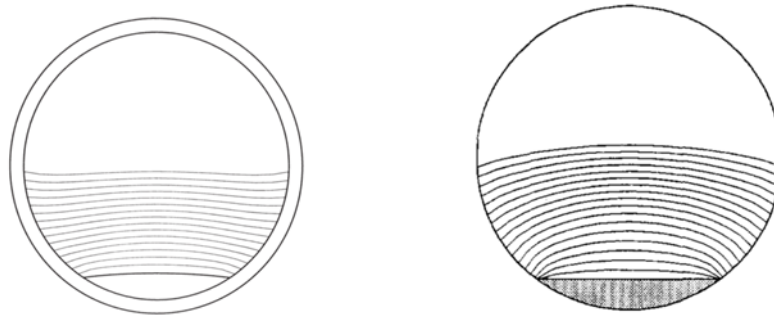


Figure 2.22: Influence of a circumferential stress concentration (left) on the fatigue crack shape development compared to a smooth bar (right) loaded in cyclic tension [29].

Where the majority of studies investigate the effect of one specific circumferential notch geometry (which results in one specific stress concentration factor) on the FCG behaviour, it would be of practical interest to know how a *range* of circumferential SCF values affects the FCG behaviour in solid round structures. The benefit would be that it would be able to do FCG predictions in circumferential notched solid round bars within a *range* of SCF values rather than just a single specific SCF value. Surprisingly, a very limited amount of studies have been done to the effect of a *range* of circumferential stress concentration factors on the FCG behaviour in a solid round metallic bar. Only a few numerical studies have investigated how a *range* of stress concentration factors influences the FCG behaviour, which will be shortly discussed here.

In a numerical study of *Carpinteri* [32][33] it is investigated what the influence of circular-arc shaped notches with different radii ρ , as illustrated in figure 2.23, is on the FCG behaviour. The investigation was done for three different notch radii ρ and a smooth bar as comparison. The resulting SCFs introduced under tension loading by the different notch radii (and the smooth bar) were: 1, 1.316, 1.591 and 2.262. The general trend observed by this paper was that the higher the SCF, the higher the FCG rates were, and thus the lower the fatigue crack growth lives. It was also investigated how the crack shape development is influenced by the different stress concentration factors. No attempt was made in this paper to compare the numerically found influence of the SCF on the FCG behaviour to experimental results.

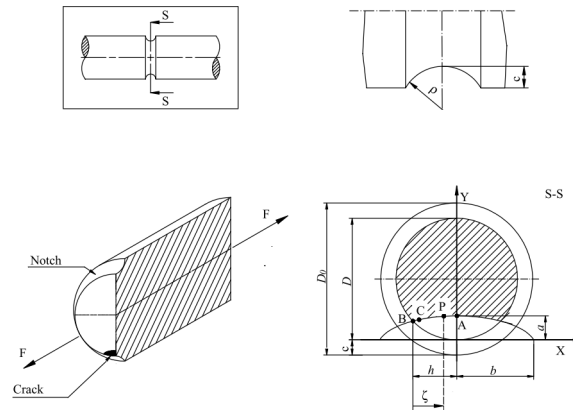


Figure 2.23: Fatigue crack emanating from circumferential circular-arc notch used in a paper of Carpinteri [33].

In a numerical study of Guo [26], two different types of circumferential notches were considered: U-shaped and V-shaped notches as illustrated in figure 2.24. It was concluded that the type of notch, U-shaped or V-shaped, did not make a difference but that the resulting SCF from the circumferential notch resulted in the same FCG behaviour. The investigation was done for notches resulting in the following values of the SCF: 1, 2.5, 4 and 5. The main result found was in agreement with what was found in the study of Carpinteri: the higher the SCF, the higher the FCG rates, especially for when the relative crack length is small. The numerically found influence of the SCF on the FCG behaviour was compared to experimental results for a single SCF. The experimental and numerical found influence of the SCF on the FCG behaviour were in agreement.

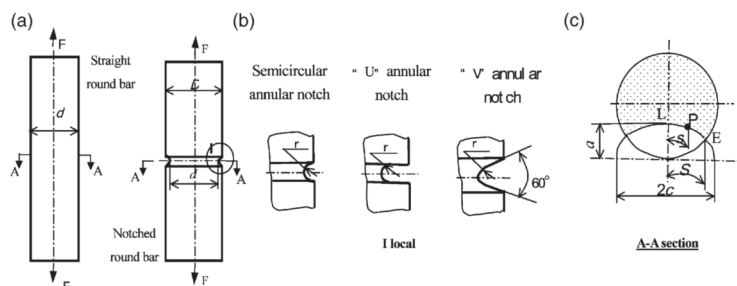


Figure 2.24: Fatigue crack emanating from circumferential stress concentrating notches used in a paper of Guo [26].

Both the studies by Carpinteri and Guo are numerical studies and the results are only compared to experimental results in the investigation of Guo [26]. This experimental study only investigates one specific circumferential notch, and thus one specific circumferential SCF. Next to that, the geometry of the circumferential notches investigated in the two studies were circular-arc, V-shaped and U-shaped. Research that investigates the effect of different shoulder fillet radii, causing different SCFs, have not been done. lastly, both studies by Carpinteri and Guo are numerical types of studies, no experimental study where the effect of a range of circumferential SCFs on the fatigue crack growth has been done.

2.3.1 Fatigue crack growth in solid round bars with a shoulder fillet

Because the research project was focussed on the influence of a shoulder fillet on the fatigue crack growth behaviour in a solid round metallic bar, studies that investigated the influence of this specific notch type are discussed here. The research done to the effect of this specific notch, a shoulder fillet, in a solid metallic round bar is rather limited: two different studies investigated the effect of a shoulder fillet in a solid round bar on the fatigue crack growth.

In an early study of Hjefeldt [34] it was investigated how a fatigue crack grows through a solid round metallic bar with a shoulder fillet with the dimensions given in figure 2.25. The bar was loaded in cyclic bending and the crack was located at 10 degrees into the fillet as illustrated in figure 2.26 as the highest stress loaded in bending was expected there. In this research only bending loads were considered and no comparison was made to the case of a smooth solid round bar. FCG was predicted using a computational procedure and experiments were conducted in laboratory environment, both results were found to be in excellent agreement.

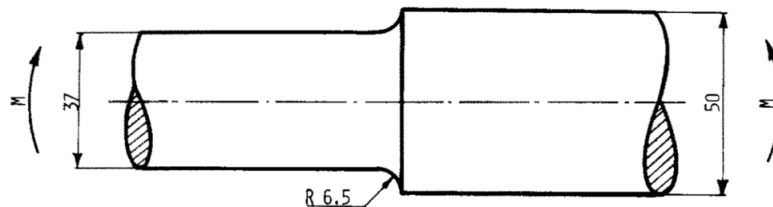


Figure 2.25: Shoulder fillet geometry investigated by Hjefeldt [34].

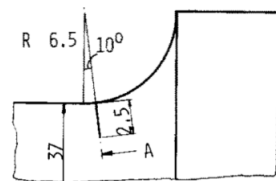


Figure 2.26: Location of the highest stress and initial crack [34].

Research done by Thompson investigated the effect of a shoulder fillet in a solid metallic round bar on the FCG loaded in cyclic tension and cyclic torsion [35] [36]. The investigated shoulder fillet geometry is illustrated in figure 2.27. The initial crack was located at the root of the shoulder fillet with a fillet radius of 3.2 mm. Both numerical research and experimental research was conducted in this study, of which the results are in good agreement. The result is compared with the FCG in a smooth solid round bar and it was concluded that the FCG through the solid round bar with the shoulder fillet is significantly quicker than through a solid round bar without a shoulder fillet.

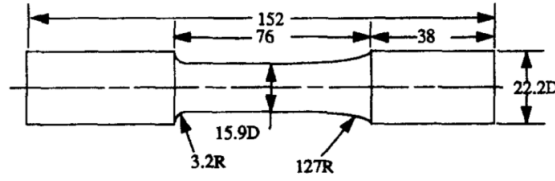


Figure 2.27: Shoulder fillet geometry investigated by Thompson, starter crack was located at the root of the 3.2 millimeter radius [35][36].

Both studies done to fatigue crack growth in a solid round metallic bar with a shoulder fillet were limited to a single shoulder fillet geometry. The study done by Thompson [35][36] is the most relevant for the proposed research project since it is the only study which investigates the behaviour under cyclic tension loading, which will be the type of loading for the proposed research project. In both studies no attempt was made to derive SIF solutions that can be used in the prediction of FCG.

2.4 Energy considerations for fatigue crack growth

As discussed before, the SIF 'K' is an important and frequently used quantity for the prediction of fatigue crack growth. Next to this stress based approach, an energy based approach is also used in literature. This energy approach for crack growth (not necessarily *fatigue* crack growth), was originally developed by Irwin. He proposed that to propagate a crack, the amount of supplied energy to the crack tip has to be equal to the surface energy of the material multiplied by the area of the newly created fracture surfaces **plus** the energy dissipated by plastic deformation. The most frequently used quantity in this energy approach is the Strain Energy Release Rate (SERR) 'G', which is the energy dissipated during the fracture per unit of new created fracture surface area ($\frac{dU}{dA}$).

In a later study by Irwin [2], the equivalence of the SERR G and the SIF K is shown, which is derived using Westergaard stress functions. The equivalence of the SERR G and the SIF K can be expressed as in equation 2.12.

$$G = \frac{K^2}{E'} \quad (2.12)$$

In equation 2.12, G is the SERR, K is the SIF and E' a stiffness term that depends on the stress/strain state at the crack tip. When the crack tip is in plane stress $E' = E$ and when the crack tip is in plane strain $E' = \frac{E}{1-\nu^2}$ where E is the Young's modulus and ν is the Poisson's ratio of the material [1].

With the equivalence known using equation 2.12, the strain energy release rate 'G' is also an often used quantity in literature for the prediction of FCG. Often similar equations like the well-known Paris equation (equation 2.8) are proposed in literature, using the SERR G instead of the SIF K .

That the FCG rate is not only dependent on the SIF range ΔK but also dependent on the stress ratio R received a lot of attention over the years as discussed in section 2.1.3 and is often attributed to the effect of *plasticity induced crack closure*. The stress ratio issues with

the current approach using the **SIF** (or equally the **SERR**) concept led to the hypothesis that the **FCG** rate is correlated to the total amount of energy lost in the complete fatigue cycle rather than to the amount of energy that would be released by a crack growth increment under the instantaneous load conditions at one point in the load cycle, e.g. G_{max} and/or G_{min} . In a recent paper of Alderliesten, it is disputed that the correction for the stress ratio R is needed because of the crack closure phenomenon only [37]. It is stated that these corrections mostly try to compensate for the fact that cyclic stress has been used in a methodology where cyclic energy should have been used instead, rather than actually correcting for crack closure alone. In a recent paper about fatigue disbond growth by Pascoe [38], it was found that the disbond growth rate of a crack was very strongly correlated to the amount of cyclic energy released during a complete cycle $\frac{dU_{cyc}}{dN}$; almost no influence of the applied stress ratio is observed in the test results.

2.5 Synthesis

From the literature reviewed in this chapter, it becomes clear that very little research has been conducted to the effect of a shoulder fillet on the **FCG** behaviour in a solid round metallic bar. The only research work done to the influence of a shoulder fillet on the **FCG** behaviour of a crack in a solid round bar loaded in tension [36] is limited to a single specific shoulder fillet geometry as illustrated in figure 2.27 and thus only a single **SCF**.

Limited numerical research was done to determine the effect of a *range* of circumferential **SCFs** on the **FCG** behaviour. The result of the numerical research done was only compared to a limited number of experimental observations for a single **SCF** in the work of Guo [26]. No experimental research has been done to the **FCG** behaviour of cracks in solid round metallic bars at a *range* of different **SCFs**.

Since there is no experimental research done to investigate the effect of different shoulder fillet radii (and thus different **SCFs**) on the **FCG** behaviour of a crack in a solid round bar under tension loading, this was one of the key points to investigate during this research.

As shown by Alderliesten [37], the nature of stress ratio corrections used in current practice in **FCG** predictions to correct for plasticity induced crack closure, can partly be explained by considering cyclic energy rather than cyclic stress. So another, more fundamental, key point that was investigated during this research was on how **FCG** can be described and predicted with the concept of cyclic energy.

Research Approach and Theory

In this chapter, the research approach and theory behind the research project is discussed. The problem of Fatigue Crack Growth (FCG) through solid round metallic bars with a shoulder fillet was approached from two different point of views: the conventional stress intensity approach and an energy approach. Before the research approaches are discussed, the investigated problem and the scope of the research is discussed in section 3.1. After that, the theory and research approach used for the two point of views is discussed in section 3.2 and section 3.3. The overall research approach is discussed in section 3.4.

3.1 Problem Description and Scope of Research

In this section, the problem that was investigated in this research is outlined. Also, the scope of the research is discussed.

The problem that initiated this research project was that in current predictions of FCG through solid round metallic bars with a shoulder fillet, the presence of the shoulder fillet is neglected: the FCG prediction is done under the assumption that the fatigue crack grows as if it is present in a solid round metallic bar without shoulder fillet. The goal of this research project was to investigate and quantify the influence of a shoulder fillet on the FCG behaviour in a solid round metallic bar to be able to do more accurate predictions. To be able to improve FCG predictions, a Stress Intensity Factor (SIF) solution for solid round bars with a shoulder fillet was developed using FCG experiments. With the developed SIF solution, a FCG prediction model was developed which takes the presence of shoulder fillets into account.

An additional point that was investigated in this research was more fundamental about FCG in general. In recent research work, it is shown that the SIF range ΔK is unable to correctly describe a load cycle. It is argued that stress ratio correction equations that are used for the prediction of FCG as proposed in literature, which claim to correct purely for plasticity induced crack closure, actually correct mainly for the fact that the SIF range ΔK is unable to describe the applied load cycle correctly. The hypothesis is that when considering the energy used for FCG during a complete load cycle, this correlates directly to the FCG rate

without any stress ratio influence. This hypothesis was investigated in this research project, furthermore it was investigated how a prediction methodology based on this knowledge could be developed.

When considering a solid round bar with a shoulder fillet, which is illustrated with its characteristic dimensions $D1$, $D2$ and r in figure 3.1, it is important to understand that every discontinuity in a structure causes a concentration of stress at that location when loaded. The severity of this concentration of stress is indicated with the Stress Concentration Factor (SCF), which is defined as the ratio between the peak stress at the discontinuity and the nominal stress which would be present if the discontinuity would not be present in the structure. Since a shoulder fillet is a circumferential discontinuity in a round bar, this causes a circumferential stress concentration. In this research it was assumed that a shoulder fillet could be characterized with the resulting SCF. It is assumed that when having a different shoulder fillet geometry, but with the same resulting SCF, the same influence on the FCG behaviour can be expected.

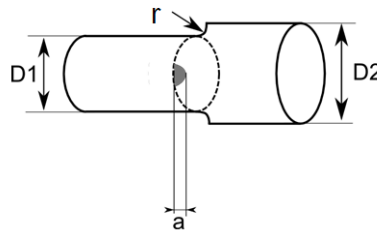


Figure 3.1: A solid round bar with small diameter $D1$, large diameter $D2$, shoulder fillet with radius r and fatigue crack with length a .

It was decided to limit the research project to FCG under Constant Amplitude (CA) tension loading, the influence of variable amplitude or other types of loading (e.g. bending or torsion) was not taken into account in this research project and the developed prediction models. The FCG behaviour in five geometrically different solid round metallic bars was investigated: a straight solid round metallic bar without shoulder fillet, and four different solid round metallic bars with different shoulder fillet geometries resulting in a SCF under tension loading of 1.5, 2, 3 and 4.1. It was decided not to investigate higher values of the SCF since this is practically never encountered in engineering practice. Furthermore, it was decided to define the initial crack as straight because of the ease of production; different initial crack shapes were not considered. In this thesis, the crack length a , crack area A and diameter of the bar at the location of the crack D are defined as in figure 3.2.

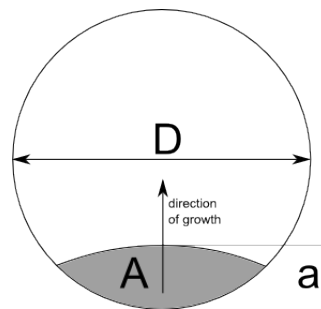


Figure 3.2: The definition of the crack length a , crack area A (grey shaded) and diameter of the bar at the location of the crack D .

3.2 Stress Intensity Approach

The SIF range ΔK is conventionally used as similarity parameter in engineering practice when predicting FCG. Theory have been developed over the past decades to determine SIF solutions for specific crack problems to be able to predict FCG. SIF solutions are expressed as values of β as defined in equation 3.1, since β captures the influence of the geometry on the SIF.

$$\Delta K = \beta \Delta S \sqrt{\pi a} \quad (3.1)$$

Since only tensional loads were considered in the research project, it was assumed that FCG only occurs in opening mode I. No subscript for ΔK or β is used to indicate the opening mode in this thesis. To be able to investigate and quantify the influence of shoulder fillets on the FCG behaviour, a SIF was determined using FCG experiments. The methodology that was used to determine SIF values using FCG experiments was successfully applied in earlier studies as discussed in section 2.2.2. First, FCG data was gathered from solid round bars without shoulder fillets (straight solid round bars): with a known one-parameter SIF solution for fatigue cracks in straight solid round bars from literature, *baseline* FCG data of the tested material was gathered. The one-parameter SIF solution used for the straight solid round bars without a shoulder fillet was determined by Forman et al [10]; this solution is used in frequently used FCG prediction software in engineering practice like NASGRO and AFGROW. The SIF solution is only dependent on the relative crack depth $\lambda = \frac{a}{D}$, where a is the crack length and D is the diameter of the bar, and is given in equation 3.2. With FCG data gathered from experiments on solid round bars with shoulder fillets, SIF values can be determined using the baseline data. This methodology to determine the SIF values from experiments is visualized in the flowchart in figure 3.3. The experimentally determined SIF values are expressed as a solution of the geometry factor β .

$$\beta(\lambda) = g \left[0.752 + 2.02\lambda + 0.37 \left(1 - \sin \left(\frac{\pi\lambda}{2} \right) \right)^3 \right] \quad (3.2)$$

Where:

$$g = \frac{0.92 \left(\frac{2}{\pi} \right) \left[\frac{(\tan(\frac{\pi\lambda}{2}))}{\frac{\pi\lambda}{2}} \right]^{0.5}}{\cos(\frac{\pi\lambda}{2})} \quad (3.3)$$

With λ as the normalized crack depth:

$$\lambda = \frac{a}{D} \quad (3.4)$$

With the experimentally determined SIF values for solid round metallic bars with shoulder fillets with four different values of the circumferential SCF under tension, an FCG prediction model was developed as will be discussed in chapter 6. The determined SIF solutions were implemented in the prediction model in such a way that FCG can be predicted in solid round metallic bars with a shoulder fillet loaded in tension.

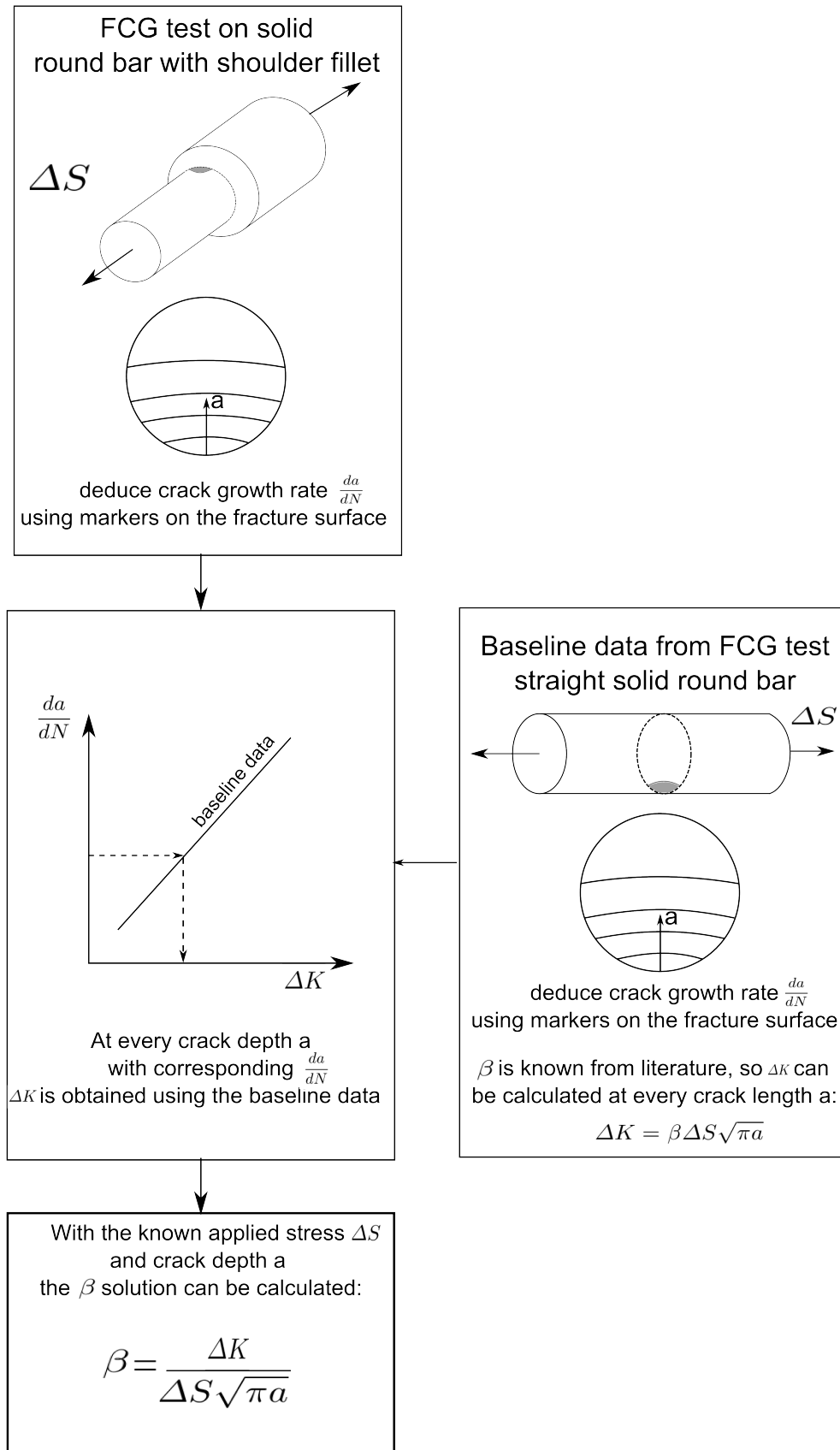


Figure 3.3: Methodology to determine SIF values from FCG experiments.

3.3 Energy Approach

The Strain Energy Release Rate (SERR) G is just as the SIF K a commonly used similarity parameter for FCG predictions. Since those two parameters are directly related as shown by Irwin [2], Paris-like equations are often proposed in literature for the prediction of FCG using the SERR. In literature often instead of the SIF range, the maximum SERR or the SERR range is used in such equations. In recent research work on fatigue disbond growth by Pascoe [38], it was shown that the disbond growth rate under fatigue loading is related to the total amount of cyclic energy released during a complete load cycle, and not the amount of energy that is released by a crack growth increment under the instantaneous load conditions at one point in the load cycle e.g. at maximum and/or minimum load. This statement was supported by experimental evidence; it was found that the relation between loss of cyclic strain energy and the disbond growth rate was independent of the applied stress ratio, where in the relationship between the disbond growth rate and the maximum SERR or SERR range a clear influence of the stress ratio was observed.

In this research, it was investigated if this correlation was also apparent in FCG through a metallic solid round bar. Furthermore, it was investigated how this knowledge could be used in the development of a prediction methodology based on the energy used for crack growth in a complete load cycle. Since the amount of energy used in a complete fatigue cycle is something which can be determined after a FCG test, but not on beforehand, it was still an open question how this could be predicted on beforehand. For an FCG prediction methodology based on the energy used for a crack to grow in a complete fatigue cycle, it is necessary to be able to predict the amount of energy used in a fatigue cycle on beforehand.

The process of FCG can be described in terms of energy: there must be an energy balance between loading and unloading a specimen with a growing fatigue crack. This energy balance can be written for a single load cycle as done in equation 3.5.

$$U_{in} = U_{out} + \frac{dU}{dN} \quad (3.5)$$

In equation 3.5, U_{in} is the strain energy supplied to the specimen during loading the specimen and U_{out} is the strain energy supplied back during unloading. $\frac{dU}{dN}$ is the energy used in that load cycle for the creation of crack area and plasticity. Because it is difficult to measure the difference between U_{in} and U_{out} during a FCG experiment, it was decided to measure the supplied strain energy U_{in} only. This will result, in the case of load-controlled experiments, in an increase of supplied energy with a growing crack because of the increase in displacement; a growing crack reduces the stiffness of the specimen. When the supplied strain energy U_{in} is plotted against the number of applied load cycles N , the derivative can be taken to obtain $\frac{dU}{dN}$. This is only true under the assumption that U_{out} of cycle N is equal to U_{in} of the cycle $N + \Delta N$ as written in equation 3.6. With this assumption, measurements of the supplied strain energy during the FCG experiments give enough information to derive $\frac{dU}{dN}$.

$$[U_{out}]_N = [U_{in}]_{N+\Delta N} \quad (3.6)$$

The increase in supplied strain energy U_{in} in the case of load-controlled fatigue experiments is a measure for the energy used in the growth of a fatigue crack, since the energy used for a

crack to grow (and formation of plasticity) between the applied load cycles N and $N + \Delta N$ is equal to the work done due to the increase in displacement by the external forces minus the difference in strain energy. This is also stated in equation 3.7.

$$U_{fracture+plasticity} = P [d_{N+\Delta N} - d_N] - 0.5P [d_{N+\Delta N} - d_N] \quad (3.7)$$

Which results in:

$$U_{fracture+plasticity} = 0.5P [d_{N+\Delta N} - d_N] \quad (3.8)$$

Where P is the applied load and d the resulting displacement. So, when the supplied strain energy $U_{in} = 0.5Pd$ is calculated for any cycle during a load-controlled FCG experiment and plotted versus the number of cycles N , the derivative $\frac{dU}{dN}$ is a measure for the amount of energy used for the growth of the fatigue crack and formation of plasticity. The amount of energy used during a fatigue cycle $\frac{dU}{dN}$ can be written as function of the energy used to create a certain crack area $\frac{dU}{dA}$ times how much crack area is created during that fatigue cycle $\frac{dA}{dN}$, which is expressed in equation 3.9.

$$\frac{dU}{dN} = \frac{dU}{dA} \frac{dA}{dN} \quad (3.9)$$

It has to be noted that the term $\frac{dU}{dA}$ in equation 3.9 relates to the total energy used for the growth of a certain crack area during complete a fatigue cycle; it is a different quantity than the conventional used SERR which is only valid at an instantaneous point in the load cycle (e.g. at maximum or minimum applied load S_{max} or S_{min}). The term $\frac{dU}{dA}$ as used in equation 3.9 will be referred to as G_{avg} since it can be seen as the average SERR during a complete fatigue cycle. When an FCG experiment is done, and the energy used during a cycle $\frac{dU}{dN}$ and the corresponding crack growth rate $\frac{dA}{dN}$ is known, this average SERR can be calculated using equation 3.9. It still was an open question at the beginning of this research project if and how this quantity G_{avg} could be used in the prediction of FCG.

It has to be noted that during this research project, no distinction was made between the energy used during FCG for plasticity (and other dissipative processes) and the formation of crack area.

3.4 Overall Research Approach

The research project took two different approaches looking at the problem of FCG through solid round bars with a shoulder fillet. Where the stress intensity approach uses an already proven methodology to investigate the influence of shoulder fillets on the fatigue crack growth behaviour, the energy approach had a more exploratory character since no proven prediction methodologies exist in current literature.

Furthermore, the research had a highly experimental character. The influence of shoulder fillets on the FCG behaviour was purely be based on experimental results. For the energy approach, a simple Finite Element (FE) model was created to investigate the relation between the crack area A and the energy input U_{in} as part of a pre-study to the possibility to characterize FCG using the energy approach. The amount of energy supplied to the specimen was also measured using force and displacement measurements during the experiments. Both the FCG prediction models that were developed, were mathematical models based on experimental results.

Chapter 4

Experiments

In this chapter, the experimental part of the research is discussed. During the research, Constant Amplitude (CA) Fatigue Crack Growth (FCG) experiments were conducted to gain the necessary FCG data. The design of experiments is discussed, as well as the specimen design, load spectrum design and experimental set-up. During the research, two different types of specimens were tested: straight solid round bars (without shoulder fillet) and solid round bars with shoulder fillet. The straight solid round bars were tested to obtain *baseline* FCG data of the material. The specimens with a shoulder fillet, of the same material, were tested to investigate the influence of a shoulder fillet on the FCG behaviour. Section 4.1 discusses the design of the experiments. After that, a pre-study to the energy approach using the FCG prediction software AFGROW and a Finite Element (FE) model is discussed in section 4.2.

4.1 Design of Experiments

To investigate the influence of a shoulder fillet on the FCG behaviour, it was decided to test specimens with different shoulder fillet radii, which caused different circumferential Stress Concentration Factor (SCF) values under tension loading. The values of the circumferential SCF under tension loading tested were: 1 (no shoulder fillet), 1.5, 2, 3 and 4.1. It was decided not to investigate higher values of the SCF since this is practically never encountered in engineering practice. Initial cracks with a depth of 1 mm were made with Electrical Discharge Machining (EDM) at the location in the shoulder fillet where the stress concentrates under tension loading.

Where in FCG experiments with a through-the-thickness fatigue crack the crack length a can be observed and measured during the experiment from the outer surface of the specimen, this is not possible in the case of a growing fatigue crack in a round bar. To be able to reconstruct how the fatigue crack grew through the solid round specimens, marker loads were implemented in the load spectrum, which became visible as clear bands on the fracture surface.

Furthermore, maximum and minimum applied force and resulting displacement are measured throughout the experiments to be able to analyse the amount of supplied energy to the specimens. Lastly, every designed specimen was produced twice to be able to analyse potential stress ratio effects. It was decided to test every designed specimen at two (very) different stress ratios: 0.5 and 0.05.

4.1.1 Specimen Design

Specimens were specifically designed for this research project. The most important criterion for the specimen design was the ability to test all the different specimens in a fatigue machine which was available in the Delft Aerospace Structures and Materials Laboratory (DASML) of the Aerospace Engineering (AE) faculty. Furthermore, the design of the specimens was as similar as possible to exclude any influence of other factors than the change in shoulder fillet geometry. All the specimens were produced from aluminium alloy 7075-T651 (the material certificate of the supplier can be found in appendix B). This material was chosen because marker loads were successfully used in this material to reconstruct how a part-through fatigue crack grew in a study of Schijve [21]. The specimens were produced from two different batches of the same material, in the test matrix in section 4.1.4 it is indicated which specimens are produced from which batch to be able to identify the possible influence of the different batches on the FCG behaviour.

The specimens with a shoulder fillet, are designed as illustrated in figure 4.1. To investigate the influence of different values of the circumferential SCF caused by a shoulder fillet under tension, it was chosen to vary only the fillet radius between the five different specimen. By only varying the fillet radius (and not the outer diameters of the bar) to obtain different circumferential SCFs, the different specimen could be very similar which makes the test procedure for the different specimen the same. The value of the circumferential SCF caused by a certain shoulder fillet geometry in a solid round bar is calculated using closed-form equations derived by Tipton [39] and the values for every specimen are indicated in the test matrix in section 4.1.4.

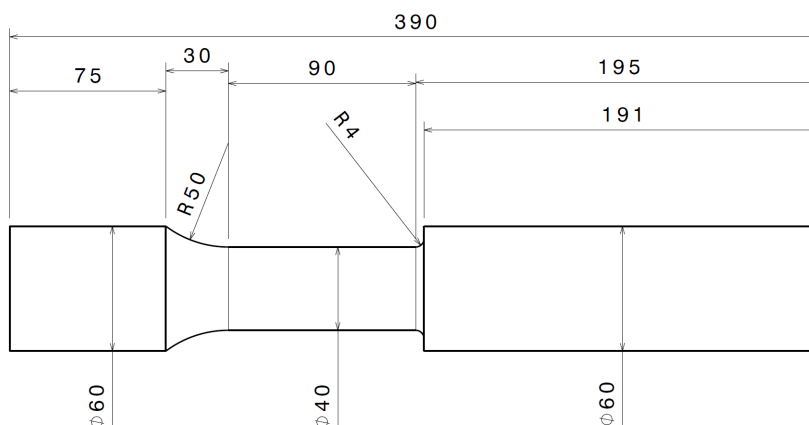


Figure 4.1: Design of specimen 1B40 and 2B40 with shoulder fillet, all values are in mm, the radius of 4 mm will vary between specimen variants, see section 4.1.4.

The smooth solid round bar *without* shoulder fillet, was very similar to the specimens with

a shoulder fillet and is illustrated in figure 4.2. All the specimen drawings can be found in appendix A.

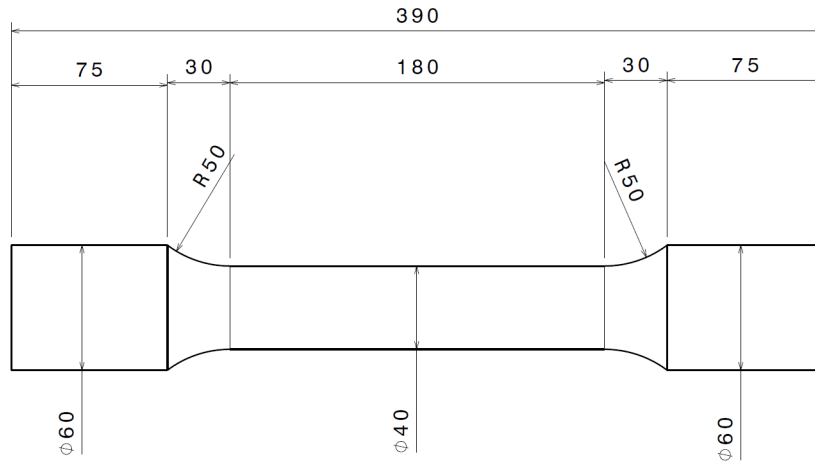


Figure 4.2: Design of the specimen without shoulder fillet, all values are in mm.

4.1.2 Location of the initial crack

An initial crack with a length of 1 mm was machined with EDM perpendicular to the axis of rotation of the solid round bar as illustrated in figure 4.3 to minimize the fatigue initiation life. The EDM machine used a thread thickness of 0.1 mm, making the thickness of the initial crack also approximately 0.1 mm. The location of the initial crack was in the shoulder fillet where the highest stress concentration is present according to Tipton [39]. This location of the highest stress concentration in the shoulder fillet will vary for every specimen and is indicated with the angle ' ϕ ' as defined in figure 4.3. The location of the highest stress concentration, and thus the initial crack, for every specimen is indicated in the test matrix in section 4.1.4 and on the specimen drawings in appendix A.

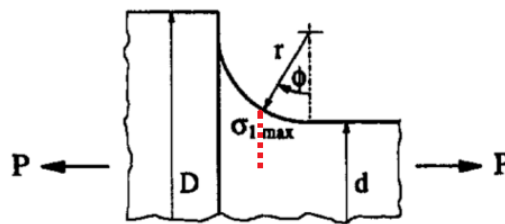


Figure 4.3: The angle ' ϕ ' which indicates where the highest stress concentrates in the fillet according to Tipton[39]. The dashed line indicates where the 1 mm deep initial crack was machined with EDM (drawing is not to scale).

4.1.3 Load spectrum design

The load spectrum was designed in such a way that FCG would occur from the initial crack machined with EDM. The specimens were loaded with a CA tensional load spectrum with a maximum stress S_{max} of 100 MPa, since an initial crack of 1 mm deep started to grow

for both stress ratio's for this material according to AFGROW. To be able to reconstruct how the fatigue crack grew after the specimen failed, marker loads were implemented in the load spectrum to create marker bands on the fracture surface. The marker loads were implemented using a study of Schijve [21]. In this study it was shown that by applying marker loads with an increased maximum stress of only 15 MPa higher than the baseline cycles, the marker loads could easily be recognised on the fracture surface as 'bands' using a Scanning Electron Microscope (SEM). It is well known that the overloads to create marker bands can lead to crack growth retardation in the subsequent CA baseline cycles because of plasticity. However, as shown in the same study by Schijve [21], an overload of 15 MPa caused negligible delay effects in the fatigue growth. Since this was concluded by Schijve for an overload of 15 MPa where the maximum stress of the baseline cycles was 60 MPa, it was assumed no delay (retardation) effects would occur when the maximum stress is equal to 100 MPa since the overload of 15 MPa is a relatively smaller overload in this case. The applied marker load block consisted out of 10 cycles and was repeated 3 times (with 50 baseline cycles in between) to make sure it could not be missed when inspecting the fracture surface. The applied CA load spectrum is visualized in figure 4.4. The amount of baseline cycles was chosen to get approximately 20 marker bands visible on the fracture surface of every specimen. Since it was not known on beforehand how fast the crack would grow under the applied loading in the tested material, the amount of baseline cycles was adjusted after the first couple of tests. The amount of baseline cycles that were applied for every specimen is indicated in the test matrix 4.1.4.

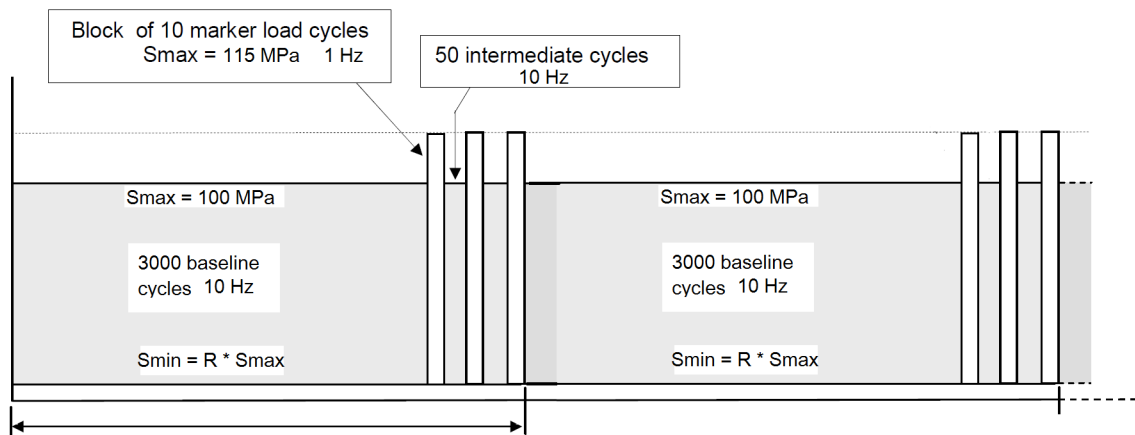


Figure 4.4: The load spectrum applied to the specimens, the amount of baseline cycles was different for every specimen, see the test matrix, and R is the applied stress ratio.

The stresses were converted to loads by multiplying the stress with the cross sectional area of the 40 mm diameter solid round bar. The load cycles applied were sinus-shaped with a frequency of 10 Hz for the baseline cycles and 1 Hz for the marker load cycles. The axial displacement between the clamps d and applied force P were measured at maximum and minimum applied load every 100th load cycle using the calibrated sensors of the MTS fatigue machine. To be able to analyse the amount of strain energy supplied to the specimen in a complete load cycle, during the last 5 cycles of every baseline block the displacement and force was measured at 10 points in every cycle. This was done to more accurately consider

the supplied strain energy rather than assuming linear force-displacement behaviour of the specimen between maximum and minimum applied load.

4.1.4 Test matrix

All the specimen that will be tested with corresponding applied load spectrum can be found in the test matrix given in table 4.1.

Table 4.1: The test matrix with tested specimens.

Specimen ID	Fillet radius [mm]	Stress concentration factor K_t [-] [39]	Stress concentration location ϕ [deg.] [39]	Material Batch	Maximum applied stress S_{max} [MPa]	Stress ratio R [-]	Amount of base-line cycles [-]
1B	-	1	-	B	100	0.5	25000
1Z	-	1	-	Z	100	0.5	10000
1B116	11.6	1.5	11.1	B	100	0.05	3000
2B116	11.6	1.5	11.1	B	100	0.5	5000
1B40	4.0	2	16.7	B	100	0.05	3000
2B40	4.0	2	16.7	B	100	0.5	10000
1Z13	1.3	3	22.3	Z	100	0.05	3000
2Z13	1.3	3	22.3	Z	100	0.5	10000
1Z06	0.6	4.1	25.8	Z	100	0.05	3000
2Z06	0.6	4.1	25.8	Z	100	0.5	10000

4.1.5 Experimental Set-Up and Procedure

The experiments were conducted on a 1000kN MTS fatigue machine which is available in the [DASML](#) lab of the [AE](#) faculty. During the experiments, which were be load controlled, the force and displacement measurements were conducted using the calibrated sensors of the MTS fatigue machine. The specimens were designed in such a way that when clamping the specimen in the machine, the initial crack was located approximately in the middle between the clamps. The specimen is clamped using the hydraulic clamps of the machine over a length of 75 mm at both ends. The clamping of the outer 75 mm on both sides of the specimen was not an exact process and this 'clamping length' varied a bit for every specimen. The tensional load spectrum was applied to the specimens until failure of the complete specimen occurred because of the growing fatigue crack. A failed specimen in the test set-up is shown in figure 4.5. After the specimen failed, the fracture surface was inspected using an Optical Microscope (OM) to identify the marker loads on the fracture surface to be able to reconstruct how the fatigue crack grew.

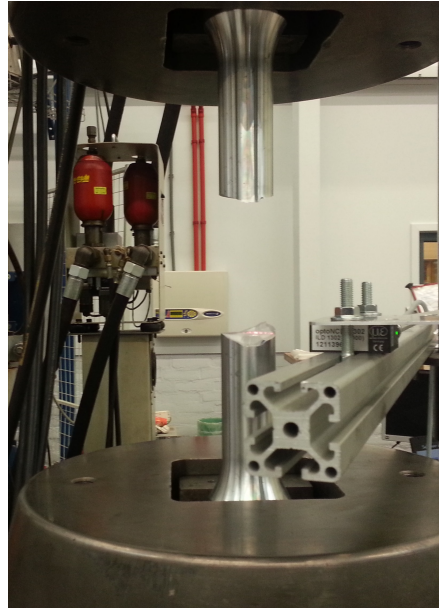


Figure 4.5: A failed specimen clamped in the 1000kN MTS fatigue machine.

Test procedure

1. Zero the force measurement before placing a specimen in the machine.
2. Clamp the outer 75 mm on both ends of the specimen using the hydraulic clamps.
3. A negative force will occur because of plastic deformation of the ends of the bar during the clamping process; when fully clamped, control the machine to zero Newton.
4. Let the machine auto-tune to be able to determine the appropriate parameters controller to control the desired applied force.
5. Control to zero Newton and assign 0 mm to the axial displacement.
6. Start the experiment. Apply the load spectrum and repeat it until failure of the specimen occurs.

4.2 Pre-study using FE and AFGROW

In preparation of the experiments, a short investigation was done using a simple **FE** model and the **FCG** prediction software AFGROW. **FCG** through a straight solid round bar was considered, of which a one-parameter Stress Intensity Factor (**SIF**) solution discussed in section 3.2 is implemented in AFGROW. The goal of this pre-study was to investigate if there was a possible correlation between the average Strain Energy Release Rate (**SERR**) G_{avg} , and the **FCG** rate $\frac{dA}{dN}$. A simple **FE** model was created to obtain a relation between the crack area A and supplied strain energy U_{in} . AFGROW was used to simulate the **FCG** process, the crack length a (which can be converted to cracked area A using the shape assumption of the **SIF** solution), number of applied load cycles N and the resulting **FCG** rate $\frac{da}{dN}$ (which can be converted to $\frac{dA}{dN}$ using the shape assumption) were taken from these simulations.

With data available on both of these aspects, it was investigated how the crack growth rate $\frac{dA}{dN}$ was correlated with an average **SERR** for several loading conditions. Furthermore, it was the question how this average **SERR** could be determined on beforehand; this is necessary to be able to do predictions of **FCG** based on the hypothesis that the total amount of energy

used during a cycle $\frac{dU}{dN}$ for a fatigue crack to grow relates directly to the FCG rate $\frac{dA}{dN}$.

To be able to calculate the average SERR G_{avg} , the energy balance as discussed in section 3.3 is considered. The energy balance of a single fatigue cycle is stated in equation 4.1.

$$U_{in} = U_{out} + \frac{dU}{dN} \quad (4.1)$$

The assumption that the strain energy that comes back during unloading U_{out} at a certain crack area A is equal to the strain energy putted in U_{in} at the next cycle (and thus at the crack area $A + \frac{dA}{dN}$) can be written as formulated in equation 4.2.

$$[U_{out}]_A = [U_{in}]_{A+\frac{dA}{dN}} \quad (4.2)$$

Now, the parameter F is introduced that describes how the strain energy input U_{in} changes with a growing crack area A compared to the energy input without a crack present, as written in mathematical form in equation 4.3.

$$[U_{in}]_A = [U_{in}]_{A=0} F(A) \quad (4.3)$$

Equation 4.1 can be rewritten using the assumption in equation 4.2 and the introduced parameter in equation 4.3:

$$[U_{in}]_{A=0} F(A) = [U_{in}]_{A=0} F\left(A + \frac{dA}{dN}\right) + \frac{dU}{dN} \quad (4.4)$$

Rewriting gives:

$$\frac{dU}{dN} = [U_{in}]_{A=0} \left[F(A) - F\left(A + \frac{dA}{dN}\right) \right] \quad (4.5)$$

Or:

$$dU = [U_{in}]_{A=0} [F(A) - F(A + dA)] \quad (4.6)$$

If both sides of equation 4.6 are divided by dA , an expression for the average SERR is obtained:

$$G_{avg} = \frac{dU}{dA} = [U_{in}]_{A=0} \frac{dF(A)}{dA} \quad (4.7)$$

A parameter H is introduced which is equal to $\frac{dF}{dA}$, this makes the equation for G_{avg} more convenient:

$$G_{avg} = \frac{dU}{dA} = [U_{in}]_{A=0} H(A) \quad (4.8)$$

A FE model was created to find an expression for the introduced parameter F in equation 4.3. This was done by calculating the energy input U_{in} at different crack areas A as will be discussed in section 4.2.2. By taking the derivative with respect to the crack area A of this function F , H as function of the crack area A was derived. By simulating the FCG process using AFGROW, it was investigated how the FCG rate $\frac{dA}{dN}$ was related to G_{avg} for different loading conditions (e.g. different applied maximum stresses S_{max} and stress ratios R).

4.2.1 The AFGROW simulations

The **FCG** process was simulated using AFGROW. A solid round bar of 40 mm with an initial crack depth of 1 mm was chosen and an **CA** load spectra were applied with several different maximum stresses and stress ratio's. The material chosen in AFGROW was 7075-T6511_Extra_L-T and the NASGRO equation was used for the prediction of **FCG**. The material properties of the used material are stated in table 4.2. A module in AFGROW for simulating **FCG** through a solid round bar was used. This module uses a one-parameter **SIF** solution only dependent on the relative crack depth $\frac{a}{D}$ and is derived by Forman et al.[10]; the solution is stated in equation 3.2. This **SIF** solution assumes that the fatigue crack front always intersects perpendicular with the outer surface of the bar during the growth as illustrated in figure 4.6. Using this shape assumption, a crack area A was calculated using the crack length a and diameter D .

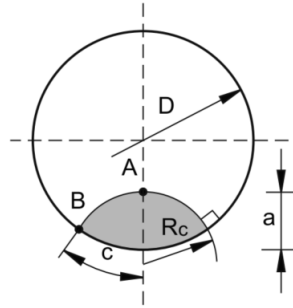


Figure 4.6: Crack shape assumed in the solution of Forman et al. [10]

Since AFGROW provides the **FCG** rate of the crack length $\frac{da}{dN}$, the **FCG** rate of the crack area $\frac{dA}{dN}$ at a certain load cycle N was calculated using the ratio between the crack length a and crack area A at that load cycle N as stated in equation 4.9.

$$\left[\frac{dA}{dN} \right]_N = \left[\frac{A}{a} \right]_N \left[\frac{da}{dN} \right]_N \quad (4.9)$$

Table 4.2: Material properties of 7075-T6511 in AFGROW.

Young's Modulus [MPa]	Poissons ratio [-]	Shear Modulus [MPa]
71705.5	0.33	26957.0

4.2.2 The FE model

An **FE** model was created using Patran to obtain the function H as stated in equation 4.8, the **FE** analysis itself was done with Nastran. Only a quarter of a solid round bar with a diameter of 40 mm and length of 180 mm was modelled due to the symmetry of the problem. Solid finite elements were used and the material properties as used in the AFGROW simulation were used for all elements in the **FE** model and are given in table 4.2. A load in the axial direction of the bar (positive x-direction) was applied on a node located next to the bar which

was aligned with the centre of the bar. The node at which the load was applied was attached to all the nodes at one end of the bar, illustrated as 'loaded side of the bar' in figure 4.7, with a Rigid Body Element (RBE). The applied load had a magnitude to introduce a stress of 100 MPa at that end of the bar. Symmetry boundary conditions were applied along the necessary surfaces of the bar and a crack was modelled by **not** applying symmetry constraints over the area of a certain part of the crack plane as illustrated in figure 4.7.

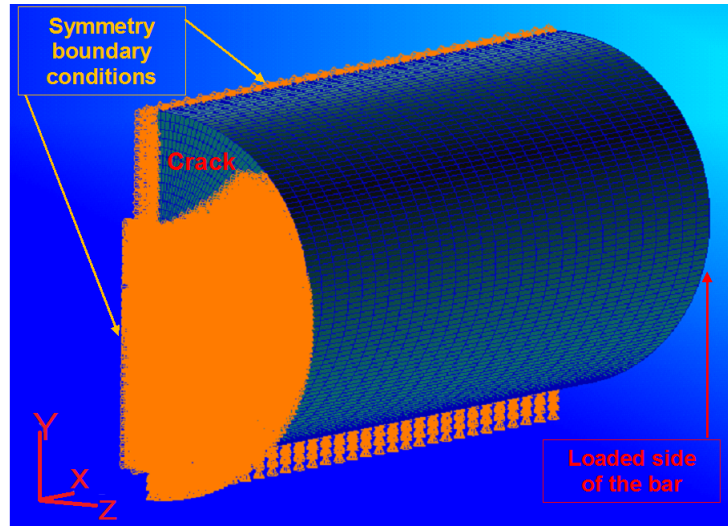


Figure 4.7: The FE model of a quarter bar with the applied boundary conditions because of symmetry and to model the crack.

Different cracks with different crack areas A were modelled while the applied load was kept constant, the supplied energy to the specimen U_{in} was calculated with the applied load P and resulting axial displacement (in positive x-direction) of the node at which the load was applied d : $U_{in} = 0.5Pd$. With the supplied strain energy when no crack was present $[U_{in}]_{A=0}$, the earlier introduced parameter F as function of the crack area A could be calculated using equation 4.10. This was done for several modelled cracks with corresponding crack areas A , of which the results are visualized in figure 4.8.

$$F(A) = \frac{[U_{in}]_A}{[U_{in}]_{A=0}} \quad (4.10)$$

A 4th order polynomial function was fitted through the data points to obtain a closed form equation for F as stated in equation 4.11, the derivative with respect to A gives the function H as function of the crack area A and is stated in equation 4.12.

$$F(A) = p_1A^4 + p_2A^3 + p_3A^2 + p_4A + p_5 \quad (4.11)$$

$$H(A) = \frac{dF(A)}{dA} = 4p_1A^3 + 3p_2A^2 + 2p_3A + p_4 \quad (4.12)$$

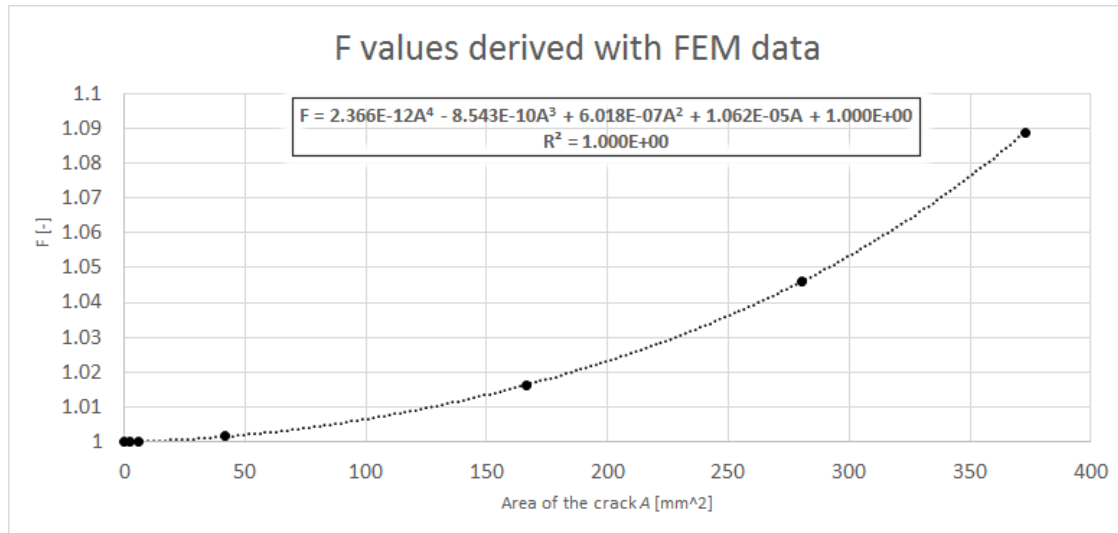


Figure 4.8: The values of F as calculated with equation 4.10 and the fitted fourth-order polynomial equation through the data indicated with the dotted line.

The fitted equation 4.10 is plotted in figure 4.8, and the parameters for the fitted equation are given in table 4.3.

Table 4.3: Fit coefficients and goodness of the fit for equation 4.11.

Fitted equation	R^2
Equation 4.11	1.000
Coefficient	Value
$p1$	2.366E-12
$p2$	-8.543E-10
$p3$	6.018E-7
$p4$	1.062E-5
$p5$	1.000

It has to be noted here, that where in the experiments the ends of the bar were fully clamped because of the hydraulic clamps, and thus the rotation of the ends of the bar because of the growing crack was constrained, this was not the case in this FE model: the ends were free to rotate with a crack present. The goal of this pre-study was not to simulate the experiments, but to investigate if there was a correlation between the FCG rate and an average SERR through a round bar in general. The experimental part of this thesis was done after this pre-study to further investigate the results of this pre-study and to provide experimental evidence of the findings.

4.2.3 Results of the Pre-study

AFGROW simulations were done for a fatigue crack in a solid round metallic bar with an initial crack of 1 mm. Several stress ratios R and maximum applied stresses S_{max} to generate some simulated FCG data. To be able to calculate G_{avg} , H as function of A as stated in

equation 4.12 was used.

It was argued that for the energy input at zero crack length $[U_{in}]_{A=0}$ in equation 4.13, the strain energy *density* input at zero crack length as defined in equation 4.14 or equation 4.15 can be used (instead of the strain energy) since the volume of the specimen does not change during the FCG process.

$$G_{avg} = [U_{in}]_{A=0} H(A) \quad (4.13)$$

Which results in, when using the strain energy *density*:

$$G_{avg,tot} = \frac{S_{max}^2}{2E} H(A) \quad (4.14)$$

Or, when considering the cyclic energy density input:

$$G_{avg,cyc} = \frac{S_{max}^2}{2E} (1 - R^2) H(A) \quad (4.15)$$

In both of above equations, S_{max} is the maximum applied stress in MPa, E is the Young's Modulus of the material in MPa and R is the stress ratio which is equal to $\frac{S_{min}}{S_{max}}$. It has to be noted that the unit of G_{avg} is $\frac{mJ}{mm^5}$ when using the strain energy *density* input for $[U_{in}]_{A=0}$. It indicates how much strain energy *density* is used for the growth of a certain fatigue crack area (in mm^2) during a complete load cycle.

When the FCG rate $\frac{dA}{dN}$ is plotted against $G_{avg,tot}$ as defined in equation 4.14, the curves in figure 4.9 are derived. When the FCG rate $\frac{dA}{dN}$ is plotted against $G_{avg,cyc}$ as defined in equation 4.15, the curve in figure 4.10 are derived.

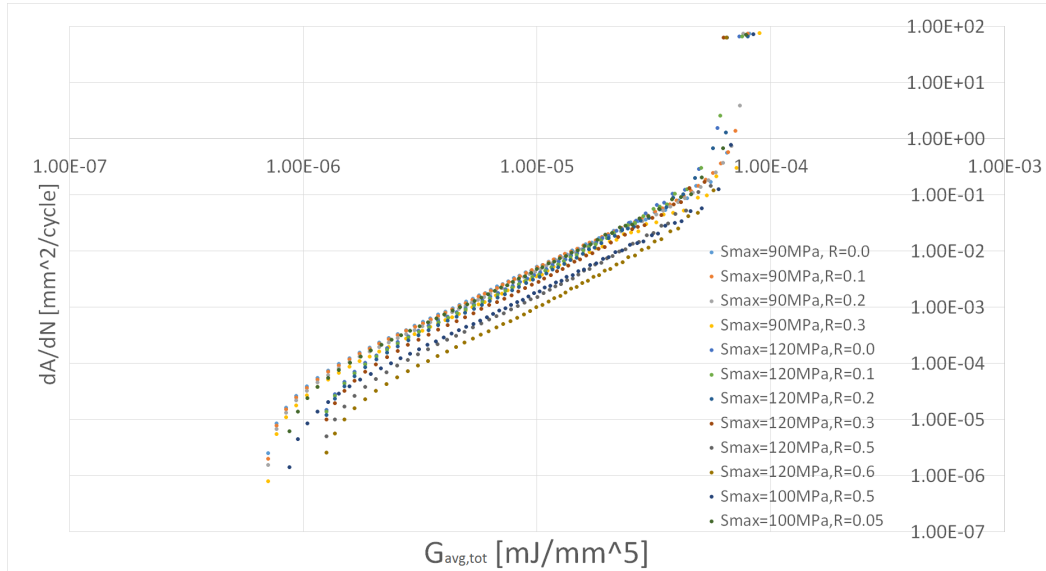


Figure 4.9: The crack growth rate versus the total energy used during the formation of crack area.

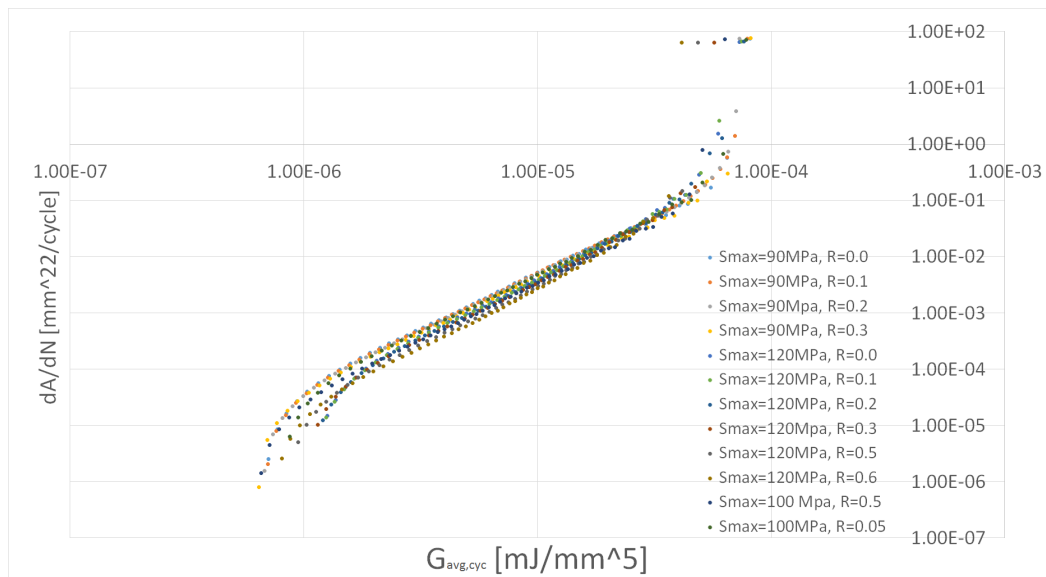


Figure 4.10: The crack growth rate versus the cyclic energy used during the formation of crack area.

When comparing the graphs in figure 4.9 and figure 4.10, it can be observed that when considering the *cyclic* energy almost a single curve is obtained for the different load cases. It seems that the crack growth rate $\frac{dA}{dN}$ correlates better with the average *cyclic* energy (density) used for the formation of crack area $G_{avg,cyc}$ during the complete load cycle than with the *total* energy (density) used for the formation of crack area $G_{avg,tot}$ during the complete load cycle. This observation was further investigated using FCG experiments in chapter 4 and 5. Furthermore, it was investigated how this observation could be used in a prediction methodology for FCG in chapter 6.

Chapter 5

Results

The results of the experiments are discussed in this chapter. The two main results are the crack growth measurements and the energy measurements which are discussed separately. First of all, some general remarks are made about the tested specimens in section 5.1. Then, the process of digitizing the fracture surface to obtain data about the crack length a and crack area A is explained in section 5.2. After that, the obtained crack length and crack area data is presented in section 5.3 and Stress Intensity Factor (SIF) solutions for the specimens with shoulder fillets are determined in section 5.4. The influence of the stress ratio is discussed in section 5.5 and how the crack shape developed during growth for the different specimen is discussed in section 5.6. The energy data is discussed in section 5.7 and the correlation with the Fatigue Crack Growth (FCG) rate is shown in section 5.8.

5.1 Test Results

In this section, the general test results are discussed, an overview is given in table 5.1. For specimen 1B, the force and displacement data was not successfully retrieved during the experiment and energy calculations were not possible. During the test of specimen 1Z06, multiple fatigue cracks initiated (next to the initial crack) in the shoulder fillet of the bar, as can be seen in figure 5.2. This made it not possible to compare it to the other specimen where this phenomenon did not occur: the fracture surfaces of all the other specimen had the characteristics as can be seen in figure 5.1. That this phenomenon happened for this specimen can be explained by the fact that it was loaded with a low stress ratio R (0.05) and had a high circumferential Stress Concentration Factor (SCF) (4.1). A low stress ratio means a high applied stress amplitude and fatigue cracks initiate quicker at higher applied stress amplitudes than lower applied stress amplitudes. Furthermore, fatigue cracks initiate quicker when a higher SCF is present. The combination of both of these factors caused that multiple fatigue cracks initiated next to the initial crack. Specimen 1B was not taken into account for the energy considerations since no data was gathered and specimen 1Z06 was not considered at all in further analysis of the test results.

Table 5.1: Test results.

Specimen ID	Stress ratio R [-]	SCF K_t [-]	Material Batch	Applied cycles at failure N_f [-]	Remarks
1B	0.5	1	B	933098	No energy data retrieved
1Z	0.5	1	Z	910170	-
1B116	0.05	1.5	B	61370	-
2B116	0.5	1.5	B	351928	-
1B40	0.05	2.0	B	99430	-
2B40	0.5	2.0	B	303771	-
1Z13	0.05	3.0	Z	95900	-
2Z13	0.5	3.0	Z	237372	-
1Z06	0.05	4.1	Z	61963	Multiple fatigue cracks
2Z06	0.5	4.1	Z	228169	-

The amount of applied cycles when failure did occur N_f in table 5.1 can be somewhat misleading since this also included the amount of cycles needed for the initiation of a fatigue crack from the initial crack made with Electrical Discharge Machining (EDM). It was not possible to detect when FCG exactly started to occur during the test. Marker loads were implemented in the load spectrum to be able to reconstruct how the fatigue crack grew during the experiment and this will be discussed in the next section.

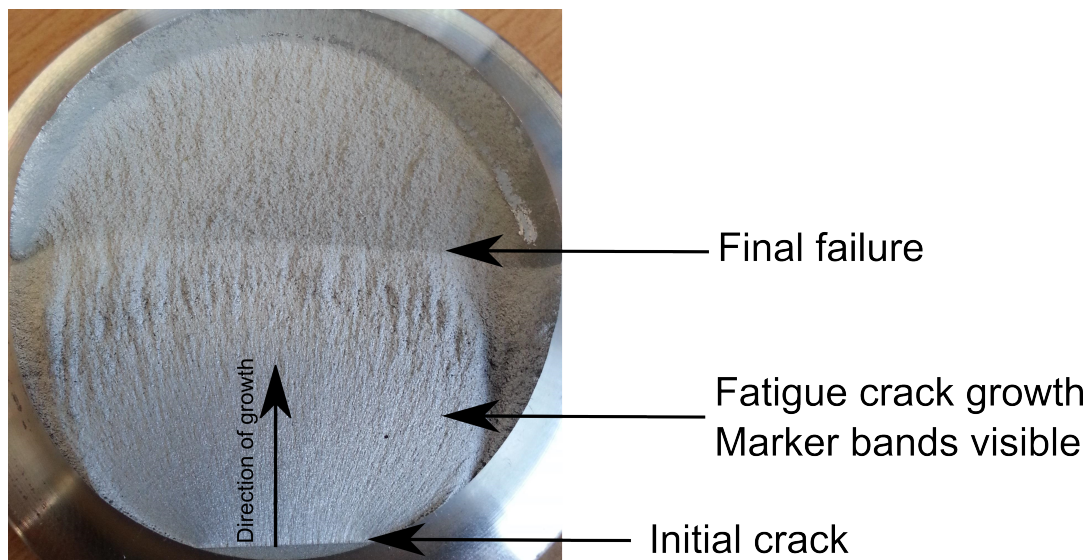


Figure 5.1: Overview of the fracture surface of specimen 2B116; the fracture surfaces of the other specimen had the same characteristics (except for specimen 1Z06).

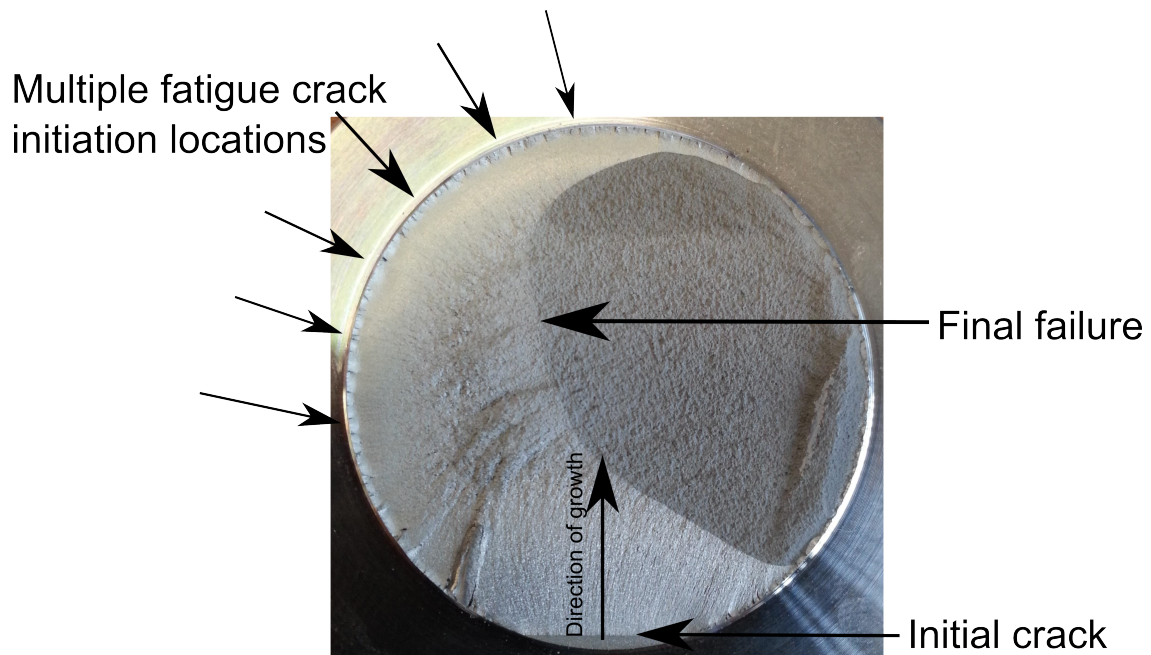


Figure 5.2: Overview of the fracture surface of specimen 1Z06 where multiple fatigue cracks initiated.

5.2 Digitizing the Fracture Surface

Data on the crack length a and crack area A were retrieved by inspecting the fracture surface of the specimens. The marker loads that were implemented in the applied load spectrum were clearly visible as darker bands on the fracture surface using an Optical Microscope (OM). As example, a picture of the fracture surface as seen with an OM of specimen 2B40 is shown in figure 5.3.

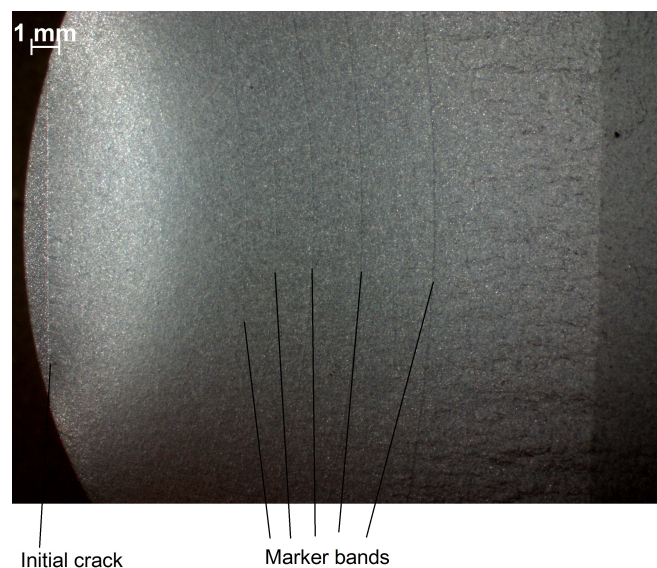


Figure 5.3: Picture of the fracture surface of specimen 2B40 seen with an OM, the applied marker loads clearly visible as darker bands.

The lens of the OM was always perpendicular positioned with respect to the fracture surface when a picture was made. Furthermore, it was made sure that the initial crack was always vertical positioned in every picture to be able to find the correct location of the reference point. Using the software of the OM, which takes into account at which magnification the picture is taken, the correct x- and y- location of a point manually indicated on a picture can be retrieved. This is done manually for several points along every marker band observed on the fracture surface. Because of the magnification of the OM, not the complete fracture surface was visible: the crack front near the outer edge of the bar was not visible as can be seen in the picture of the fracture surface of specimen 2B40 in figure 5.3. It is important that the x- and y-location of the reference point is also known for every picture made; then the location of every marker band on the fracture surface can be reconstructed. The reference point for every picture was on the outer edge of the round bar, in the middle of the initial crack as indicated in figure 5.4.

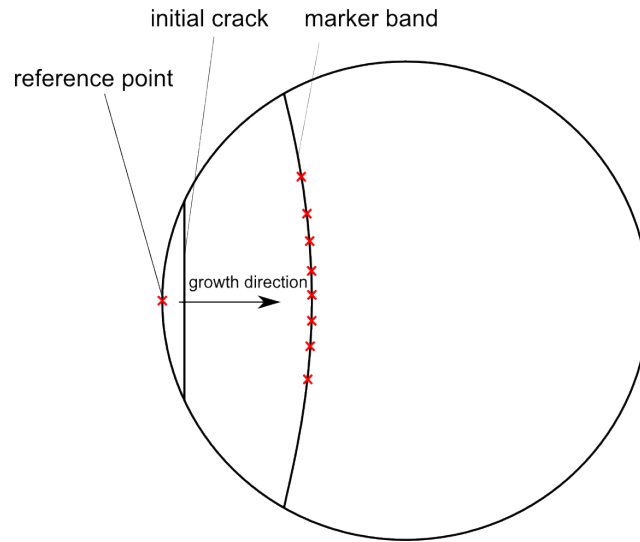


Figure 5.4: Schematic overview (not to scale) of the fracture surface with reference point and points along a marker band indicated with marks.

With knowledge of the x- and y- location of the reference point and several points along the marker bands, the fracture surface was digitized using MATLAB. The outer diameter of the bar at the location of the crack was plotted (this is a different diameter for every specimen because of the location of the initial crack at the highest stress concentration), the coordinates of the middle point of the bar was chosen to be (0,0). The marked points for every marker band observed were plotted at the correct location with respect to the outer diameter using the reference point. By fitting a second order polynomial equation through every set of points corresponding to a marker band, the complete crack front was reconstructed. The fitted equation is given in equation 5.1, this equation was chosen since the marker bands were symmetric with respect to the y-axis. An example of a completely digitized fracture surface is given in figure 5.5. It has to be noted that the to closer to the initial crack, the more difficult it became to recognize marker bands on the fracture surface using the OM.

$$y = c_1x^2 + c_2 \quad (5.1)$$

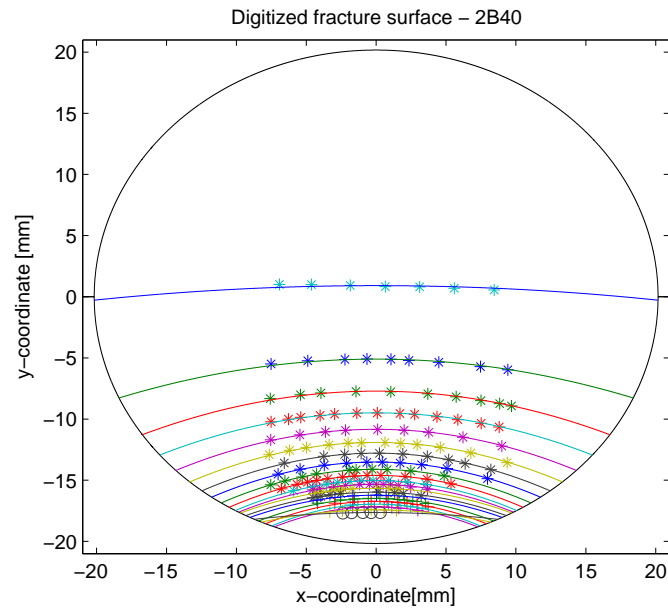


Figure 5.5: Digitized fracture surface of specimen 2B.4,0 with fitted equations to reconstruct marker bands.

Using the digitized fracture surfaces of the tested specimens, the crack length a and crack area A were obtained using MATLAB.

Fracture surface inspection procedure

1. Make sure that the fracture surface is perpendicular with respect to the lens of the OM.
2. Make sure that a picture is made with the initial crack positioned vertical.
3. Adjust the lightning and magnification in a way that the marker bands become visible.
4. Check the correct magnification is selected in the software and make a picture.
5. Use the software to mark points (the software saves the x- and y-location of every point marked automatically) on the picture where a marker band is visible.
6. Make sure that for every picture made, the reference point is marked and the x- and y-location is known.

5.3 Crack Growth Rate Data

With the process discussed in the previous section, the fracture surface of every tested specimen was digitized. For every digitized marker band on the surface, a crack length a and crack area A were calculated from the digitized image using MATLAB. The amount of load cycles applied N at every marker band observed is retrieved from the data file of the MTS machine. Since the marker load block was applied in three separate blocks of 10 cycles with 50 baseline cycles in between (in total 130 cycles), there was some uncertainty in the amount of cycles corresponding which corresponded to the marker band observed. It was chosen to take the amount of applied cycles half-way through the applied marker block of 130 cycles, which is indicated as example as N_{marker} in figure 5.6.

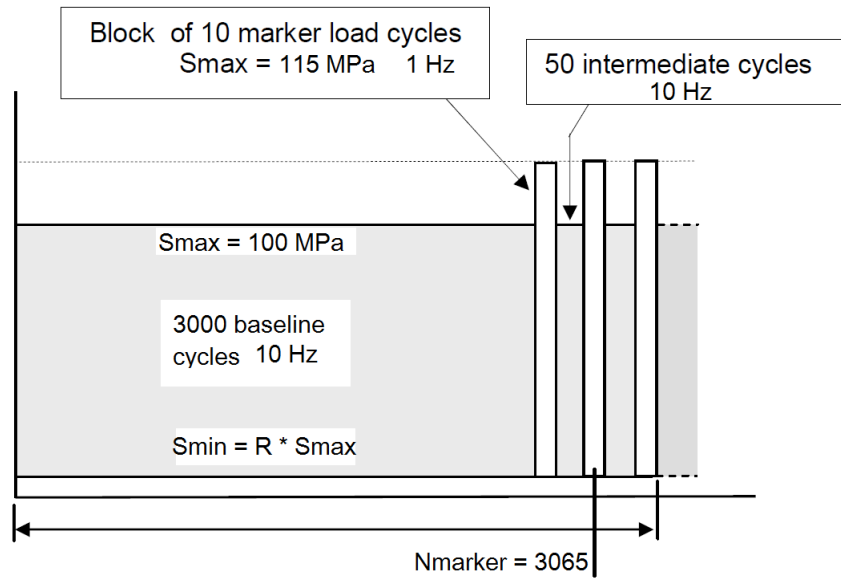


Figure 5.6: Applied load spectrum with cycle N_{marker} indicated which is assigned to a marker band observed on the fracture surface.

The second order exponential equations 5.3 and 5.5 were fitted through both data sets for every specimen. To obtain better fitting, the number of cycles were shifted along the x-axis in such a way that the first marker observed, the closest to the initial crack, on the fracture surface was assigned 1 number of shifted cycles, this shifted amount of cycles N_s was calculated using equation 5.2. The growth rates $\frac{da}{dN}$ and $\frac{dA}{dN}$ were obtained by differentiating the fitted second order exponential equation. The crack length a and crack area A plotted against the amount of shifted cycles N_s and fitted second order exponential equation is shown for specimen 2B40 in figure 5.7 and figure 5.8. The parameters for both fitted equations can be found in tables 5.2 and 5.3.

$$N_s = N_{marker} - \min(N_{marker}) + 1 \quad (5.2)$$

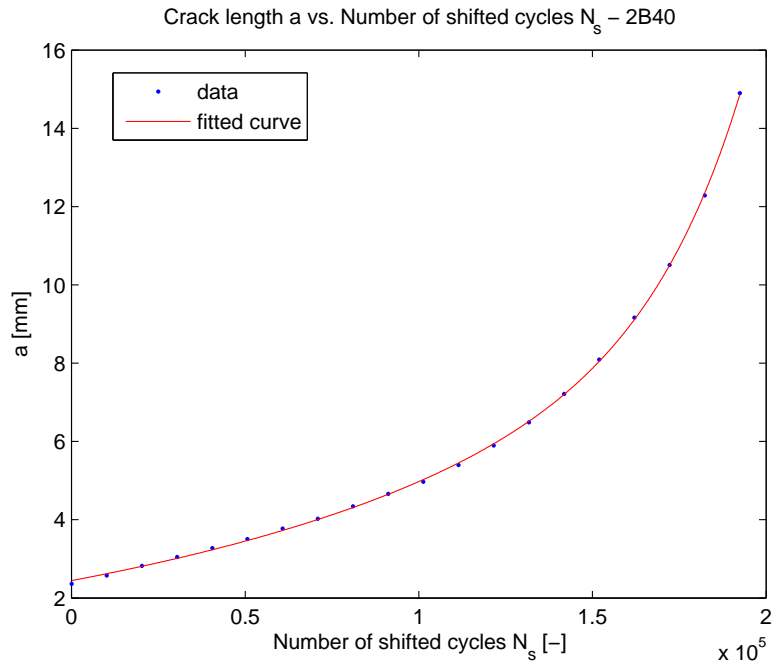


Figure 5.7: Crack length versus the shifted amount of cycles for specimen 2B40

$$a = c_1 e^{c_2 N_s} + c_3 e^{c_4 N_s} \quad (5.3)$$

$$\frac{da}{dN} = c_1 c_2 e^{c_2 N_s} + c_3 c_4 e^{c_4 N_s} \quad (5.4)$$

Table 5.2: Fit coefficients and goodness of the fit for equation 5.3 for specimen 2B40.

Fitted equation	RMSE	R^2
Equation 5.3 (and 5.4)	0.0473	0.9998
Coefficient	Value	95% Confidence Bounds
c_1	2.443	2.489 2.397
c_2	6.804E-6	7.117E-6 6.491E-6
c_3	2.919E-3	4.939E-3 8.989E-4
c_4	3.948E-5	4.277E-5 3.619E-5

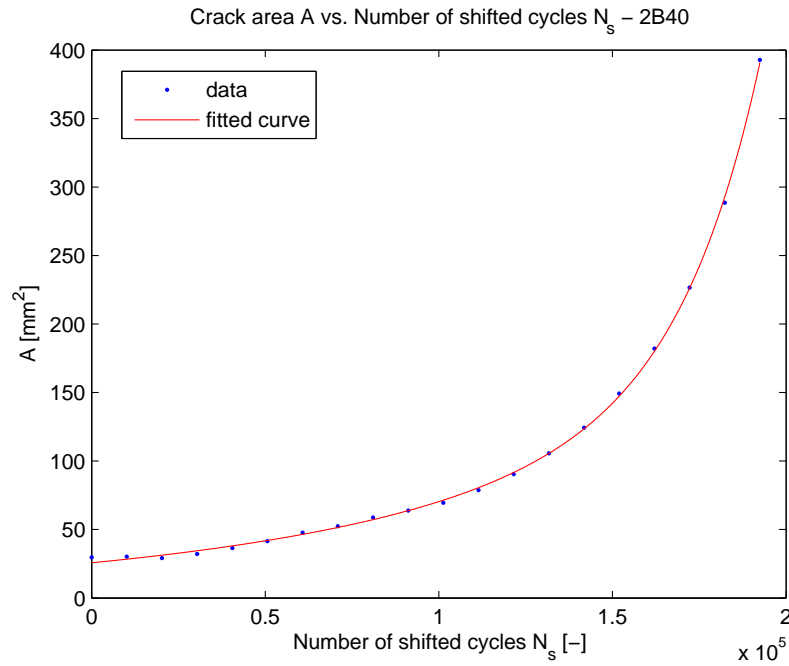


Figure 5.8: Crack area versus the shifted amount of cycles for specimen 2B40

$$A = c_1 e^{c_2 N_s} + c_3 e^{c_4 N_s} \quad (5.5)$$

$$\frac{dA}{dN} = c_1 c_2 e^{c_2 N_s} + c_3 c_4 e^{c_4 N_s} \quad (5.6)$$

Table 5.3: Fit coefficients and goodness of the fit for equation 5.5 for specimen 2B40.

Fitted equation	RMSE	R^2
Equation 5.5 (and 5.6)	2.1797	0.9996
Coefficient	Value	95% Confidence Bounds
c_1	26.67	27.57 23.78
c_2	9.524E-6	1.057E-5 8.479E-6
c_3	0.0453	0.08945 0.001154
c_4	4.434E-5	4.897E-5 3.971E-5

This process was repeated for every tested specimen to obtain the necessary data on the FCG rates. All the test results can be found in appendix C.

5.4 Development of a Stress Intensity Factor Solution

Using the gathered baseline FCG data, SIF values for the solid round bars with a shoulder fillets causing different values of the circumferential SCF under tension loading could be determined.

Baseline FCG data was derived using the same one-parameter SIF solution as used in commonly used FCG prediction software like AFGROW and NASGRO. This SIF solution is derived by Forman et al. [10] and stated in equation 5.8. When applying this SIF solution to the FCG data gathered with the experiments on the specimens without shoulder fillets, the crack growth rate as function of the SIF range ΔK is found as shown in figure 5.9.

$$\Delta K = \beta \Delta S \sqrt{\pi a} \quad (5.7)$$

With, for a solid round bar:

$$\beta(\lambda) = g \left[0.752 + 2.02\lambda + 0.37 \left(1 - \sin \left(\frac{\pi\lambda}{2} \right) \right)^3 \right] \quad (5.8)$$

With g defined as:

$$g = \frac{0.92 \left(\frac{2}{\pi} \right) \left[\frac{(\tan(\frac{\pi\lambda}{2}))}{\frac{\pi\lambda}{2}} \right]^{0.5}}{\cos(\frac{\pi\lambda}{2})} \quad (5.9)$$

Where λ is the relative crack length:

$$\lambda = \frac{a}{D} \quad (5.10)$$

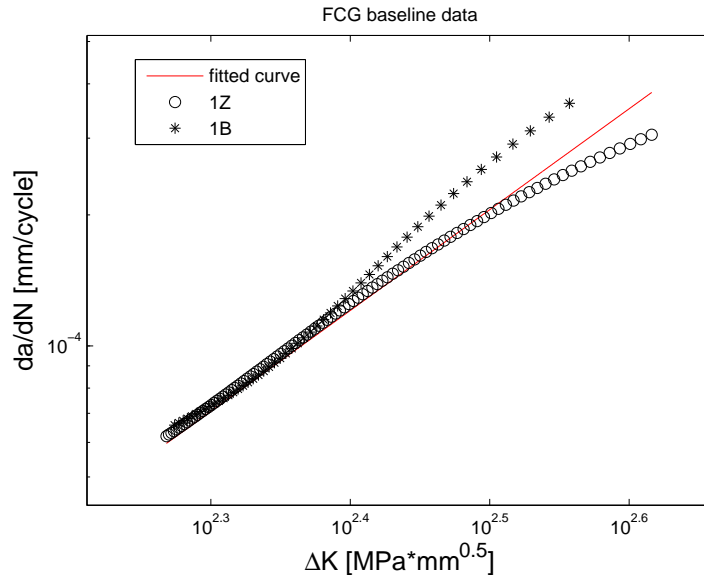


Figure 5.9: FCG baseline data

It can be observed that the two straight specimen from a different batch of material show FCG behaviour that is very similar at lower crack growth rates and at higher crack growth

rates a difference is observed. This difference can be explained by the fact that specimen 1B only had 3 observable marker bands on the fracture surface (see appendix C). To make fitting through the crack length versus amount of cycles possible, an extra data point had to be added for specimen 1B: the crack length at final failure. The process to determine the crack length at final failure was less accurate than for the marker bands: the marker bands were better visible than the exact location of the final fracture. That this extra data point had to be added for specimen 1B, could be an explanation for the difference in FCG behaviour at higher crack growth rates. It was decided to fit a power-law curve through the FCG data of both specimen to obtain one closed-form equation for the baseline FCG data. It is assumed that FCG occurred in the 'Paris-law' region and the power-law equation stated in equation 5.11 is fitted through the baseline data. The fitted equation was used as *baseline* FCG data to be able to calculate SIF values for the specimens with a shoulder fillet.

$$\frac{da}{dN} = C \Delta K^m \quad (5.11)$$

The fitted equation in figure 5.9 and stated in equation 5.11 has the C and m values as stated in table 5.4. The goodness of the fitted equation is indicated by the adjusted R-squared (R^2) value and the Root Mean Squared Error (RMSE).

Table 5.4: Fit coefficients and goodness of the fit for equation 5.11.

Fitted equation	RMSE	R^2
$\frac{da}{dN} = C \Delta K^m$	2.1397E-5	0.9078
Coefficient	Value	95% Confidence Bounds
C	3.318E-10	5.375E-10 1.261E-10
m	2.317	2.425 2.209

The fitted Paris-law equation 5.11 with the parameters as defined in table 5.4 was used as baseline to develop SIF values for the specimens with shoulder fillets using the methodology described in section 3.2. Only the specimens tested with a stress ratio of 0.5 were used to determine SIF values, the specimens tested at the stress ratio of 0.05 were used in section 5.5 to investigate the influence of the stress ratio. The experimentally determined SIF values for the specimens with a shoulder fillet are visualized in figure 5.10.

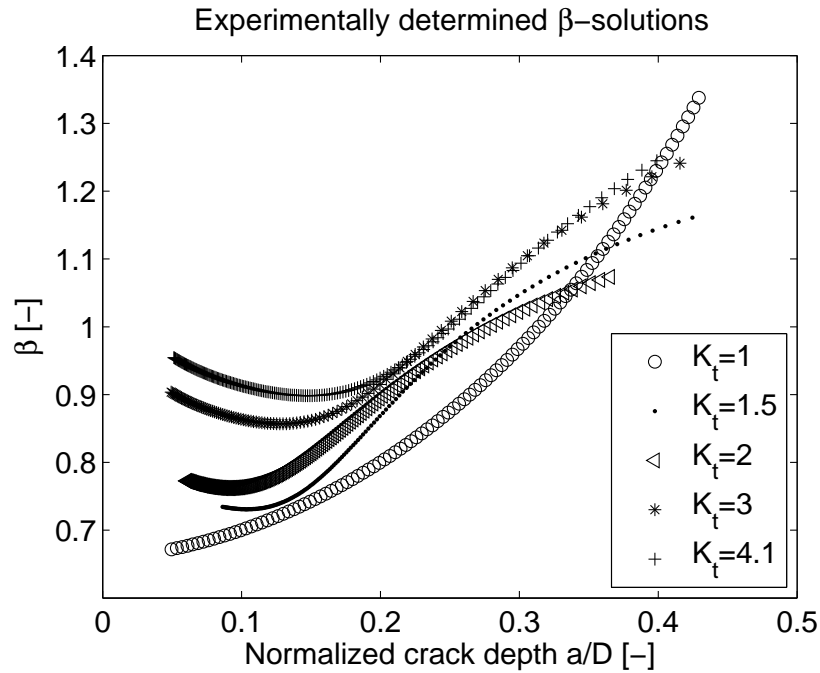


Figure 5.10: The determined **SIF** solutions expressed as values of β .

Now, a new parameter β_{corr} is introduced which is defined as the determined β value divided by the β value for a solid round bar without shoulder fillet ($K_t = 1$), in mathematical form stated in equation 5.12.

$$\beta_{corr} = \frac{\beta}{\beta_{K_t=1}} \quad (5.12)$$

This parameter is introduced because it enables that the current **SIF** solution for a solid round bar without shoulder fillet can be used in **FCG** predictions, but have to be adjusted with β_{corr} when a shoulder fillet is present. The **SIF** range ΔK for a solid round bar with a shoulder fillet can be calculated using β_{corr} as defined in equation 5.13.

$$\Delta K = \beta \beta_{corr} \Delta S \sqrt{\pi a} \quad (5.13)$$

The **SIF** values for a solid round bar with shoulder fillet expressed as values of β_{corr} are visualized in figure 5.11.

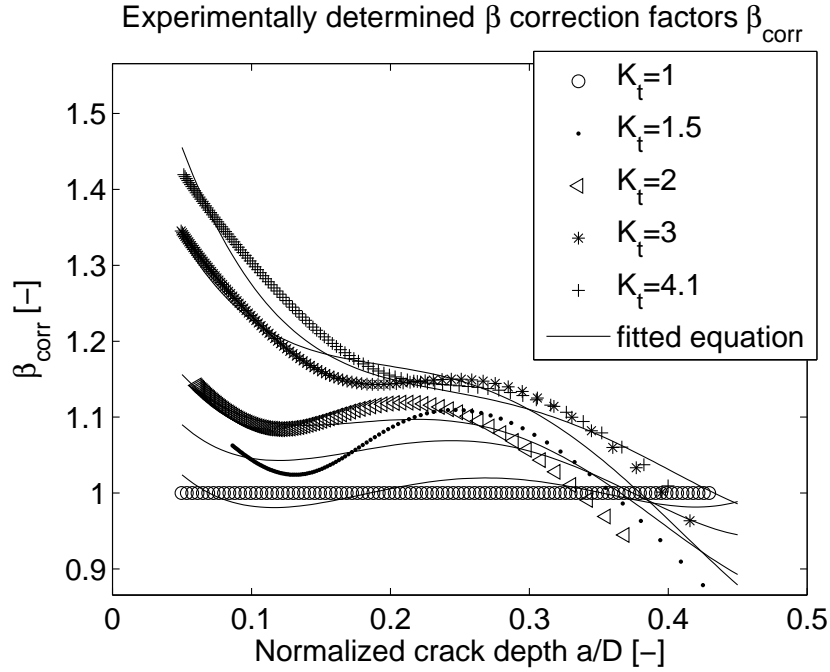


Figure 5.11: The determined correction factors β_{corr} .

It can be seen in figure 5.11 that the higher the SCF K_t , the larger the correction factor β_{corr} is. Also, the smaller the (normalized) crack depth, the larger the influence of the SCF on β_{corr} . This result can be explained by the fact that when the (normalized) crack length is lower, a large part of the crack front is closer to the shoulder fillet which causes a concentration of stress which is higher when the SCF is higher. When the fatigue crack grows, a large part of the crack front grows away from the shoulder fillet and this decreases the influence of the shoulder fillet on the FCG behaviour.

All the data in figure 5.11 was used in a two-parameter fitting technique to obtain a closed-form equation for the correction factor β_{corr} as function of the normalized crack length $\lambda = \frac{a}{D}$ and the SCF K_t . The fitted equation is given in equation 5.14 and visualized in figure 5.11. The corresponding goodness of the fit and values for the fit coefficients is given in table 5.5.

$$\begin{aligned} \beta_{corr}(\lambda, K_t) = & p00 + p10\lambda + p01K_t + p20\lambda^2 + p11\lambda K_t + p02K_t^2 + p30\lambda^3 \\ & + p21\lambda^2 K_t + p12\lambda K_t^2 + p03K_t^3 + p40\lambda^4 + p31\lambda^3 K_t + p22\lambda^2 K_t^2 + p13\lambda K_t^3 + p04K_t^4 \end{aligned} \quad (5.14)$$

The fitted equation for β_{corr} as defined in equation 5.14, was used in the developed prediction model as discussed in section 6.1. The fitted equation β_{corr} as defined in equation 5.14, is considered valid between a SCF of 1 and 4.1 and relative crack depth λ of 0.05 and 0.45 since there is only experimental data available between those limits.

Table 5.5: Fit coefficients and goodness of the fit for equation 5.14.

Fitted equation	RMSE	R²
Equation 5.14	0.0164	0.9802
Coefficient	Value	95% Confidence Bounds
p_{00}	0.8864	1.027 0.7463
p_{10}	-4.495	-3.359 -5.63
p_{01}	0.4676	0.7359 0.1993
p_{20}	27.6	34.43 20.78
p_{11}	1.492	2.162 0.8222
p_{02}	-0.302	-0.1186 -0.4855
p_{30}	-72.37	-54.06 -90.68
p_{21}	-0.8863	0.7841 -2.557
p_{12}	-0.8267	-0.622 -1.031
p_{03}	0.1137	0.1658 0.06153
p_{40}	72.07	90.1 54.04
p_{31}	-4.963	-3.225 -6.701
p_{22}	1.064	1.258 0.8704
p_{13}	0.05621	0.08007 0.03235
p_{04}	-0.01338	-0.008135 -0.01862

5.5 Influence of the Stress Ratio

The SIF solution stated in equation 5.14 was determined using the specimens tested at a stress ratio of 0.5. Now, the developed SIF solution as stated in equation 5.14 is applied to all the specimens tested (also at the specimens tested at a stress ratio of 0.05) and the FCG rate $\frac{da}{dN}$ versus the SIF range ΔK is plotted in figure 5.12.

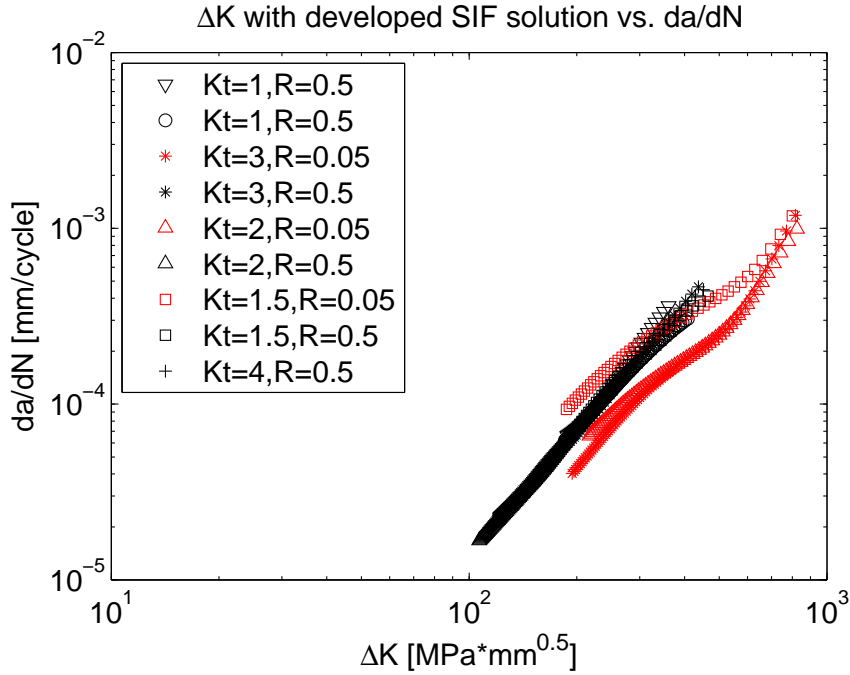


Figure 5.12: All the test data plotted with the determined β_{corr} solution of equation 5.14.

As expected, a stress ratio effect is observed in figure 5.12. The specimens tested at a stress ratio of 0.5 condense to a single curve and the specimens tested at a stress ratio of 0.05 condense to a single curve (except for specimen 1B116, with a $K_t = 1.5$ and $R = 0.05$, which is considered as outlier). To be able to predict FCG at different stress ratios, a correction equation is proposed to condense the gathered FCG data at the two stress ratios on a single curve. The correction equation proposed is one derived by Schijve for 2024-T3 as stated in equation 5.15 [40]. Although the tested material is a different aluminium alloy, a large part of the stress ratio effect disappears when equation 5.15 is applied as visualized in figure 5.13. It is believed that this can be explained by the fact that these correction equations don't correct for crack closure only, but largely correct for the fact that the SIF range is not able to describe the load cycle correctly. Since a large part of the stress ratio effect disappeared with the use of equation 5.15, it was assumed that this correction equation for the stress ratio R could be used in a prediction model based on the stress intensity concept and will be discussed in section 6.1. That the FCG data obtained at both stress ratios do not fall exactly on a single curve, there is still some scatter present when applying the correction equation, has an effect on the FCG predictions done with the developed model as will be discussed in chapter 6.

$$\frac{\Delta K_{eff}}{\Delta K} = 0.55 + 0.33R + 0.12R^2 \quad (5.15)$$

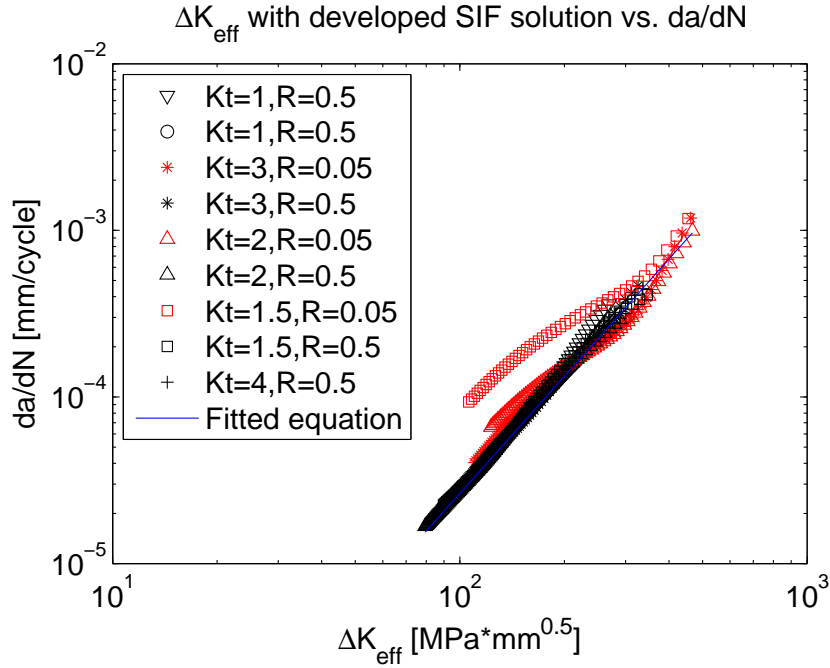


Figure 5.13: All the test data plotted with the determined β_{corr} solution of equation 5.14 and corrected to obtain an effective SIF range with equation 5.15.

Excluding the specimen with $K_t = 1.5$ and tested at a stress ratio $R = 0.05$, the power law equation stated in equation 5.16 is fitted through the data in figure 5.13. The resulting coefficients for C and m in equation 5.16 were used in the developed prediction model that is discussed in section 6.1.

$$\frac{da}{dN} = C \Delta K_{eff}^m \quad (5.16)$$

Table 5.6: Fit coefficients and goodness of fit for equation 5.16

Fitted equation	RMSE	R^2
$C \Delta K_{eff}^m$	2.2715E-5	0.9660
Coefficient	Value	95% Confidence Bounds
C	5.615E-10	6.612E-10 4.617E-10
m	2.336	2.367 2.305

5.6 Crack shape development

Since the presence of a circumferential stress concentration not only influences the FCG rate $\frac{da}{dN}$, but also how the crack shape develops when growing, this was investigated in this section. The test results results were used to derive an empirical based equation between the relative crack depth $\lambda = \frac{a}{D}$ and shape of the crack for the different stress concentration factors K_t . This empirical derived equation will be used in the developed prediction model to be able to also a crack shape and not only the crack depth.

The shape of the crack front is determined by a second order polynomial equation, as fitted through every marker band observed on the fracture surface with equation 5.17 and visualized in figure 5.14. In this equation, c_2 indicates the length of the crack and c_1 indicates the shape of the crack. How this shape, captured by the coefficient c_1 , changes with the relative crack depth for the different specimens, is plotted in figure 5.15. When c_1 is equal to 0, the crack front is straight, as is the case for the initial cracks. The more negative c_1 is (higher absolute value), the more circular-shaped the front crack is.

$$y = c_1x^2 + c_2 \quad (5.17)$$

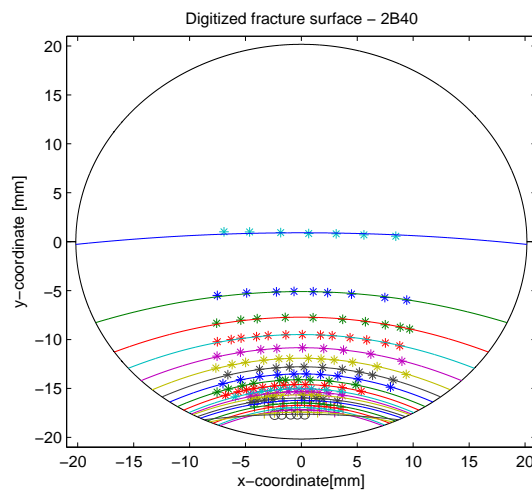


Figure 5.14: Digitized fracture surface of specimen 2B.4,0 with fitted equations to reconstruct marker bands.

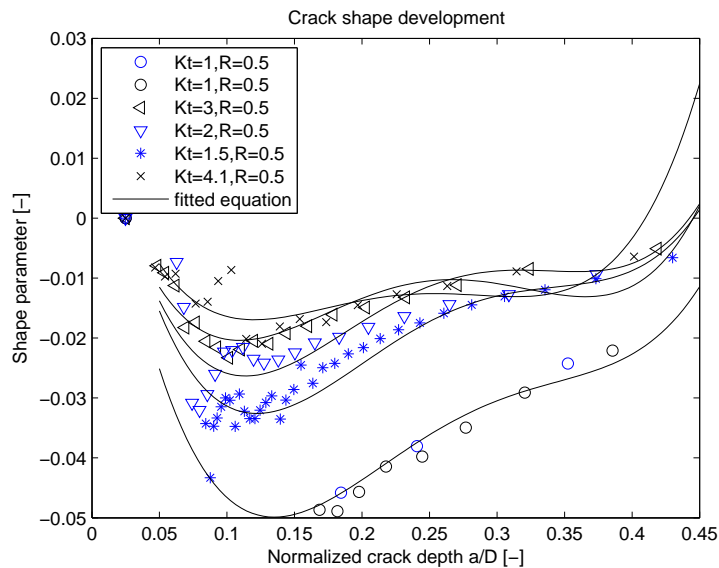


Figure 5.15: The crack shape parameter versus the normalized crack depth for the specimens tested.

In figure 5.15, it can be seen that all the cracks become more circular shaped (the absolute value of c_1 increases) from the straight initial crack until a normalized crack depth of approximately 0.13 is reached. When the relative crack depth becomes larger, the crack front tends to become more straight in all cases (the absolute value of c_1 decreases). It can also be seen in figure 5.15 that the higher the SCF, the crack shape stays more straight (the absolute values of c_1 are lower for a higher SCF).

A two-variable fitting technique through all the data was used to obtain a closed-form equation for c_1 , which indicates the shape of the crack, as function of the normalized crack depth $\lambda = \frac{a}{D}$ and SCF K_t . The fitted equation is given in equation 5.18 and visualized in figure 5.15. The values of the coefficients and the goodness of the fit is given in table 5.7.

$$c_1(\lambda, K_t) = p00 + p10\lambda + p01K_t + p20\lambda^2 + p11\lambda K_t + p02K_t^2 + p30\lambda^3 + p21\lambda^2 K_t + p12\lambda K_t^2 + p03K_t^3 + p40\lambda^4 + p31\lambda^3 K_t + p22\lambda^2 K_t^2 + p13\lambda K_t^3 + p04K_t^4 \quad (5.18)$$

The fitted equation for the crack shape c_1 as defined in equation 5.18, was used in the developed prediction model as discussed in section 6.1. The fitted equation c_1 as defined in equation 5.18, is considered valid between a SCF K_t of 1 and 4.1 and relative crack depth λ of 0.05 and 0.45 since there is only experimental data available between those limits.

Table 5.7: Fit coefficients and goodness of the fit for equation 5.18.

Fitted equation	RMSE	R ²
Equation 5.18	0.004009	0.8927
Coefficient	Value	95% Confidence Bounds
p_{00}	-0.03275	0.02961 -0.09511
p_{10}	-2.085	-1.803 -2.367
p_{01}	0.1286	0.2498 0.007418
p_{20}	11.36	13.28 9.444
p_{11}	0.7152	0.9495 0.4809
p_{02}	-0.08944	-0.008315 -0.1706
p_{30}	-25.77	-20.2 -31.33
p_{21}	-1.834	-1.299 -2.369
p_{12}	-0.136	-0.0535 -0.2186
p_{03}	0.02431	0.04703 0.001594
p_{40}	21.74	27.69 15.78
p_{31}	1.425	2.036 0.8128
p_{22}	0.1535	0.2253 0.08164
p_{13}	0.008816	0.01895 -0.001315
p_{04}	-0.002287	-3.334e-05 -0.00454

5.7 Energy Data

With the measured maximum and minimum force and displacement for every 100th applied load cycle, the total strain energy U_{tot} and cyclic strain energy U_{cyc} for every 100th applied load cycle could be calculated. Linear force-displacement behaviour was assumed between minimum and maximum applied load and the supplied energy is calculated as area below this curve. This assumption was verified by the force and displacement measurements done during the last five cycles of a baseline block. The force and displacement was measured 10 times during every cycle in the last 5 cycles; when the applied force and corresponding displacement is plotted, linear behaviour can be observed. These measurements are shown for

the first baseline and last baseline block in figure 5.16 for specimen 1B40. All tested specimen showed this linear load-displacement behaviour. Since the measurements of the first and last baseline block showed linear load-displacement behaviour, linear load-displacement behaviour was assumed for every load cycle applied during the FCG experiment.

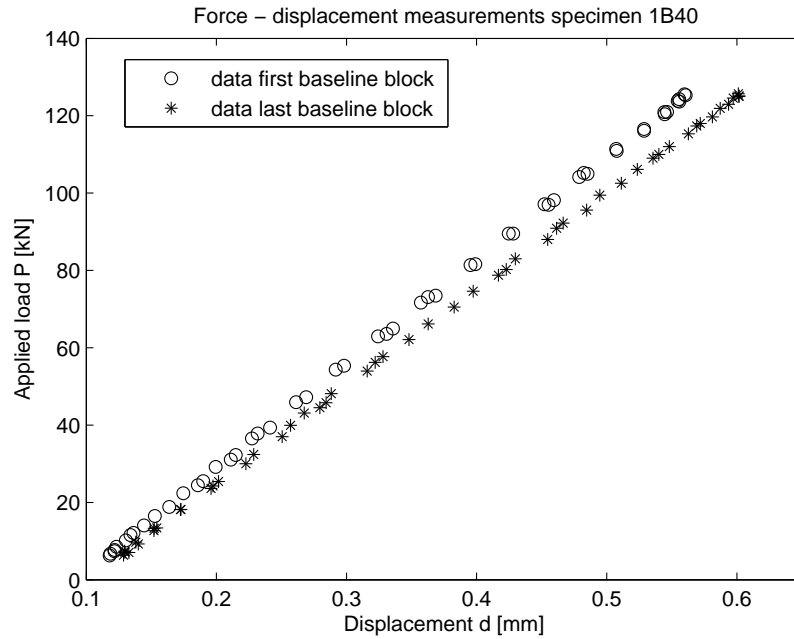


Figure 5.16: Linear load-displacement behaviour of specimen 1B40.

Now this linear behaviour was assumed and verified by measurements, the total and cyclic energy supplied to the specimen were calculated using the measured maximum and minimum value of the applied force and corresponding displacement. Since this linear curve did not necessarily pass through the origin when extrapolated, the location where this linear curve intersects with the displacement-axis d^* as visualized in figure 5.17 had to be calculated for a correct calculation of the total and cyclic energy.

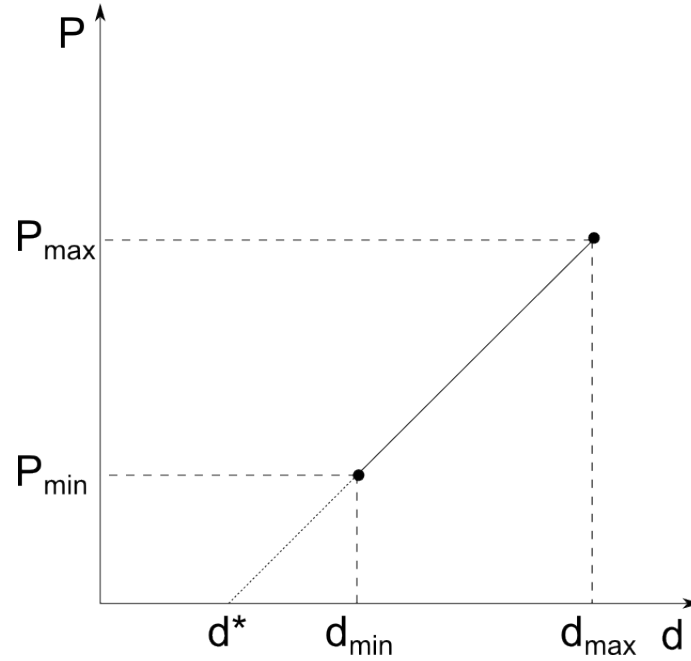


Figure 5.17: Linear load-displacement behaviour where d^* indicated the location of the intersection with the displacement axis.

With the two data points measured for a load cycle as indicated in figure 5.17, the point where the load-displacement curve intersects the displacement-axis d^* is calculated using equation 5.19.

$$d^* = d_{min} - \left(\frac{d_{max} - d_{min}}{P_{max} - P_{min}} \right) P_{min} \quad (5.19)$$

Now, the total energy U_{tot} can be calculated with equation 5.20 and the cyclic energy U_{cyc} with equation 5.21.

$$U_{tot} = 0.5P_{max} (d_{max} - d^*) \quad (5.20)$$

$$U_{cyc} = U_{tot} - 0.5P_{min} (d_{min} - d^*) \quad (5.21)$$

When the total and cyclic energy is calculated for every measured load cycle, the total and cyclic energy is plotted versus the amount of applied cycles and it was possible to fit a second order power-law equation as stated in equation 5.23 through the data. To ensure better fitting, the amount of cycles N was translated with equation 5.22. The energy data versus the amount of cycles N with fitted equations is plotted for specimen 2B40 in figure 5.18 to coefficients of the fitted equations are shown in table 5.8 and 5.9. The amount of strain energy used in a complete load cycle $\frac{dU}{dN}$ is obtained by taking the derivative of the fitted equation as stated in equation 5.24. For some specimens, two different power-law equations were fitted through the energy data to obtain better fitting.

$$N_* = (\max(N) + \min(N)) - N \quad (5.22)$$

$$U = c_1 N_*^{c_2} + c_3 \quad (5.23)$$

$$\frac{dU}{dN} = c_1 c_2 N_*^{c_2-1} \quad (5.24)$$

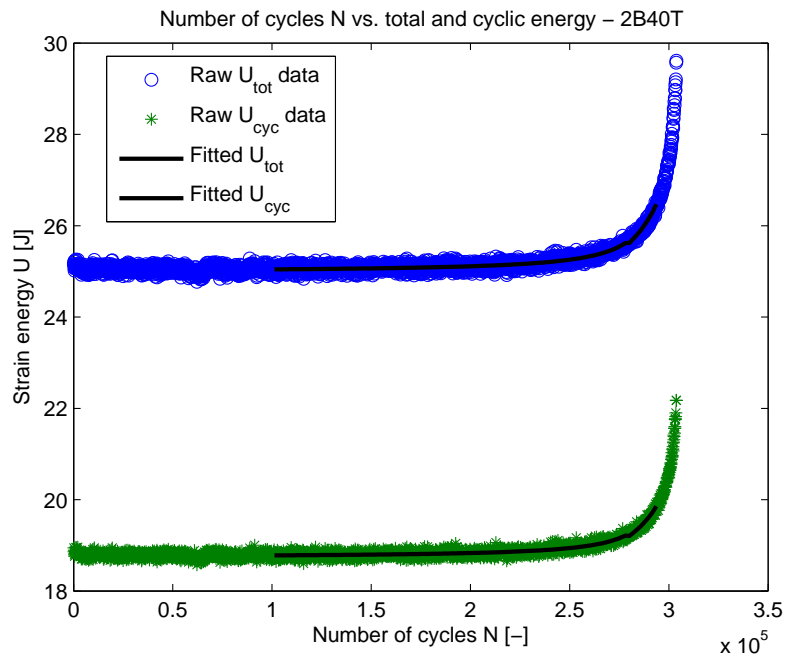


Figure 5.18: Cyclic and total energy versus the amount of cycles with fitted power-law equations.

The derivatives $\frac{dU_{tot}}{dN}$ and $\frac{dU_{cyc}}{dN}$ give information about how much (total or cyclic) energy was used during that complete cycle for the fatigue crack to grow. How this correlates to the FCG rate is discussed in section 5.8.

Table 5.8: Fit coefficients and goodness of the fit for equation 5.23 fit through **total** energy data for specimen 2B40.

Fitted equation	RMSE	R ²
$U_{tot} = c_1 N_*^{c_2} + c_3$	0.0185	0.9996
Coefficient	Value	95% Confidence Bounds
c_1	-15.86	-14.07 -17.64
c_2	0.042	0.04549 0.0385
c_3	49.83	51.71 47.95

Table 5.9: Fit coefficients and goodness of the fit for equation 5.23 fit through cyclic energy data for specimen 2B40.

Fitted equation	RMSE	R ²
$U_{cyc} = c_1 N_*^{c_2} + c_3$	0.0145	0.9995
Coefficient	Value	95% Confidence Bounds
c_1	-5.972	-5.446 -6.498
c_2	0.06718	0.07096 0.06341
c_3	30.96	31.55 30.37

5.8 Relation Between the Fatigue Crack Growth Rate and Energy

To investigate if the FCG rate $\frac{dA}{dN}$ correlates with the total or cyclic energy used in the complete fatigue cycle, the data gathered in the previous sections is plotted. The crack growth rate $\frac{dA}{dN}$ is plotted against the amount of total and cyclic energy used for FCG during that complete fatigue cycle $\frac{dU_{tot}}{dN}$ or $\frac{dU_{cyc}}{dN}$ for all the specimens.

In figure 5.19, the total energy used for FCG $\frac{dU_{tot}}{dN}$ is plotted against the FCG rate $\frac{dA}{dN}$ for all the specimens. In figure 5.20, the cyclic energy used for FCG $\frac{dU_{cyc}}{dN}$ is plotted against the FCG rate $\frac{dA}{dN}$. Note that both plots have logarithmic axes.

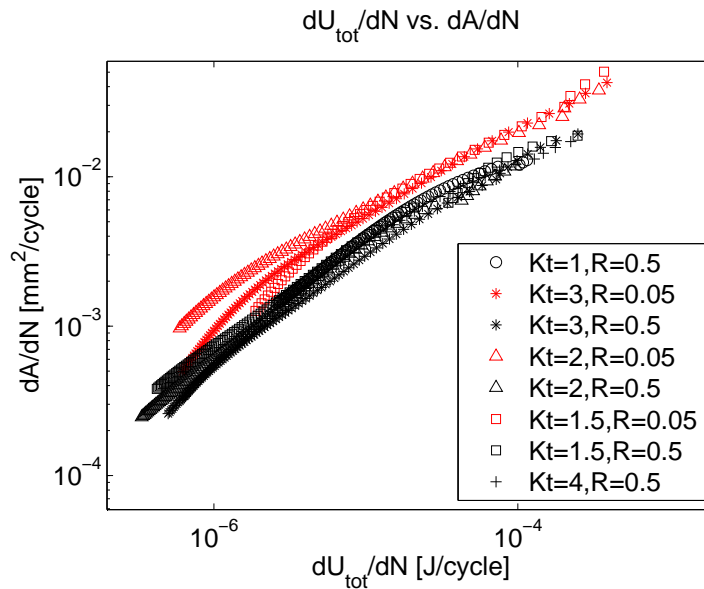


Figure 5.19: The total strain energy used for crack growth in a load cycle versus the crack growth rate.

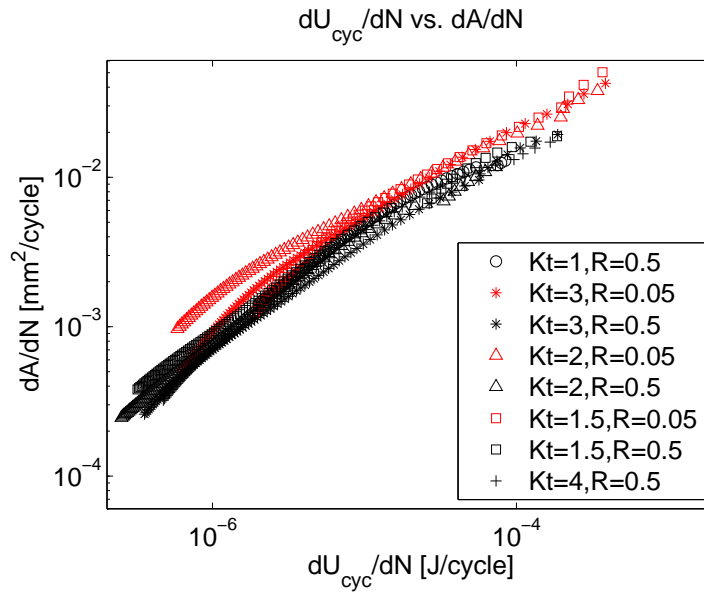


Figure 5.20: The total cyclic strain energy used for crack growth in a load cycle versus the crack growth rate.

When comparing both graphs, it can be noted that in the total energy used for FCG a stress ratio effect can be observed, and the cyclic energy used almost no stress ratio effect is present and the data almost falls on a single curve. Furthermore, it can be observed that no clear influence of the specimen with a different SCF is observed in the graphs.

Using equation 5.25, the FCG rate $\frac{dA}{dN}$ is plotted against $\frac{dU_{tot}}{dA}$ in figure 5.21 and $\frac{dU_{cyc}}{dA}$ in figure 5.22.

$$\frac{dU}{dN} = \frac{dU}{dA} \frac{dA}{dN} \tag{5.25}$$

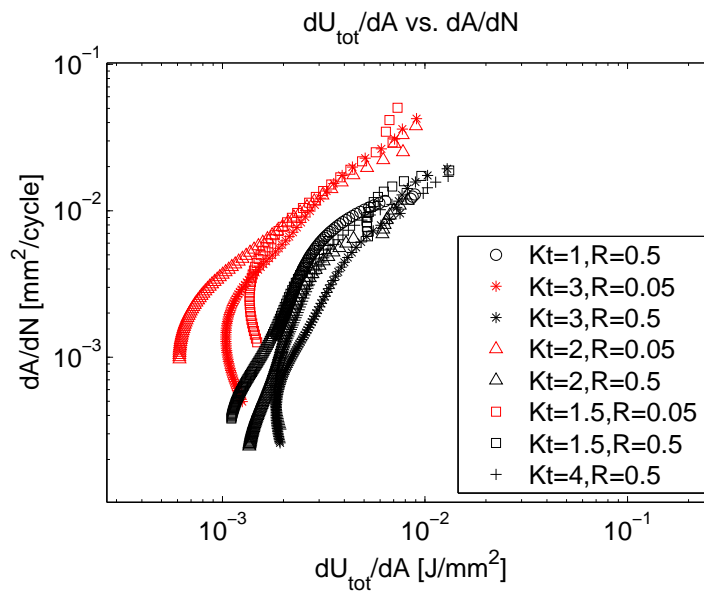


Figure 5.21: The total strain energy used for crack growth in a load cycle versus the crack growth rate.

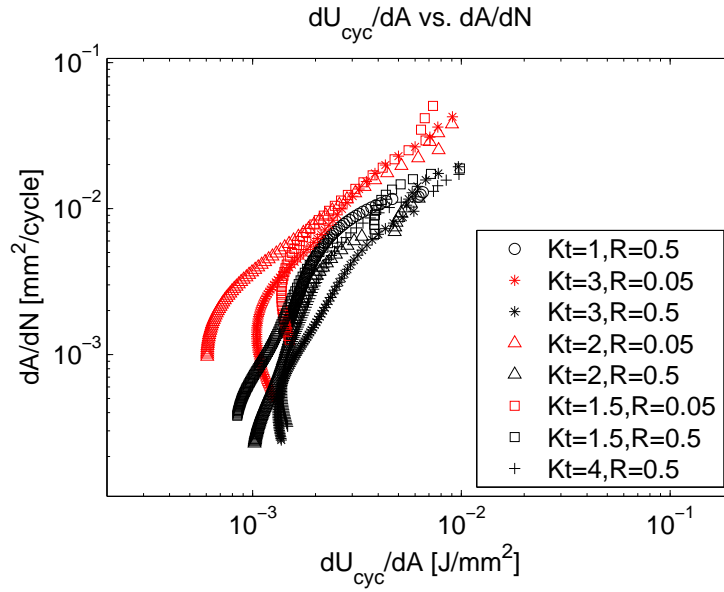


Figure 5.22: The total cyclic strain energy used for crack growth in a load cycle versus the crack growth rate.

Again it is noted that a larger effect of the stress ratio is present when comparing the total energy in figure 5.21 with the cyclic energy in figure 5.22. It seems that the cyclic energy used for FCG correlates better with the FCG rate than the total energy used. The same was observed in the pre-study using a Finite Element (FE) model and AFGROW in section 4.2.

For a FCG prediction model, knowledge about the correction parameter H as introduced in section 4.2 and as defined in equation 5.26 is a prerequisite. This parameter H as function of the (normalized) crack area can be derived from the test results using equation 5.27.

$$\frac{dU}{dA} = [U_{in}]_{A=0} H(A) \quad (5.26)$$

Or, rewritten to obtain H :

$$H(A) = \frac{\frac{dU}{dA}}{[U_{in}]_{A=0}} \quad (5.27)$$

Since $\frac{dU}{dA}$ is already known from experiments (see figure 5.21 and 5.22), only the term $[U_{in}]_{A=0}$ was needed to be able to derive H values from the experiments. Values for H could be calculated using the cyclic energy U_{cyc} or the total energy U_{tot} , which didn't make a difference in the values for H as long as one of both is consistently used for both terms $\frac{dU}{dA}$ and $[U_{in}]_{A=0}$ in equation 5.27.

The term $[U_{in}]_{A=0}$, is the (total or cyclic) energy input at zero crack area. This quantity was determined using the measured energy versus the corresponding crack area A . Since the specimens contained an initial crack, this quantity could not be directly measured during the experiments but was determined by extrapolating a fitted curve through the measured data. As example, the measured cracked area A versus the measured cyclic energy input U_{cyc} for specimen 2B40 and a fitted curve through the data is visualized in figure 5.23.

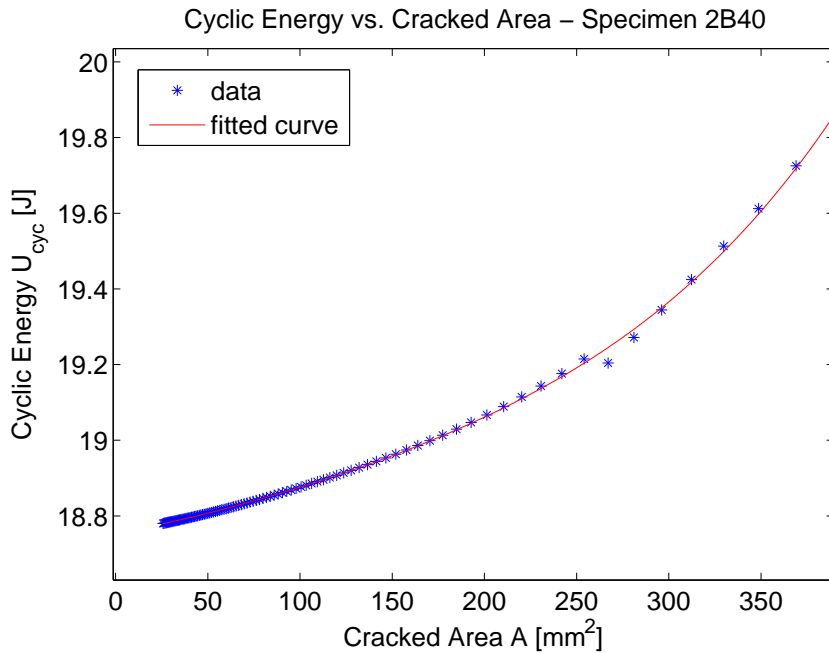


Figure 5.23: The cyclic strain energy input versus the crack area for specimen 2B40.

A fourth order polynomial equation was fitted through the data in figure 5.23 to find the cyclic energy input at zero crack area $[U_{cyc}]_{A=0}$. This was done for all specimens and was used to determine H values with equation 5.27. The derived H values as function of the *normalized* crack area for all the specimens is visualized in figure 5.24. The normalized crack area, Λ , is defined as the crack area A divided by the total cross-sectional area of the bar at the location of the crack with diameter D :

$$\Lambda = \frac{A}{\pi \left(\frac{D}{2}\right)^2} \tag{5.28}$$

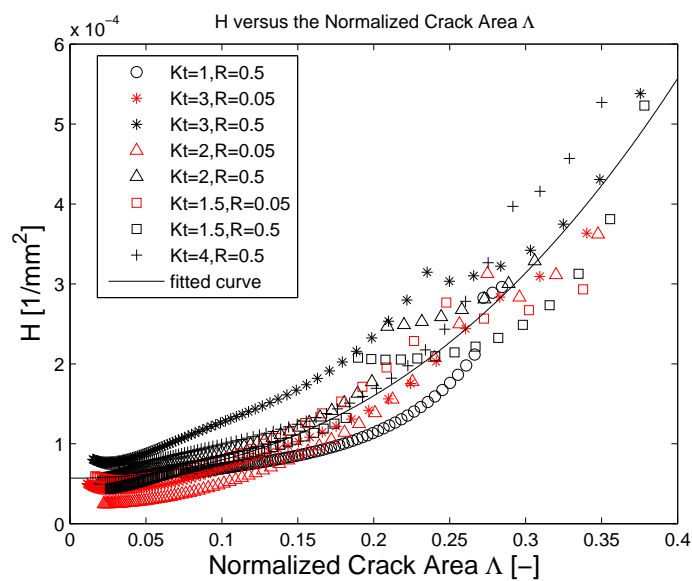


Figure 5.24: Experimental H versus normalized crack area Λ for all specimen with fitted curve.

As can be seen in figure 5.24, there is quite some scatter in H for the different specimen. The scatter is thought to be the same as observed in figure 5.22 for the different specimen and will be discussed in chapter 7. A third-order polynomial equation was fitted through all the data to obtain a single closed-form equation for the correction function H for all the specimens. The fitted equation 5.29 is visualized in figure 5.24 and the fit coefficients and goodness of the fitted equation is given in table 5.10.

$$H(\Lambda) = p_1\Lambda^3 + p_2\Lambda^2 + p_3\Lambda + p_4 \quad (5.29)$$

Table 5.10: Fit coefficients and goodness of the fit for equation 5.29.

Fitted equation	RMSE	R ²
Equation 5.29	2.5970E-05	0.8730
Coefficient	Value	95% Confidence Bounds
p_1	0.002645	0.005486 -0.000196
p_2	0.002086	0.00351 0.0006612
p_3	-7.277E-06	0.0001887 -0.0002033
p_4	5.691E-05	6.368e-05 5.013e-05

The closed-form equation for the correction function H as function of the normalized crack area Λ was now used to calculate $G_{avg,cyc}$ based on the energy density with equation 5.30. When $G_{avg,cyc}$ is plotted versus the FCG rate $\frac{dA}{dN}$, the graph in figure 5.25 is obtained.

$$G_{avg,cyc} = \frac{S_{max}^2}{2E} (1 - R^2) H(\Lambda) \quad (5.30)$$

In this equation S_{max} is the maximum applied stress, which was 100 MPa for all specimens, R the stress ratio, which is 0.5 or 0.05 for the different specimen, en E the Young's Modulus which is 71700 MPa for the material of the specimen, Aluminium 7075-T6511.

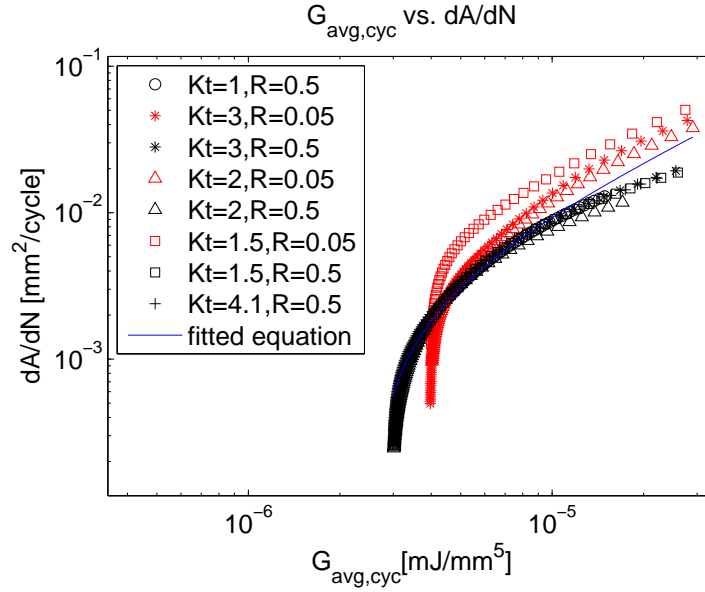


Figure 5.25: Crack growth rate versus the average cyclic energy release rate for all specimen.

It can be seen in figure 5.25 that there is still a stress ratio effect present; the data for the two tested stress ratios don't fall exactly on a single curve. This effect was also observed in the pre-study and it remains the question if the average cyclic energy release rate $G_{avg,cyc}$ as derived in this thesis is indeed a correct similarity parameter to predict FCG. To be able to develop a FCG prediction model with $G_{avg,cyc}$ as similarity parameter, a linear equation as defined in equation 5.31 is fitted through the data to obtain a closed-form and single relation between $G_{avg,cyc}$ and the crack growth rate $\frac{dA}{dN}$. The fitted equation 5.31 is visualized in figure 5.25 and the goodness of the fitted equation and the corresponding values for the coefficients F and K are given in table 5.11.

$$\frac{dA}{dN} = F + KG_{avg,cyc} \quad (5.31)$$

Table 5.11: Fit coefficients and goodness of the fit for equation 5.31.

Fitted equation	RMSE	R ²
Equation 5.31	0.0016	0.9022
Coefficient	Value	95% Confidence Bounds
F	-0.003144	-0.002935 -0.003352
K	1240	1272 1209

The closed-form relation between G_{avg} and $\frac{dA}{dN}$ as expressed in equation 5.31, and the closed-form equation for the correction function H as function of the normalized crack area Λ as expressed in equation 5.29 were the basis for a FCG prediction model based on the energy concept. The developed energy based FCG prediction model is discussed in section 6.2.

The Prediction of Fatigue Crack Growth

In this section, the developed prediction models for Fatigue Crack Growth (FCG) through a solid round metallic bar with a shoulder fillet is discussed. Based on the results of the experiments, a closed-form Stress Intensity Factor (SIF) solution was derived in chapter 5. This closed-form SIF solution was used in a FCG prediction model for solid round bars with a shoulder fillet and is discussed in section 6.1. Furthermore, an FCG prediction model for a solid round bar with a shoulder fillet with the average cyclic Strain Energy Release Rate (SERR) $G_{avg,cyc}$ as similarity parameter was developed and is discussed in section 6.2.

6.1 Stress intensity based FCG prediction model

The developed SIF solution and parameters C and m for the Paris-equation obtained in chapter 5 were used to develop a FCG prediction model for solid round metallic bars with a shoulder fillet. The model works according to the flowchart diagram in figure 6.1.

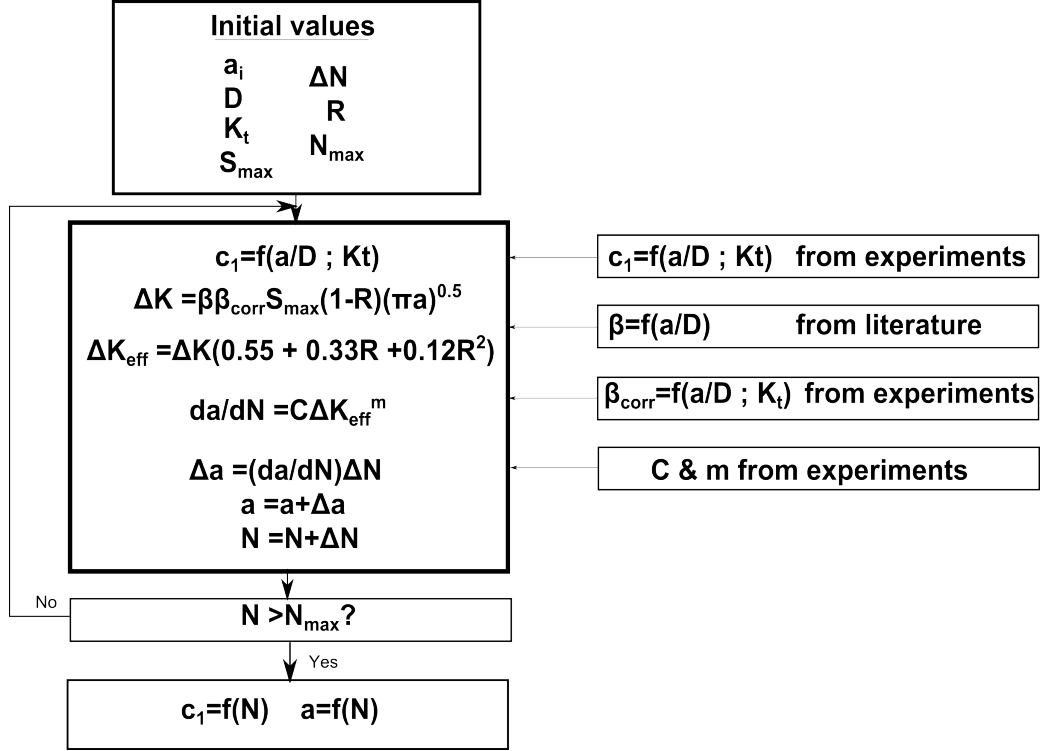


Figure 6.1: Flowchart of SIF based FCG prediction model which predicts the crack length a and crack shape c_1 as function of the number of applied load cycles N .

The initial values are loading parameters (of a Constant Amplitude (CA) tensional load spectrum), geometrical parameters and run parameters. The loading parameters are the maximum stress S_{max} acting away from the crack in the smallest diameter of the bar D_1 and the stress ratio R . The geometrical parameters are the diameter of the bar at the location of the crack D , the Stress Concentration Factor (SCF) K_t and the initial crack length a_i . The run parameters are the step size of the model ΔN , and the maximum applied number of cycles N_{max} after which the prediction is stopped.

The model uses iterative numerical integration to predict the crack length a and crack shape c_1 as function of the number of applied cycles N . The algorithm as visualized in figure 6.1 was implemented in a MATLAB code which gives as output a vector of crack lengths a , crack shapes c_1 for each number of cycle increment. Another output of the model is a graph of the crack length a and crack shape c_1 versus the number of applied load cycles N to visualize the FCG process.

6.2 Energy based prediction model

The experimentally derived correction function H , and the experimentally derived relation between the similarity parameter $G_{avg,cyc}$ and the FCG rate $\frac{dA}{dN}$ in chapter 5 were used to develop a FCG prediction model for solid round metallic bars with a shoulder fillet. The model works according to the flowchart diagram in figure 6.2.

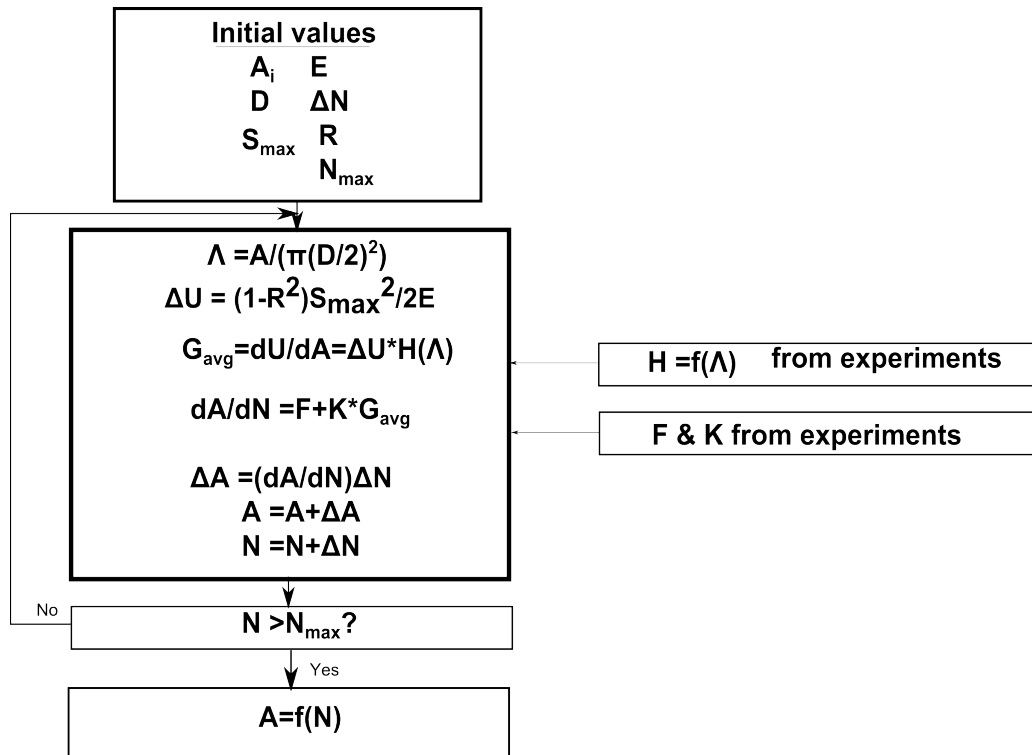


Figure 6.2: Flowchart of energy based prediction model which predicts the crack area A as function of the applied number of load cycles N .

The initial values are loading parameters (of a CA tensional load spectrum), geometrical parameters and run parameters. The loading parameters are the maximum stress S_{max} acting away from the crack in the smallest diameter of the bar D and the stress ratio R . The geometrical parameters are the diameter of the bar at the location of the crack D , the initial crack area A_i and the Young's Modulus of the material E . The run parameters are the step size of the model ΔN , and the maximum applied number of cycles N_{max} after which the prediction is stopped.

The model uses iterative numerical integration to predict the crack area A as function of the number of applied cycles N . The algorithm as visualized in figure 6.2 was implemented in a MATLAB code which gives as output a vector of crack areas A for each number of cycle increment. Another output of the model is a graph of the crack area A versus the number of applied load cycles N to visualize the FCG process.

6.3 Comparison Between Predictions and Experiments

In this section, it is compared how both models predict FCG compared with the some of the test results. This is not a validation of the models, since the models are based on the test result with which the predictions are compared, but the comparisons give can give an insight into the behaviour of the models.

It was chosen to compare how the models predict FCG with the test results of the specimen listed in table 6.1. Those specimen were chosen because they cover all the tested values of the SCF and stress ratio.

Table 6.1: Specimen of which the test results are compared with the prediction.

Specimen ID	Applied Maximum Stress S_{max} [MPa]	Applied Stress Ratio R [-]	SCF K_t [-]	Material Batch
2B116	100	0.5	1.5	B
1B40	100	0.05	2.0	B
1Z13	100	0.05	3.0	Z
2Z06	100	0.5	4.1	Z

How well the SIF based model and energy based model predict FCG compared to the test results is discussed in the next two sections.

6.3.1 Predictions with the stress intensity based model

For all the specimen listed in table 6.1, FCG is predicted using the model as described in section 6.1. How well the model predicts the crack length a and crack shape c_1 compared with the test results is shown in graphs.

Crack length predictions

The predictions of the crack length a are done with the SIF based FCG model as discussed in section 6.1. As observed in the graphs, the prediction of the crack length a for the specimens tested at a stress ratio of 0.5 (2B116 and 2Z06) are more accurate than for the specimens tested at a stress ratio of 0.05 (1B40 and 1Z13). This is caused by the scatter in the ΔK_{eff} versus $\frac{da}{dN}$ data: it can be observed that the FCG data of the specimen tested at 0.05 is consistently higher than the fitted curve (which results in the parameters C and m) which is used for the prediction.

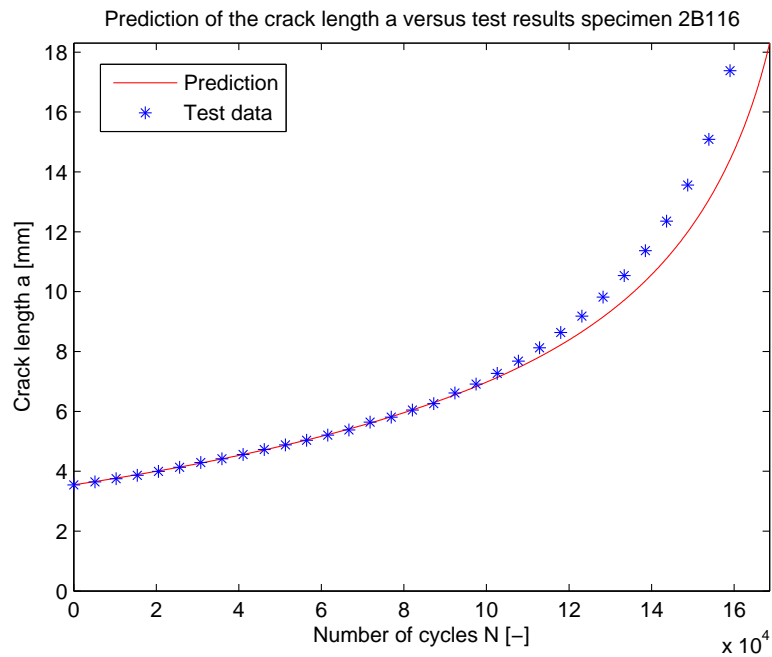


Figure 6.3: Prediction of the crack length a compared with the test result of specimen 2B116.

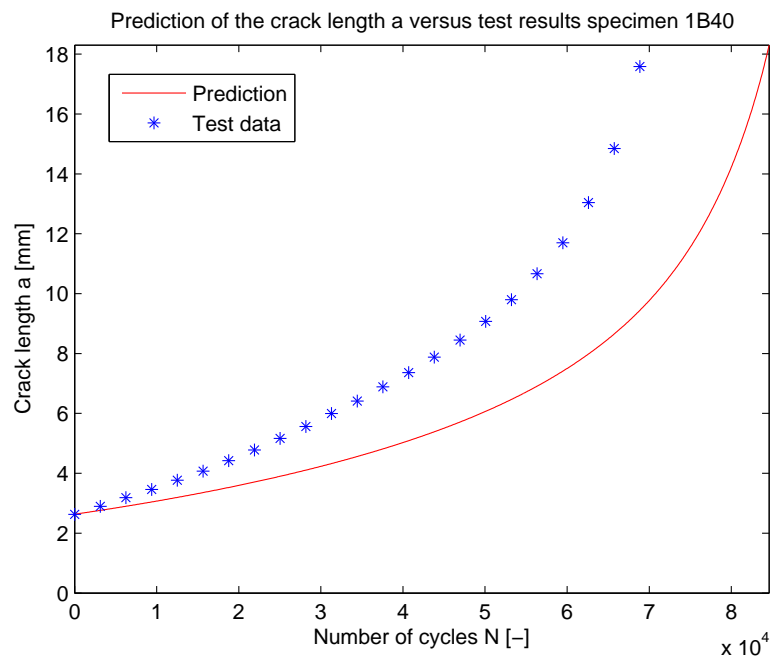


Figure 6.4: Prediction of the crack length a compared with the test result of specimen 1B40.

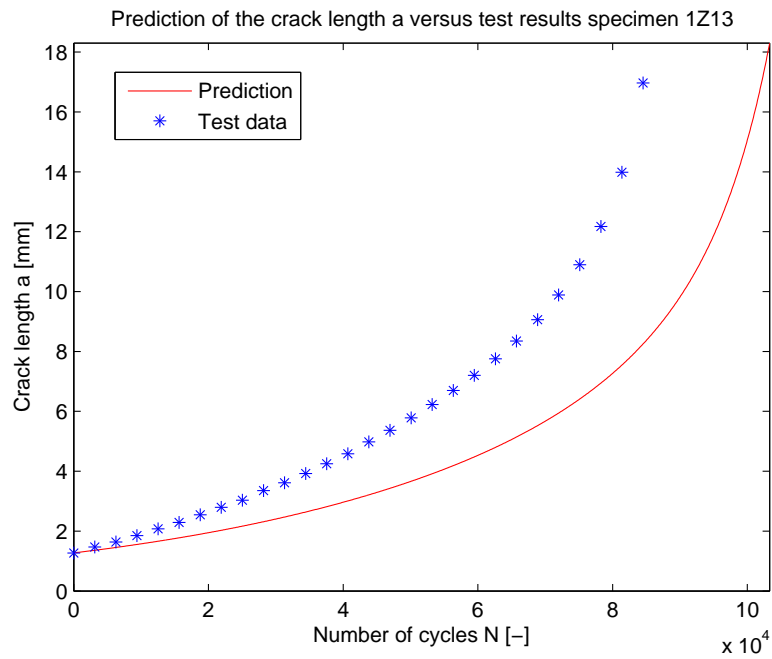


Figure 6.5: Prediction of the crack length a compared with the test result of specimen 1Z13.

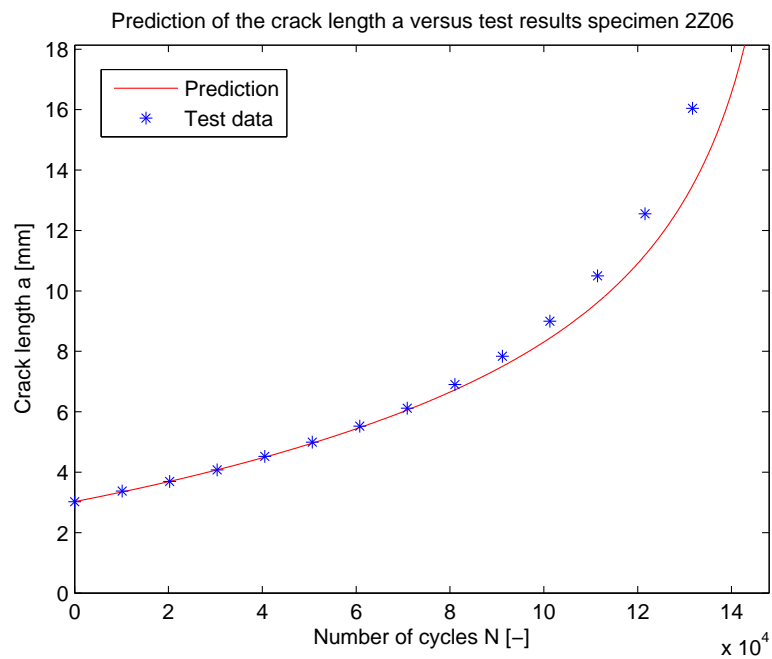


Figure 6.6: Prediction of the crack length a compared with the test result of specimen 2Z06.

Crack shape predictions

The prediction of the crack shape c_1 is quite accurate for the specimen tested at 0.5 as can be seen in the graphs in figure 6.7 and figure 6.10. Only at higher crack lengths, a steep increase in c_1 is observed in the prediction which is not present in the test results. The order of the fitted equation (4th) which is used to obtain a closed-form equation for c_1 could be the explanation for this behaviour; a lower order might improve the shape predictions. The comparison with the specimens tested at the stress ratio of 0.05 (1B40 and 1Z13) are quite inaccurate. Since the experimentally derived closed-form equation for c_1 is only based on the test results of the specimen tested at 0.5, there might be an influence of the stress ratio on how the crack shape c_1 which is not taken into account currently.

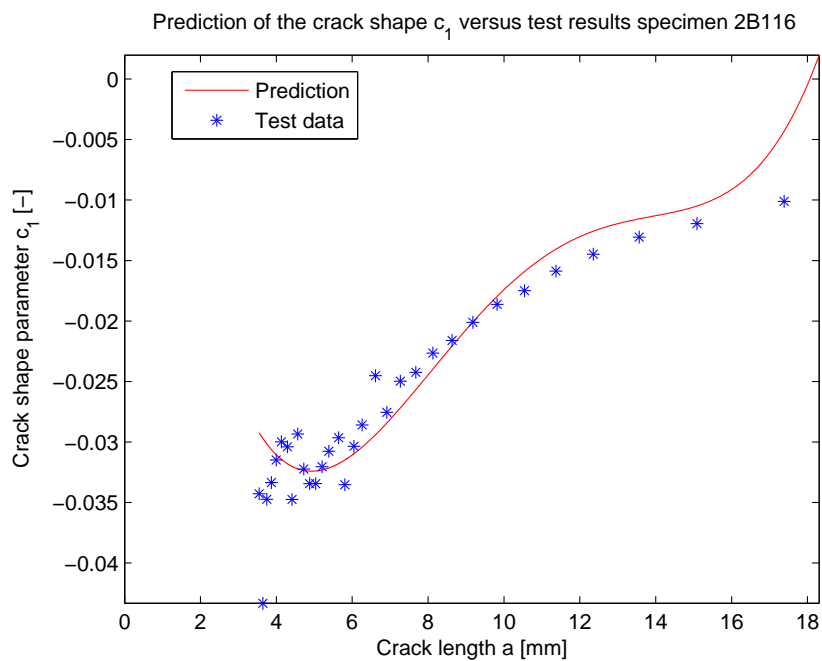


Figure 6.7: Prediction of the crack shape c_1 compared with the test result of specimen 2B116.

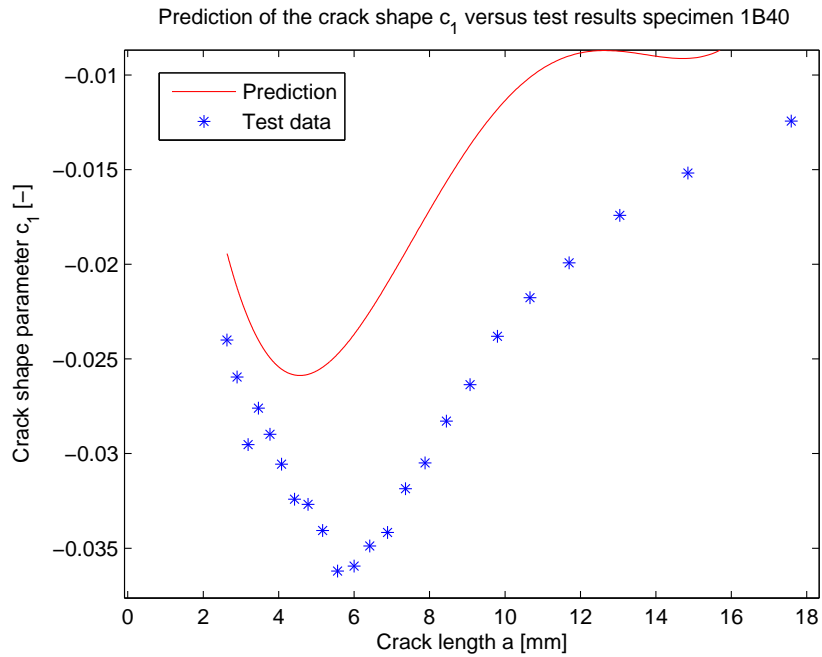


Figure 6.8: Prediction of the crack shape c_1 compared with the test result of specimen 1B40.

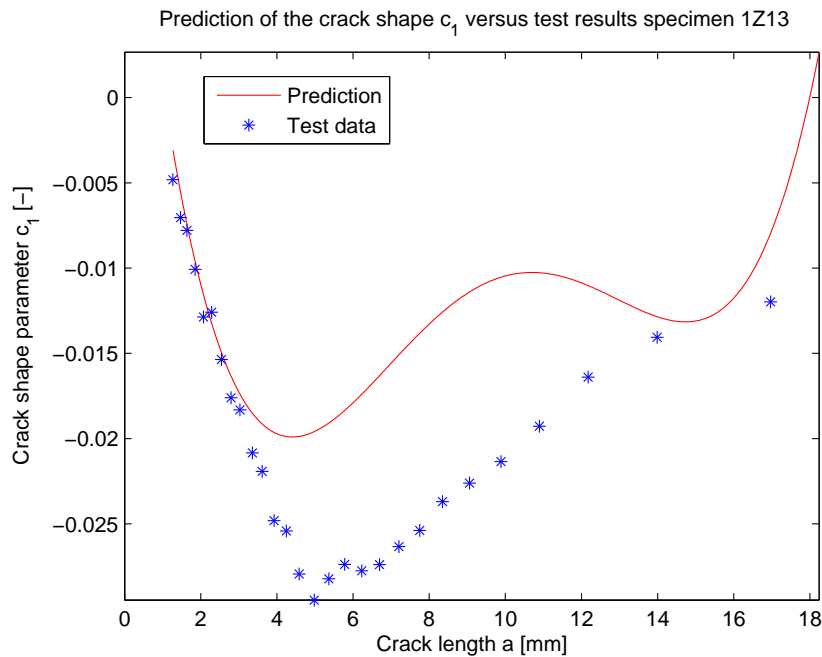


Figure 6.9: Prediction of the crack shape c_1 compared with the test result of specimen 1Z13.

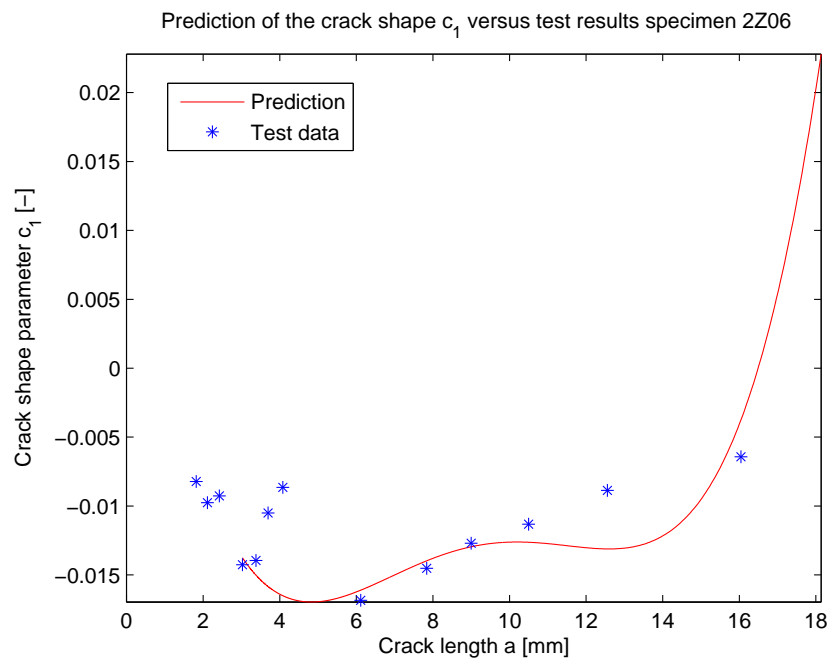


Figure 6.10: Prediction of the crack shape c_1 compared with the test result of specimen 2Z06.

6.3.2 Predictions with the energy based model

For all the specimen listed in table 6.1, FCG is predicted using the model as described in section 6.2. How well the model predicts the crack area A compared with the test results is shown in the graphs in this section.

As can be observed in the graphs in this section, the prediction of the crack area A based on the energy method is quite accurate for all specimens.

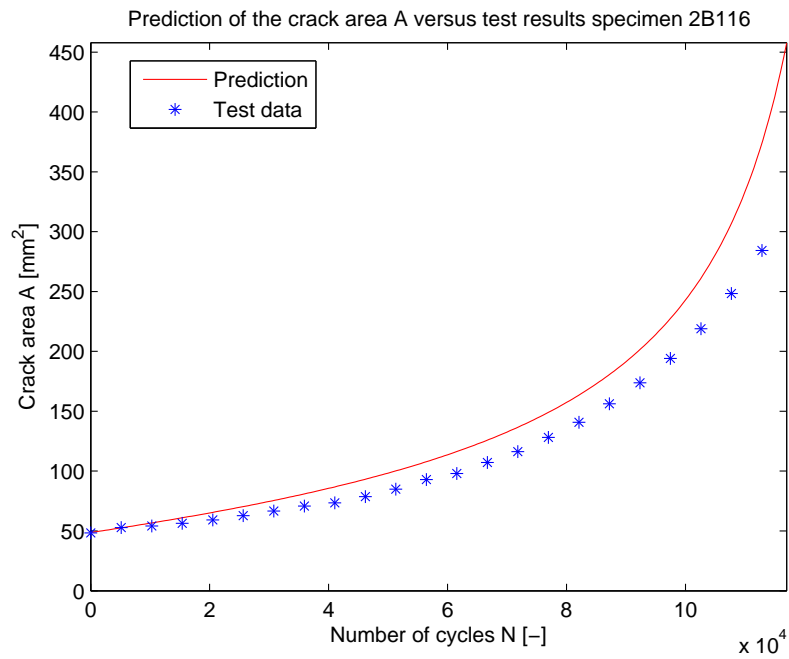


Figure 6.11: Prediction of the crack area A compared with the test result of specimen 2B116.

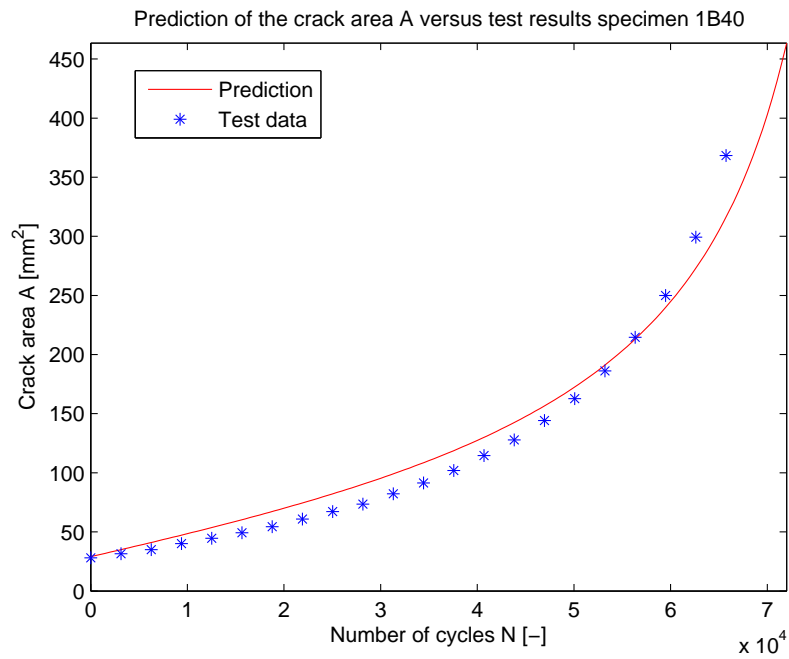


Figure 6.12: Prediction of the crack area A compared with the test result of specimen 1B40.

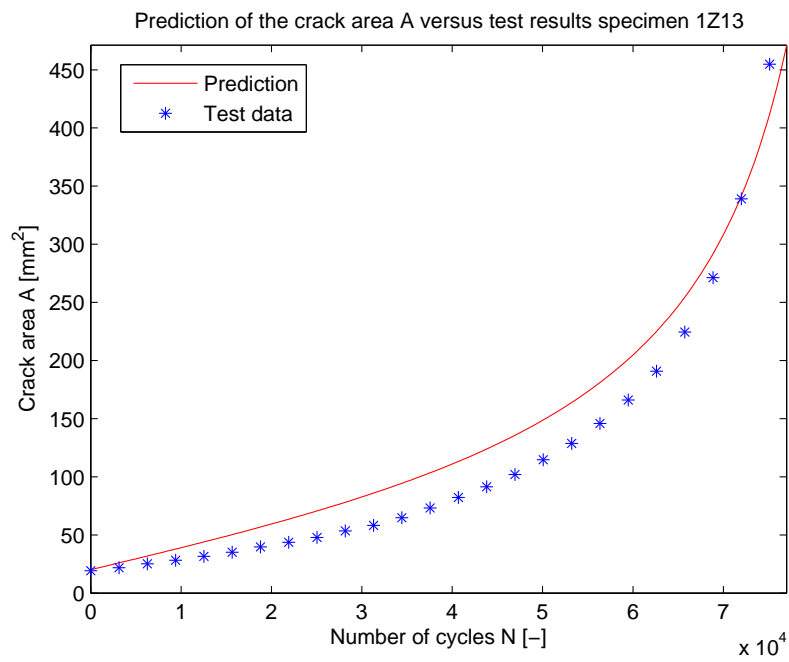


Figure 6.13: Prediction of the crack area A compared with the test result of specimen 1Z13.

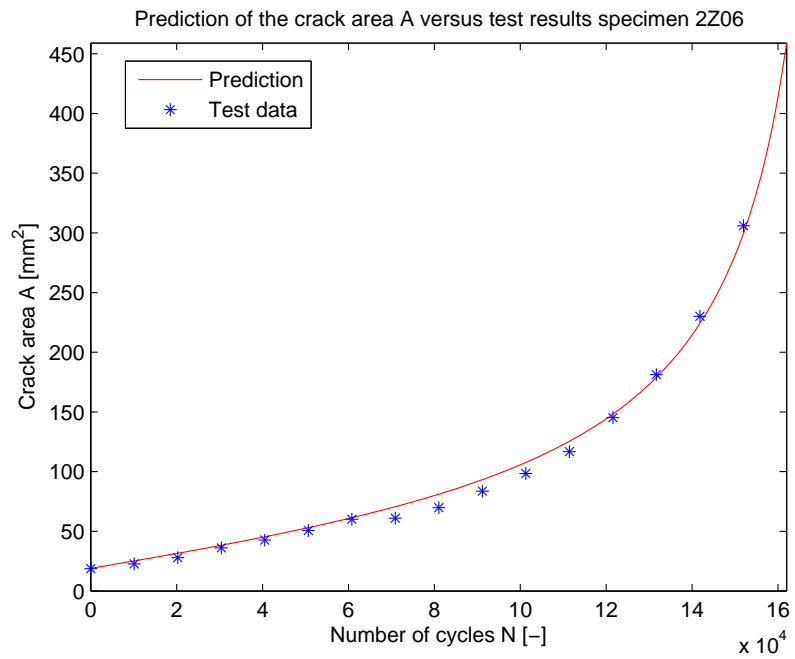


Figure 6.14: Prediction of the crack area A compared with the test result of specimen 2Z06.

Chapter 7

Discussion

In this section, the results of the research project are discussed. The research approached the problem of Fatigue Crack Growth (FCG) through a solid round bar with a shoulder fillet from two different point of views: the conventional stress intensity approach and an energy approach. For the energy approach, a prediction methodology was proposed with the average cyclic Strain Energy Release Rate (SERR) $G_{avg,cyc}$ as similarity parameter. For both point of views, a FCG prediction model for solid round bars with a shoulder fillet loaded in tension was developed. The results of the stress intensity approach are discussed in section 7.1, the results of the energy approach in section 7.2 and the results of the research in general are discussed in section 7.3.

7.1 Stress intensity approach

For the stress intensity approach, an experimental technique was used to determine Stress Intensity Factor (SIF) values for solid round bars with a shoulder fillet using *baseline* FCG data. The *baseline* FCG data was obtained with FCG experiments on straight solid round bars without shoulder fillet, of which a SIF solution was available from literature. A closed-form SIF solution for solid round bars with a shoulder fillet was obtained by fitting a two-parameter equation through the experimentally determined SIF values. The derived closed-form SIF solution for solid round bars with a shoulder fillet under tension loading was expressed as values of an extra correction factor β_{corr} for the presence of the shoulder fillet. The developed FCG model based on the stress intensity approach can predict FCG for different values of the Stress Concentration Factor (SCF) caused by the presence of the shoulder fillet. When comparing the FCG predictions done with the developed model with the test results, it predicts FCG quite well for the specimens tested at a stress ratio of 0.5; it predicts less accurate for the specimens tested at a stress ratio of 0.05. That the developed model predicts FCG less accurate at a stress ratio of 0.05 is attributed to the scatter that is present between the FCG rate $\frac{da}{dN}$ and effective SIF range ΔK_{eff} for the two tested stress ratios. A point of discussion that deserves attention for the results of this stress intensity approach is:

- **Fitted equations for the crack shape c_1 and correction factor β_{corr}**

To be able to predict FCG at all in-between values of the tested SCF and normalized

crack depth λ , a two-parameter equation was fitted through the test data. For both the correction factor β_{corr} and shape of the crack front c_1 a two-parameter equation, where the parameters were the SCF and the normalized crack depth λ , was fitted through the test data. Both equations were 4th order equations for both parameters. This order of fitting was chosen because it resulted in a reasonable fit for both β_{corr} and c_1 through the test data. It has to be noted that the 4th order of the fitted equation for c_1 might be not appropriate since the fitted equation shows a upwards curvature for higher normalized crack lengths λ which is not in agreement with the measured data. In general it should be investigated if the fourth-order fitted equations through the test data for c_1 and β_{corr} give reasonable results when comparing the predictions with more test results, which is necessary for validation. It could also be interesting to investigate if other fitted equations (of a lower order) through the test data of β_{corr} and c_1 give very different prediction results.

7.2 Energy approach

For the energy approach, a prediction methodology was proposed where the average cyclic SERR $G_{avg,cyc}$ is used as *similarity* parameter. This similarity parameter was proposed after the observation that the cyclic energy used for FCG during a complete load cycle correlates strongly with the FCG rate $\frac{dA}{dN}$. It was observed that the stress ratio R still had some influence on this correlation, but that effect was neglected in the developed FCG model. When comparing the FCG predictions done with the developed model with the test results, the model can predict FCG quite well independently of the applied stress ratio R or SCF.

To be able to use the similarity found between $G_{avg,cyc}$ and the crack growth rate $\frac{dA}{dN}$ in the prediction of FCG, it was necessary to be able to calculate $G_{avg,cyc}$ given the loading condition and geometry of the crack problem. To be able to calculate $G_{avg,cyc}$ on beforehand, it was expressed as written in equation 7.1.

$$G_{avg,cyc} = \frac{S_{max}^2}{2E} (1 - R^2) H(\Lambda) \quad (7.1)$$

In the above equation, $\frac{S_{max}^2}{2E} (1 - R^2)$ calculates the remotely applied cyclic strain energy density; the correction equation H takes the geometry of the crack problem into account and is only dependent on the normalized crack area Λ . To be able to do FCG predictions, knowledge about the correction factor H for the specific crack problem is a prerequisite. Some points of discussion that deserves attention based on this energy approach are:

- **Scatter in experimentally determined correction factor H .**

There is some significant scatter in the derived correction factor H values for the different specimen as can be seen in figure 7.1. An important source of scatter in the correction factor H values, is the scatter in the measured energy data which introduced uncertainty in the fitted curves through the energy data. There might also be other sources of scatter such as different clamping lengths or that the axial location of the initial crack was different for the different specimen. For now, an equation was fitted through all the data to obtain a single closed-form equation for the correction equation H as function of the normalized crack area Λ . The derived closed-form equation for the correction

factor H worked quite well in the prediction model, but the sources of scatter should be further investigated.

- **Difference in H determined experimentally and with the Finite Element (FE) model.**

In figure 7.1 the experimentally determined values for the correction factor H are plotted together with the values for H determined with the FE model in section 4.2.

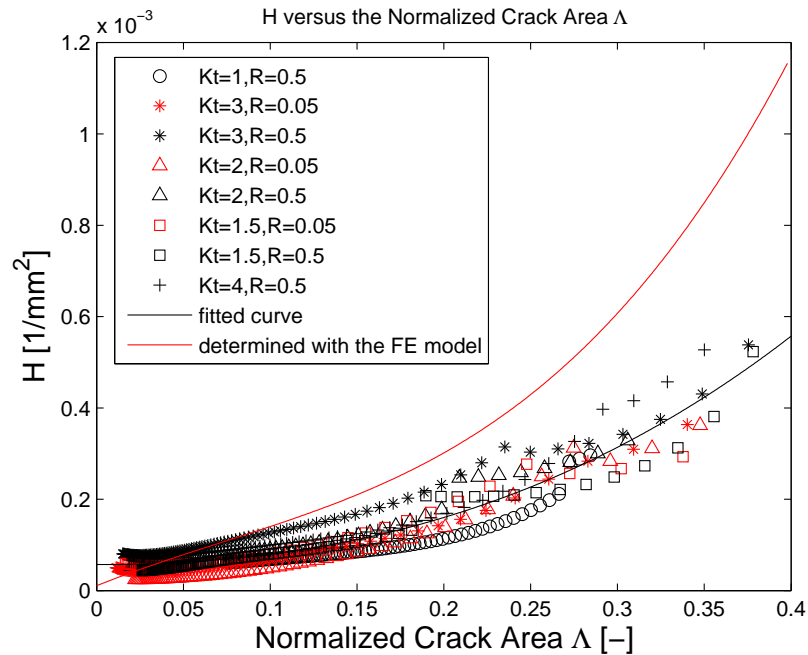


Figure 7.1: Experimental H values and H values determined with the FE model versus the normalized crack area Δ .

It can be seen that the values for H determined with the FE model are in general higher for larger (normalized) crack areas. This is attributed to the fact that in the FE model, the end of the bar was not clamped and free to rotate because of the growing crack. The larger the (normalized) crack area becomes, the larger the discrepancy between the two becomes. This is attributed to the fact that the larger the crack area becomes, the more the bar is constraint against rotation because of the clamped ends in the experiments which is not the case in the FE model. The influence of the clamped ends during the FCG experiments is also shortly discussed in section 7.3.

7.3 General research approach

Since the problem of FCG through a solid round bar with a shoulder fillet was approached from two different point of views, but the results were obtained from the exact same experiments, there are some points of discussion that deserves attention for the research approach in general:

- **The influence of the initial crack shape.**

The influence of the initial crack shape is not taken into account in the development of the SIF solution. If the initial crack had a different shape, and not straight as in

this research, this could have led to different values of the **SIF**. Also, it should be investigated if a different initial crack shape has influence on the energy method and in particular on the correction function H .

- **Prediction of the crack shape in general.**

In both approaches, the prediction of the crack length a or crack area A is done with the assumption that the crack shape develops during the **FCG** process as observed in the experiments. Both developed prediction models are not able to take different crack shapes into account; they are unable to predict how the crack shape would develop in the case of a different initial crack length or crack shape.

- **The influence of clamped ends during the **FCG** experiments of the specimen.**

That the ends of the specimen were clamped during the experiments may have a significant effect on the absolute values of the **SIF** solution. Because of the clamped ends of the bar, rotation was constrained which would not occur in the case of free ends. For the energy approach, this could explain the large difference between the H values derived with the **FE** model and experiments. It remains a question if the clamped ends have influence on the derived correction factor β_{corr} for the **SIF** approach since both the specimen to obtain *baseline* **FCG** data and the specimens with a shoulder fillet had clamped ends in the **FCG** experiments.

- **Stress ratio effect still present in both approaches.**

For both the stress intensity approach as the energy approach there is still a stress ratio effect present using their corresponding similarity parameter:

There is an effect of the stress ratio observed in the **SIF** approach when using the *effective* **SIF** range ΔK_{eff} as similarity parameter as can be seen in figure 7.2.

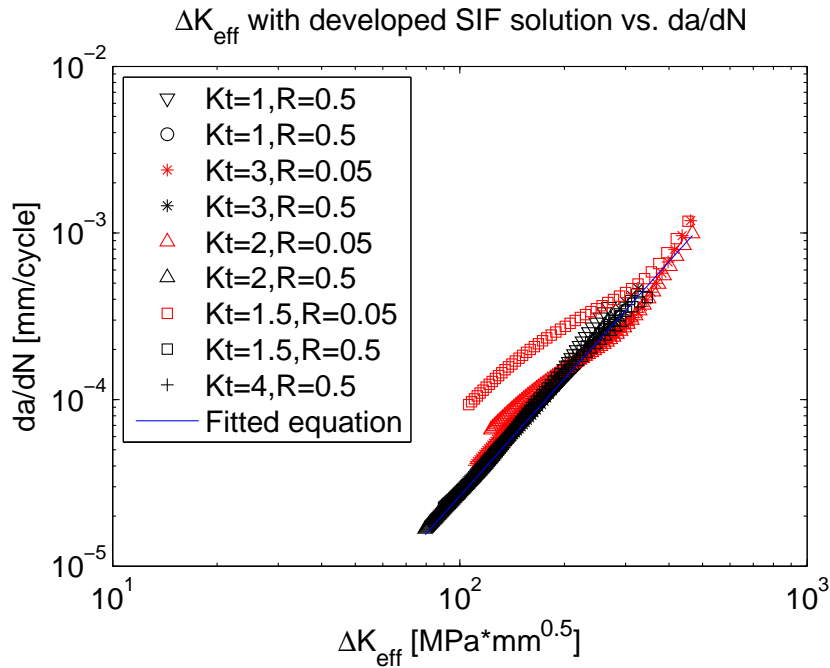


Figure 7.2: All the **FCG** test data plotted with the effective **SIF** range ΔK_{eff} as similarity parameter.

There is also a stress ratio effect observed in the energy approach when using the average cyclic **SERR** as similarity parameter as can be seen in figure 7.3.

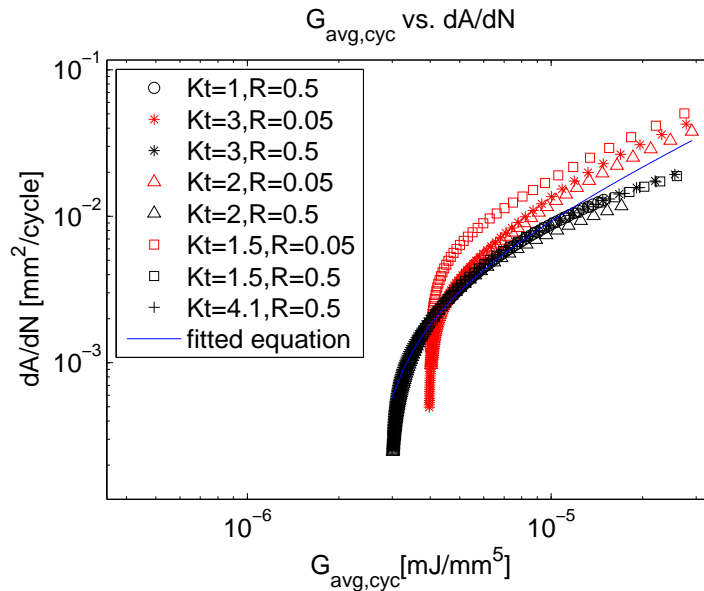


Figure 7.3: Crack growth rate versus the average cyclic energy release rate for all specimen.

Especially in the **FCG** prediction model based on the **SIF** approach, the scatter has significant influence on the **FCG** predictions at an applied stress ratio of 0.05 as was showed in chapter 6.

- **Both the **SIF** solution and energy methodology are not validated.**

The developed **SIF** solution to take the effect of the shoulder fillet into account is not validated. It should be validated using more test data on different types of solid round bars with shoulder fillets under different types of loading conditions. Also, the developed energy methodology should be validated with **FCG** experiments in general.

Both developed models were able to predict **FCG** through solid round bars with a shoulder fillet under Constant Amplitude (**CA**) tension loading. The **SIF** approach needed a correction equation for the applied stress ratio R to correct the ΔK values to ΔK_{eff} values to be able to do **FCG** predictions at different stress ratios. The energy approach uses the average cyclic **SERR** as similarity parameter, only a small influence of the stress ratio was observed. It is believed that ΔK only is not able to uniquely describe the applied load cycle and that the stress ratio effect which is observed in this approach is a reflection of this inadequacy. From an academical point of view, I would recommend to further investigate the energy approach since it is able to describe the applied load cycle uniquely, which is not the case in the conventional stress intensity approach. From an engineering point of view, I would recommend Atkins, and engineering practice in general, to implement the correction factor β_{corr} in **FCG** prediction software that is used to account for the presence of a shoulder fillet since the stress intensity methodology is accepted current practice. More research is required to the energy approach to validate that the average cyclic **SERR** is indeed a correct similarity parameter for the prediction of **FCG**.

If a different type of structure than a solid round bar with a shoulder fillet would be considered, both approaches could be used for the prediction of FCG by adjusting the prediction models. For the SIF prediction model, a SIF solution for the specific crack problem should be determined to be able to do FCG predictions. For the energy prediction model, the correction factor H for that specific crack problem should be determined to be able to do FCG predictions. It should be further investigated if the correction factor H is more generic than the SIF solutions used in the stress intensity approach.

Conclusions and Recommendations

In this chapter, the conclusions of the research project are presented. Furthermore, recommendations for further research are given.

8.1 Conclusions

The conclusions of this research project are given in this section.

- The marker load spectrum used in this research project was successfully applied to reconstruct crack fronts. Marker bands became visible because of the applied marker load spectrum and could be detected using an Optical Microscope (OM) rather than with a Scanning Electron Microscope (SEM), which saves a lot of time when reconstructing the fracture surface.
- The influence of a shoulder fillet on the Fatigue Crack Growth (FCG) behaviour under tension loading is significant, especially for small (normalized) crack lengths. When the resulting Stress Concentration Factor (SCF) of the shoulder fillet is higher, the influence becomes larger and the fatigue crack will grow faster.
- Shoulder fillets have a significant effect on how the fatigue crack shape develops through the solid round bar. The higher the resulting SCF, the sooner and more 'straight' the fatigue crack becomes when growing.
- Based on the test results, the influence of a shoulder fillet on the FCG rate could be quantified by the developed closed-form Stress Intensity Factor (SIF) solution. This closed-form SIF solution was used in the developed FCG prediction model.
- The developed SIF based prediction model can successfully predict FCG through a solid round bar with a shoulder fillet under Constant Amplitude (CA) tension loading using the developed SIF solution when comparing it with the test results tested at a stress ratio of 0.5.

- The influence of the stress ratio R in the **SIF** based model on the **FCG** behaviour was not well captured by the used correction equation: **FCG** was consistently under-predicted at a stress ratio of 0.05 when compared with the test results.
- The **FCG** rate $\frac{dA}{dN}$ correlates better with the cyclic energy used during that complete cycle $\frac{dU_{cyc}}{dN}$ than the total energy used during that complete cycle $\frac{dU_{tot}}{dN}$.
- Although there was still some influence of the stress ratio observed, the average cyclic Strain Energy Release Rate (**SERR**) $G_{avg,cyc}$ was successfully used as similarity parameter for the prediction of **FCG**.
- The energy based **FCG** model can successfully predict the crack area A as function of the number of applied load cycles N when comparing it with the test results at both stress ratios and different values of the **SCF**.
- The **SCF** seems to have no effect on the energy approach: the crack area A can be predicted independently of the **SCF**.

8.2 Recommendations

In this section, recommendations are given for further research.

- To be able to validate the developed **SIF** solution, it is recommended to do multiple **FCG** experiments on solid round bars shoulder fillets causing different values of the **SCF**, different sizes (different diameters $D1$ and $D2$), and different load spectra. By comparing the test results with the predictions done with the developed **SIF** solution, the **SIF** solution can be validated.
- It is recommended to do more fundamental research to the energy approach. There is still a, not desired, stress ratio effect present when using the proposed similarity parameter $G_{avg,cyc}$.
- The effect of plasticity induced crack closure is currently not taken into account in the energy based approach. It is recommended to do further research on how to take this phenomenon into account.
- This research was limited to investigate tensional, constant amplitude fatigue loads. It would be of practical interest to investigate the effect of variable amplitude loading and different types of (combined) loading (e.g. bending and/or torsion).
- It is recommended to investigate the effect of the clamped ends of the tested specimens on the **FCG** rate. In real engineering structures clamped conditions at the ends may not apply.

References

- [1] J. Schijve, *Fatigue of Structures and Materials*. Springer, 2nd ed., 2009.
- [2] G. Irwin, “Analysis of stresses and strains near end of crack traversing plate,” *Journal of Applied Mechanics*, vol. 24, pp. 361–364, 1957.
- [3] P. Paris, M. Gomez, and W. Anderson, “A rational analytical theory of fatigue,” *The Trend of Engineering*, vol. 13, p. 914, 1961.
- [4] P. Paris and F. Erdogan, “A cirical analysis of crack propagation laws,” *Trans. ASME, Series D*, vol. 85, pp. 528–535, 1963.
- [5] H. Tada, P. Paris, and G. Irwin, *The Stress Analysis of Cracks Handbook*. New York: ASME, 3rd ed., 2000.
- [6] X. Huang and T. Moan, “Improved modeling of the effect of R-ratio on crack growth rate,” *International Journal of Fatigue*, vol. 29, pp. 591–602, Apr. 2007.
- [7] W. Elber, “The significance of fatigue crack closure. Damage tolerance in aircraft structures.,” *ASTM STP 486*, pp. 230–242, 1971.
- [8] S. Zhang, R. Marissen, K. Schulte, K. Trautmann, H. Nowack, and J. Schijve, “Crack Propagation Studies on Al7475 on the Basis of Constant Amplitude and Selective Variable Amplitude Loading Histories,” *Fatigue & Fracture of Engineering Materials & Structures*, vol. 10, no. 4, pp. 315–332, 1987.
- [9] J. Toribio, N. Álvarez, B. González, and J. Matos, “A critical review of stress intensity factor solutions for surface cracks in round bars subjected to tension loading,” *Engineering Failure Analysis*, vol. 16, pp. 794–809, Apr. 2009.
- [10] R. Forman and V. Shivakumar, “Growth Behavior of Surface Cracks in the Circumferential Plane of Solid and Hollow Cylinder,” in *Fracture Mechanics: Seventeenth Volume, ASTM STP 905* (J. H. Underwood, R. Chait, C. Smith, D. Wilhem, W. Andrews, and J. Newman, eds.), (Philadelphia), pp. 59–74, American Society for Testing and Materials, 1986.

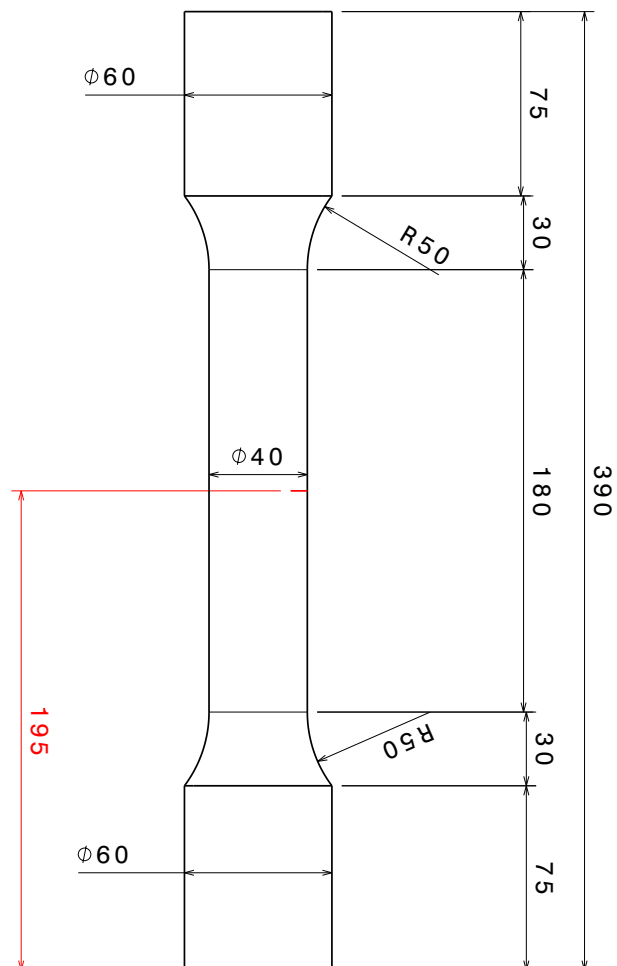
- [11] A. Carpinteri, "Shape change of surface cracks in round bars under cyclic axial loading," *International Journal of Fatigue*, vol. 15, pp. 21–26, Jan. 1993.
- [12] C. Shin and C. Cai, "Experimental and finite element analyses on stress intensity factors of an elliptical surface crack in a circular shaft under tension and bending," *International Journal of Fracture*, vol. 129, pp. 239–264, Oct. 2004.
- [13] I. Raju and J. Newman, "Stress-intensity factors for a wide range of semi-elliptical surface cracks in finite-thickness plates," *Engineering Fracture Mechanics*, vol. 11, pp. 817–829, 1979.
- [14] C. Shin, "The stress intensity of corner cracks emanating from holes," *Engineering Fracture Mechanics*, vol. 37, pp. 423–436, Jan. 1990.
- [15] L. James and W. Anderson, "A simple experimental procedure for stress intensity factor calibration.," *Engineering Fracture Mechanics*, vol. 1, no. 3, pp. 565–568, 1969.
- [16] J. Schijve, "Comparison between empirical and calculated stress intensity factors of hole edge cracks," *Engineering Fracture Mechanics*, vol. 22, pp. 49–58, Jan. 1985.
- [17] D. Child, N. Moyle, and A. Grandt, "Experimental Validation of Stress Intensity Factor Solutions for the Pin Loaded Lug," in *ICAF 2009, Bridging the Gap between Theory and Operational Practice* (M. Bos, ed.), no. May, (Rotterdam, the Netherlands), pp. 871–898, Springer Science, 2009.
- [18] D. Wilhem, J. FritzGerald, J. Carter, and D. Dittmer, "An Emperical Approach To Determining K For Surface Cracks," in *Advances in Fracture Research*, pp. 11–21, 1981.
- [19] R. Piascik and S. Willard, "The characteristics of fatigue damage in fuselage riveted lap splice joint.," tech. rep., NASA, 1997.
- [20] I. S. Putra and J. Schijve, "Crack Opening Stress Measurements of Surface Cracks in 7075-T6 Aluminium Alloy Plate Specimen Through Electron Fractography," *Fatigue & Fracture of Engineering Materials and Structures*, vol. 15, pp. 323–338, Apr. 1992.
- [21] J. Schijve, "Application of Marker Loads for Fractography of Fatigue Cracks," in *11th International Fatigue Congress*, (Melbourne, Australia), 2014.
- [22] J. Toribio, J. Matos, B. González, and J. Escuadra, "Numerical modelling of cracking path in round bars subjected to cyclic tension and bending," *International Journal of Fatigue*, vol. 58, pp. 20–27, Jan. 2014.
- [23] X. Lin and R. Smith, "Shape growth simulation of surface cracks in tension fatigued round bars," *International Journal of Fatigue*, vol. 19, pp. 461–469, Aug. 1997.
- [24] X. B. Lin and R. A. Smith, "An Improved Numerical Technique for Simulating the Growth of Planar Fatigue Cracks," *Fatigue & Fracture of Engineering Materials & Structures*, vol. 20, pp. 1363–1373, Oct. 1997.
- [25] X. B. Lin and R. a. Smith, "Numerical Prediction of Fatigue Crack Growth of a Surface Defect," *Fatigue & Fracture of Engineering Materials and Structures*, vol. 18, pp. 247–256, Feb. 1995.

-
- [26] W. Guo, H. Shen, and H. Li, "Stress intensity factors for elliptical surface cracks in round bars with different stress concentration coefficient," *International Journal of Fatigue*, vol. 25, pp. 733–741, Aug. 2003.
- [27] X. Lin and R. Smith, "Shape evolution of surface cracks in fatigued round bars with a semicircular circumferential notch," *International Journal of Fatigue*, vol. 21, pp. 965–973, 1999.
- [28] M. Caspers, C. Mattheck, and D. Munz, "Propagation of surface cracks in notched and unnotched rods.," in *Surface-crack growth: models, experiments, and structures, ASTM, STP1060* (W. Reuter, J. Underwood, and J. Newman Jr., eds.), (Philadelphia), pp. 365–389, American Society for Testing and Materials, 1990.
- [29] X. Lin and R. Smith, "Fatigue Growth Simulation For Cracks in Notched and Unnotched Round Bars," *International Journal of Mechanical Sciences*, vol. 40, no. 5, pp. 405–419, 1998.
- [30] F. Brennan and W. Dover, "Stress Intensity Factors for Threaded Connections," *Engineering Fracture Mechanics*, vol. 50, no. 4, pp. 545–567, 1995.
- [31] L. James and W. Mills, "Review and synthesis of stress intensity factor solutions applicable to cracks in bolts," *Engineering Fracture Mechanics*, vol. 30, no. 5, pp. 641–654, 1988.
- [32] A. Carpinteri and S. Vantadori, "Sickle-shaped surface crack in a notched round bar under cyclic tension and bending," *Fatigue & Fracture of Engineering Materials & Structures*, vol. 32, pp. 223–232, Mar. 2009.
- [33] A. Carpinteri, R. Brighenti, and S. Vantadori, "Surface cracks in notched round bars under cyclic tension and bending," *International Journal of Fatigue*, vol. 28, pp. 251–260, Mar. 2006.
- [34] E. Hjfeldt and C. Ostervigt, "Fatigue Crack Propagation In Shafts With Shoulder Fillets," *Engineering Fracture Mechanics*, vol. 25, no. 4, pp. 421–427, 1986.
- [35] K. Thompson and S. Sheppard, "Fatigue crack growth in notched and plain shafts subjected to torsion and axial loading," *Engineering Fracture Mechanics*, vol. 43, no. 1, pp. 55–71, 1992.
- [36] K. Thompson and S. Sheppard, "Stress intensity factors in shafts subjected to torsion and axial loading," *Engineering Fracture Mechanics*, vol. 42, no. 6, pp. 1019–1034, 1992.
- [37] R. C. Alderliesten, "The Explanation of Stress Ratio Effect and Crack Opening Corrections for Fatigue Crack Growth in Metallic Materials," *Advanced Materials Research*, vol. 891–892, pp. 289–294, Mar. 2014.
- [38] J. Pascoe, R. Alderliesten, and R. Benedictus, "Towards Understanding Fatigue Disbond Growth via Cyclic Strain Energy," *Procedia Materials Science*, vol. 3, pp. 610–615, 2014.
- [39] S. M. Tipton, J. R. Sorem, and R. Rolovic, "Updated stress concentration factors for filleted shafts in bending and tension," *Journal of Mechanical Design*, vol. 118, no. 3, pp. 321–327, 1996.

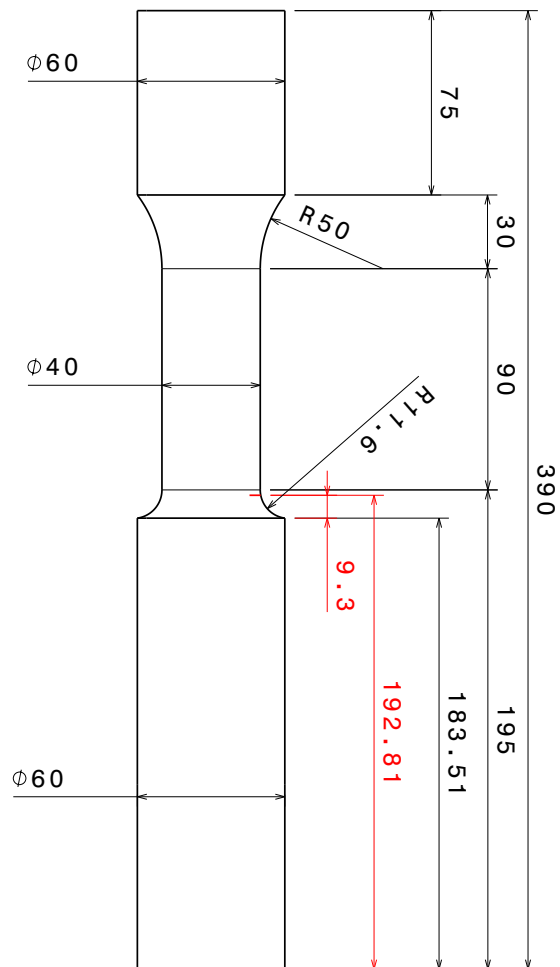
- [40] J. Schijve, "Some formulas for the crack opening stress level," *Engineering Fracture Mechanics*, vol. 14, pp. 461–465, 1981.

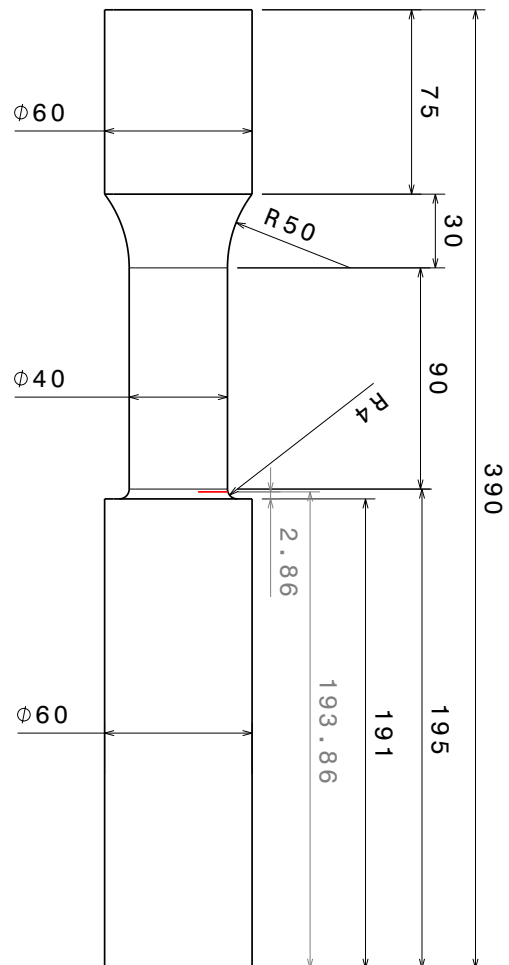
Appendix A

Specimen Drawings

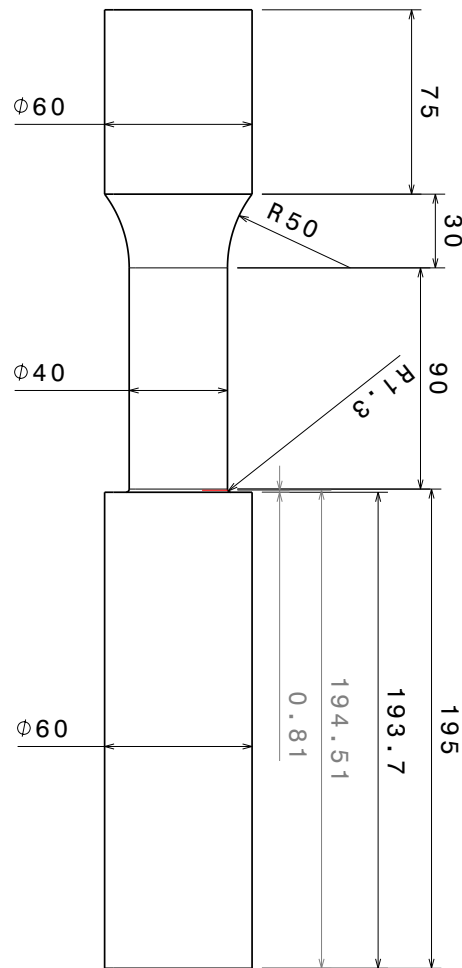
A.1 Straight specimen, $K_t = 1$ 

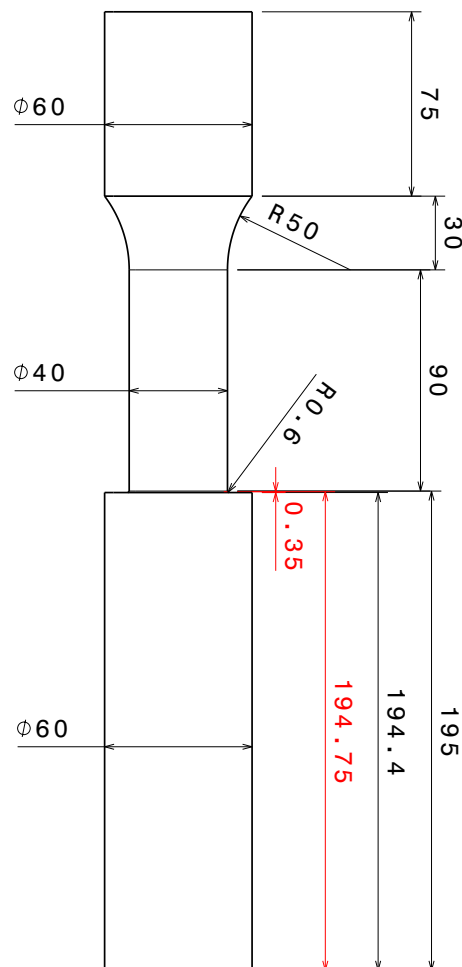
A.2 Specimen with fillet radius of 11.6 mm, $K_t = 1.5$



A.3 Specimen with fillet radius of 4.0 mm, $K_t = 2.0$ 

A.4 Specimen with fillet radius of 1.3 mm, $K_t = 3.0$



A.5 Specimen with fillet radius of 0.6 mm, $K_t = 4.1$ 

Appendix B


Material Certificate Aluminium 7075-T651



CERTIFICATO DI COLLAUDO INSPECTION CERTIFICATE ABNAHMEPRUEFZEUGNIS CERTIFICAT DE RECEPTION EN 10204 31B		DATA DATE DATUM DATE	24/07/02	NR. NO. NR. NO.	C 118780
CLIENTE CUSTOMER KUNDE CLIENT		ORDINE NR. ORDER NO. AUFTRAGS NR. NO. DE COMMANDE	02 83167 6 10		
NO. ORDINE CLIENTE CUSTOMERS ORDER NO. AUFTRAGS NR. KUNDE NO. DE COMMANDE CLIENT		NO. PROFILO SECTION NO. PROFIL NR. NO. DE PROFIL	14BT100 - B03 7075 T651		
NO. ORDINE CLIENTE CUSTOMERS ORDER NO. AUFTRAGS NR. KUNDE NO. DE COMMANDE CLIENT		PESO WEIGHT GEWICHT POIDS	ord. 02/05/02 407		
PROFILO DEL CLIENTE CUSTOMERS SECTION NO. PROFIL NR. KUNDE NO. DE PROFIL CLIENT		LEGA ALLOY LEGIERUNG ALLIAGE	ROUND BAR 60 7075 T651 EN 573-3		

COMPOSIZIONE CHIMICA / CHEMICAL COMPOSITION / CHEMISCHE ZUSAMMENSETZUNG / COMPOSITION CHIMIQUE														
COLATA CAST CHARGE	%Si	%Fe	%Cu	%Mn	%Mg	%Cr	%Ni	%Zn	%Ga	%V	%Ti	%Pb	%Zr	%Bi
2163A1	0,12	0,23	1,32	0,07	2,38	0,19	0,00	5,45	0,00	0,00	0,04	0,02	0,05	0,00
NORMA LIMIT NORM NORME	Min.	0,00	0,00	1,20	0,00	2,10	0,18	0,00	5,10	0,00	0,00	0,00	0,00	0,00
	Max.	0,40	0,50	2,00	0,30	2,90	0,28	0,05	6,10	0,05	0,05	0,20	0,05	0,05

CARATTERISTICHE MECCANICHE / MECHANICAL PROPERTIES / MECHANISCHE EIGENSCHARTEN / CARACTERISTIQUES MECANIKQUES				
NO. PROVETTA SAMPLE NO. PROBE NR. NO. D'EPROUVETTE	Rm N/mm ²	Rp0.2 N/mm ²	A5 %	HB Brinell
234741	564,0	517,0	13,5	160
NORMA LIMIT NORM NORME	Min.			0
	DIN EN 755-2			

NOTE	
<small> Noi certifichiamo che il prodotto è conforme ai requisiti dell'ordine. Es wird bestätigt, daß die Lieferung gemäß wasser und den Vereinbarungen bei der Auftragsbestätigung entspricht. We hereby certify that the material described above has been tested and complies with the terms of the sales confirmation. Nous certifions que la livraison est conforme aux spécifications de la confirmation de la commande. </small>	Responsabile Controllo Qualità 

All Test Results

C.1 Straight specimens, $K_t = 1$

C.1.1 Specimen 1B, R=0.5

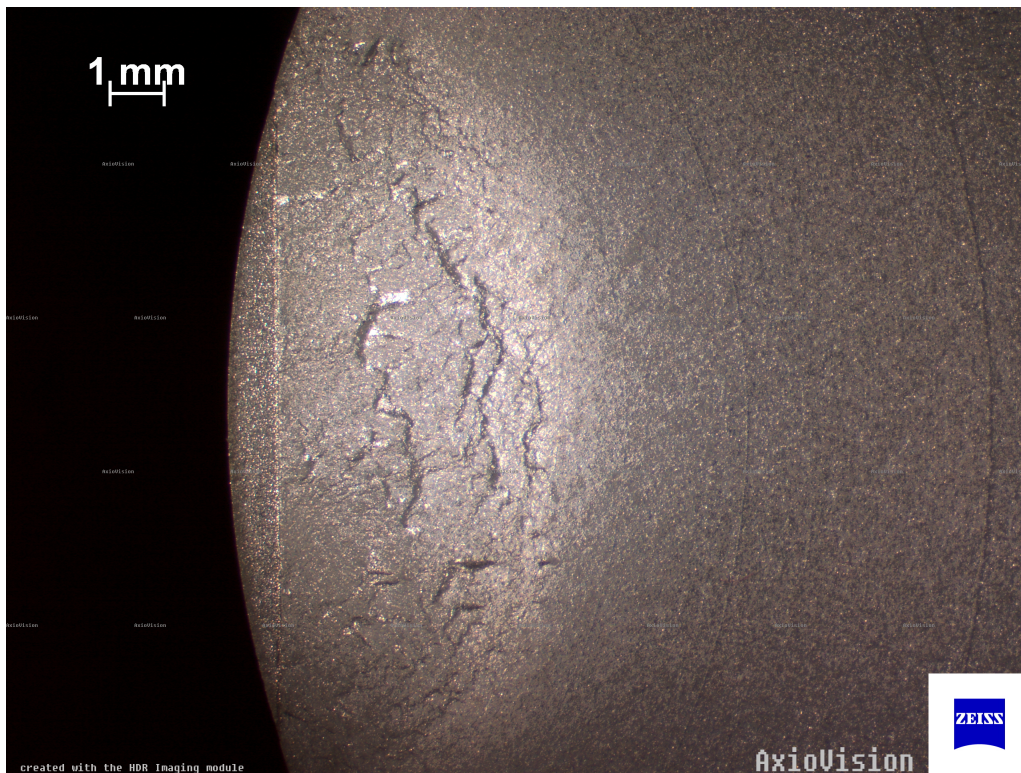


Figure C.1: Picture of the fracture surface of specimen 1B.

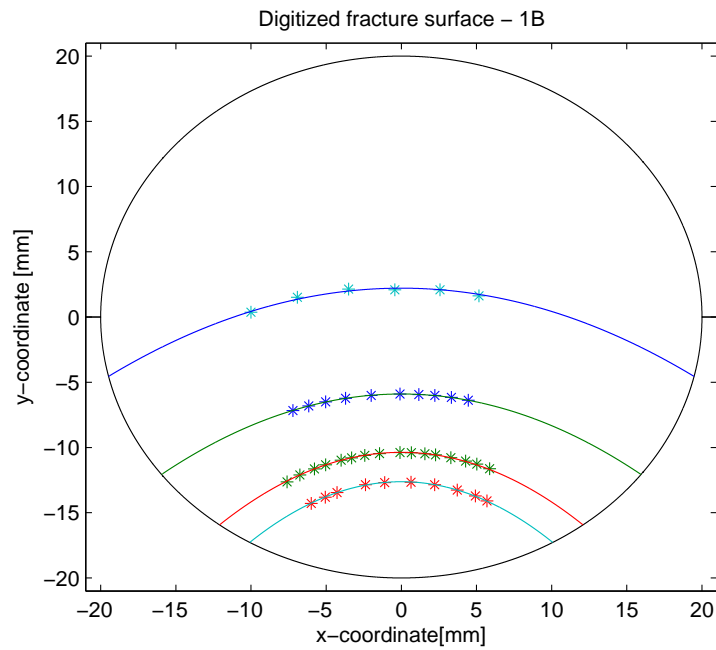


Figure C.2: Plot of the digitized fracture surface of specimen 1B.

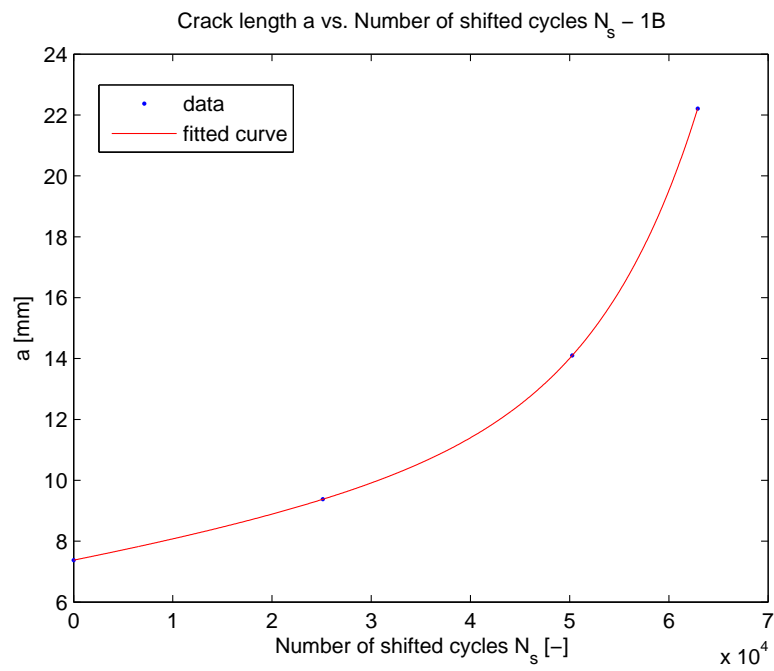


Figure C.3: Crack length a versus the shifted amount of cycles N_s for specimen 1B.

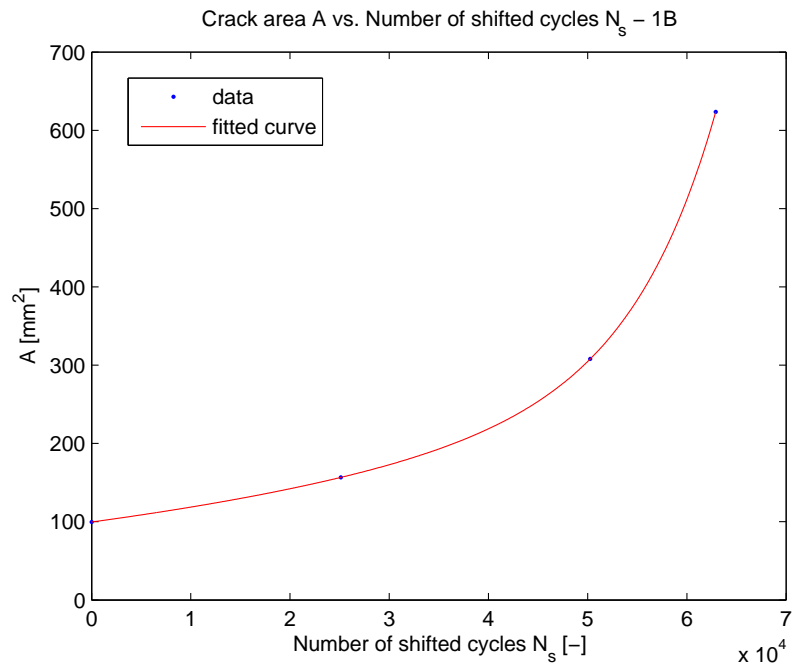


Figure C.4: Crack area A versus the shifted amount of cycles N_s for specimen 1B.

No energy data was gathered during the test of this specimen.

C.1.2 Specimen 1Z, $R=0.5$

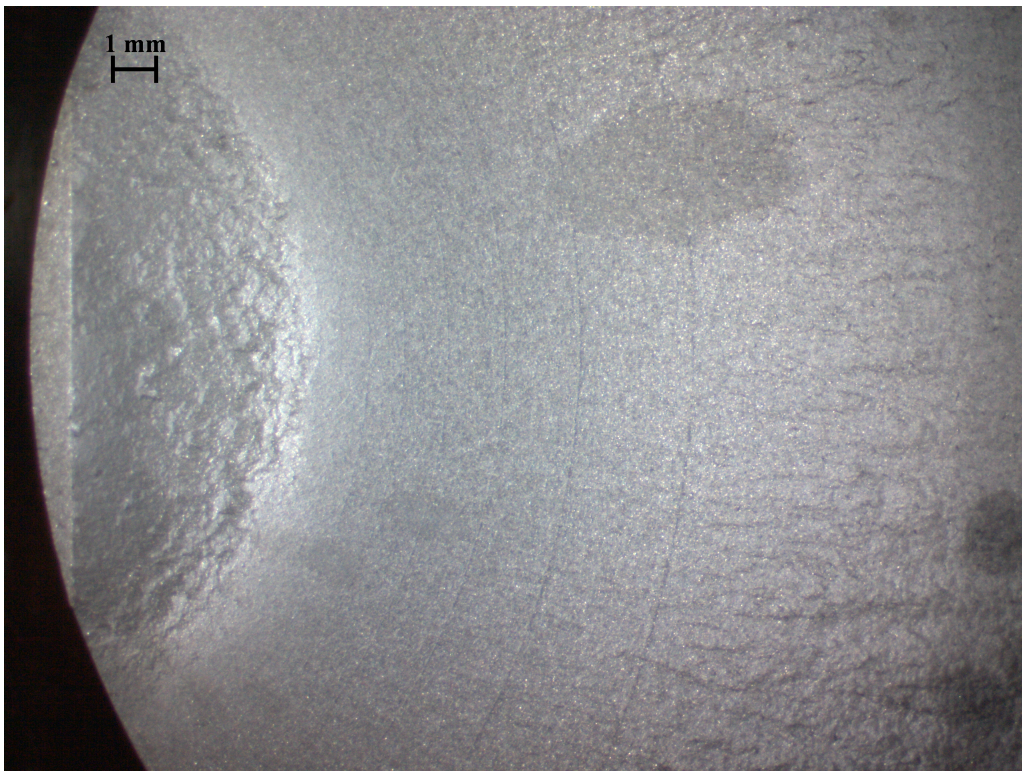


Figure C.5: Picture of the fracture surface of specimen 1Z.

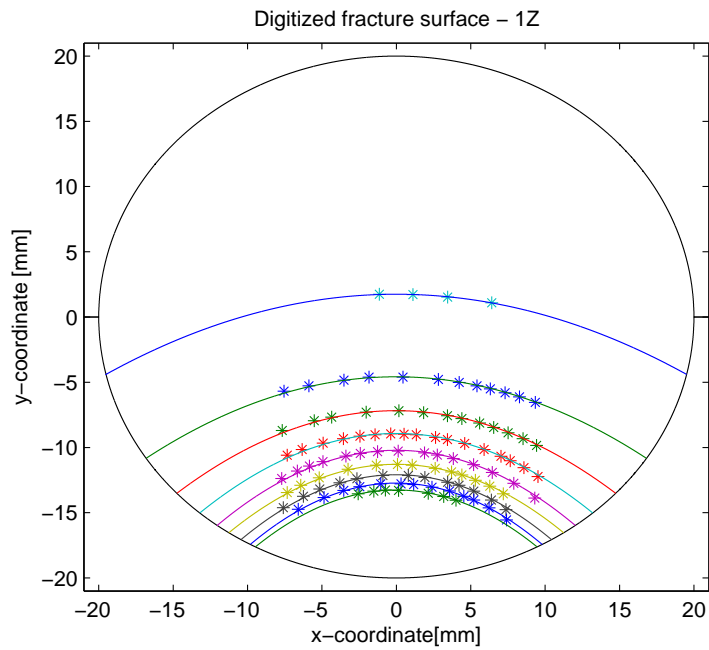


Figure C.6: Plot of the digitized fracture surface of specimen 1Z.

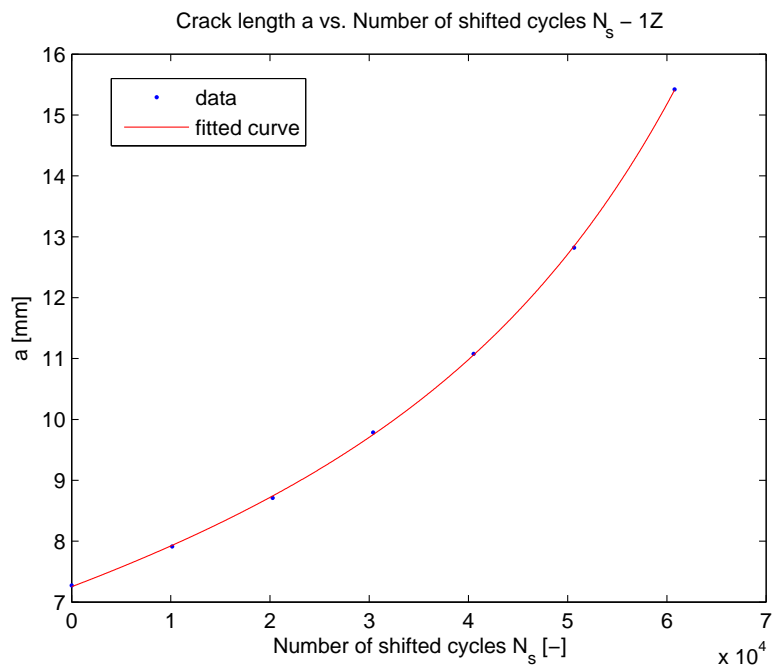


Figure C.7: Crack length a versus the shifted amount of cycles N_s for specimen 1Z.

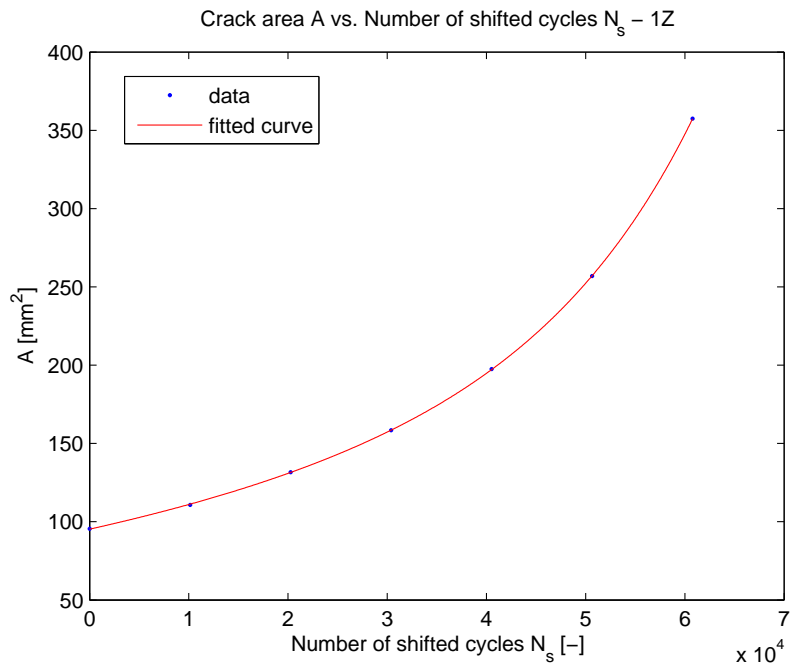


Figure C.8: Crack area A versus the shifted amount of cycles N_s for specimen 1Z.

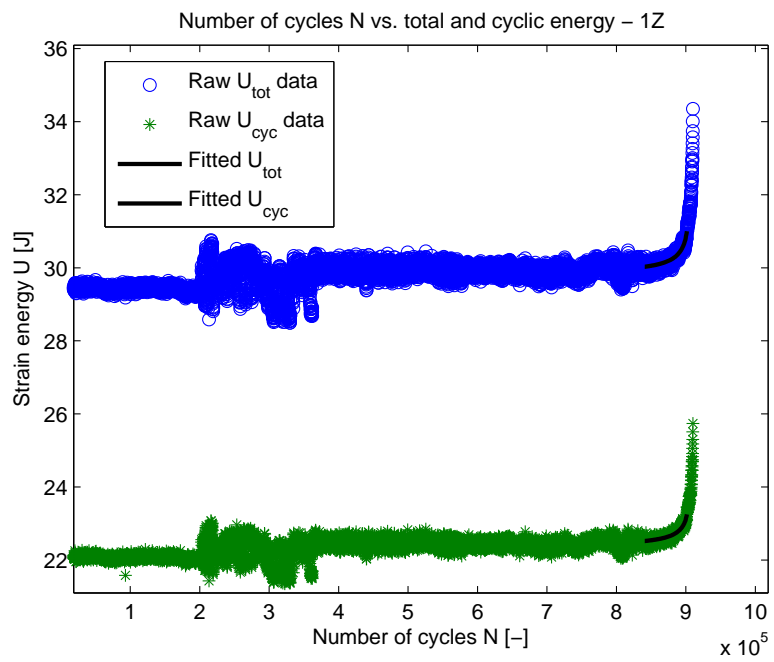


Figure C.9: Energy data for specimen 1Z.

C.2 Specimens with shoulder fillet, $K_t = 1.5$

C.2.1 Specimen 1B116, R=0.05

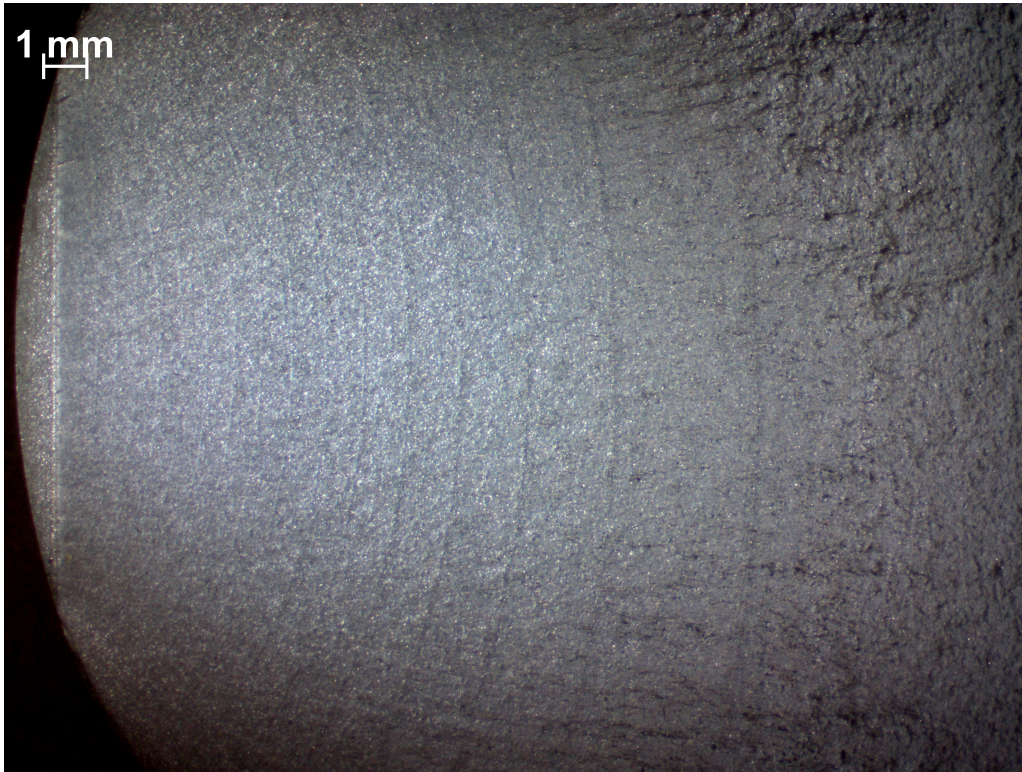


Figure C.10: Picture of the fracture surface of specimen 1B116.

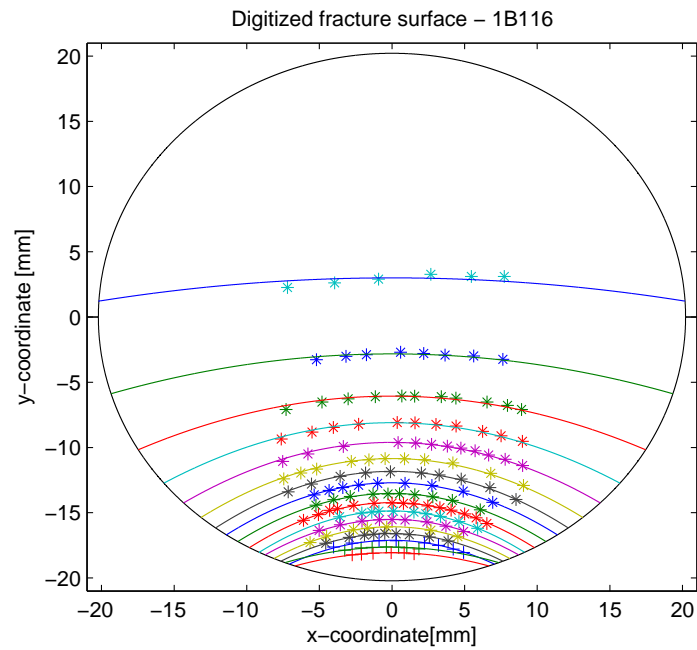


Figure C.11: Plot of the digitized fracture surface of specimen 1B116.

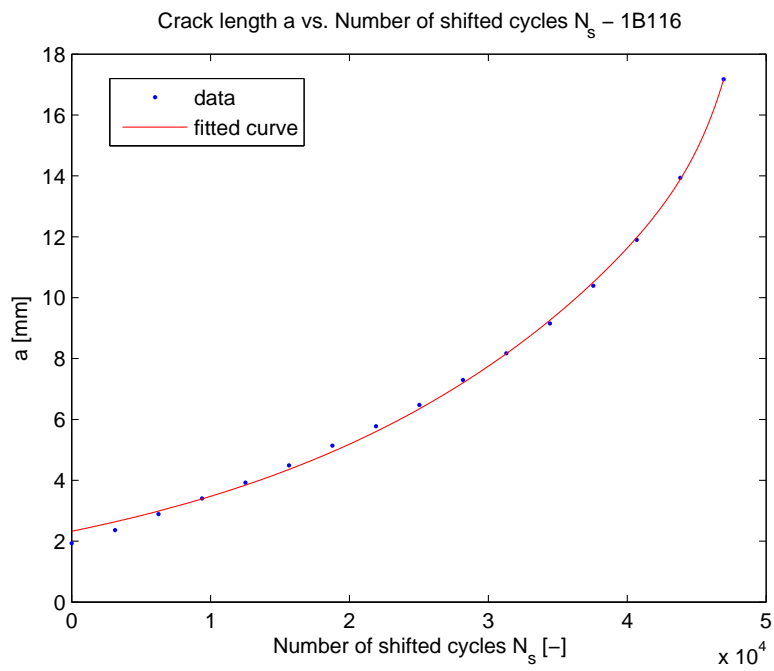


Figure C.12: Crack length a versus the shifted amount of cycles N_s for specimen 1B116.

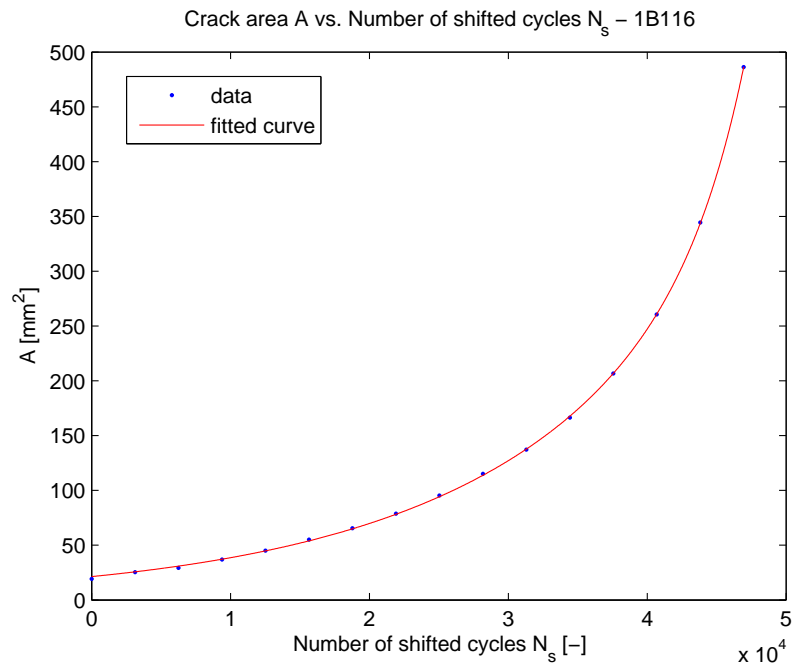


Figure C.13: Crack area A versus the shifted amount of cycles N_s for specimen 1B116.

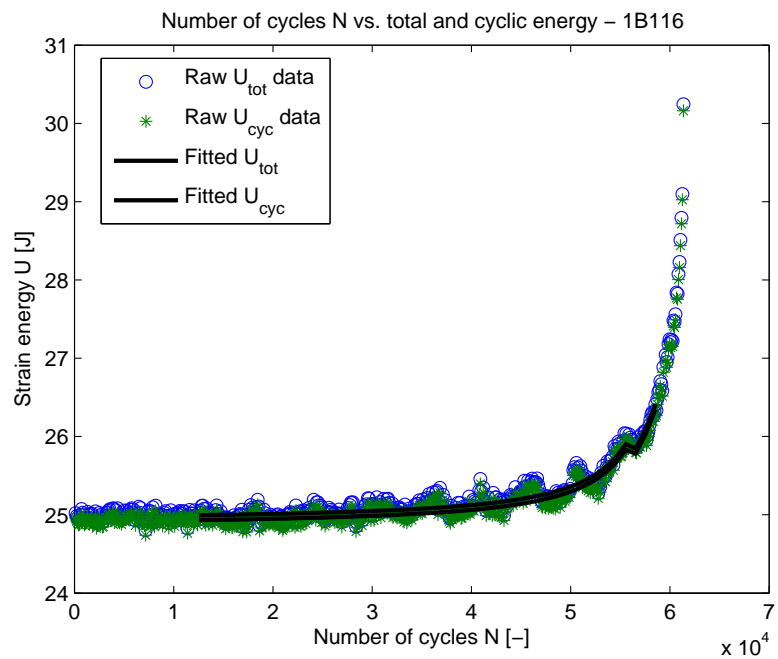


Figure C.14: Energy data for specimen 1B116.

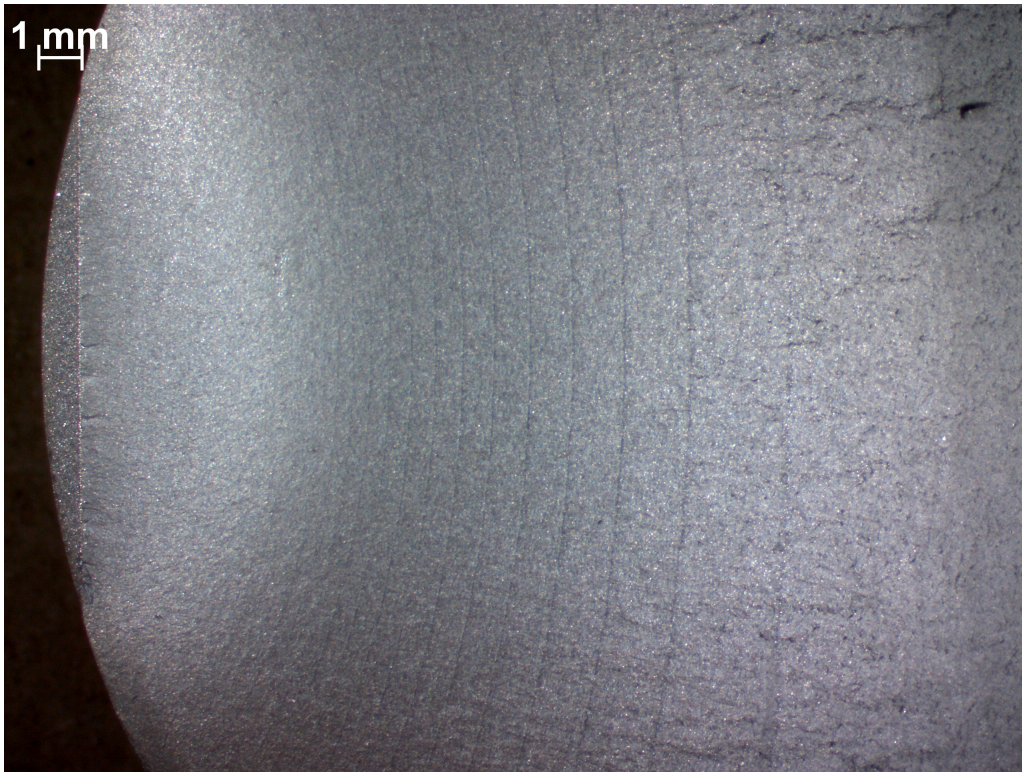
C.2.2 Specimen 2B116, $R=0.5$ 

Figure C.15: Picture of the fracture surface of specimen 2B116.

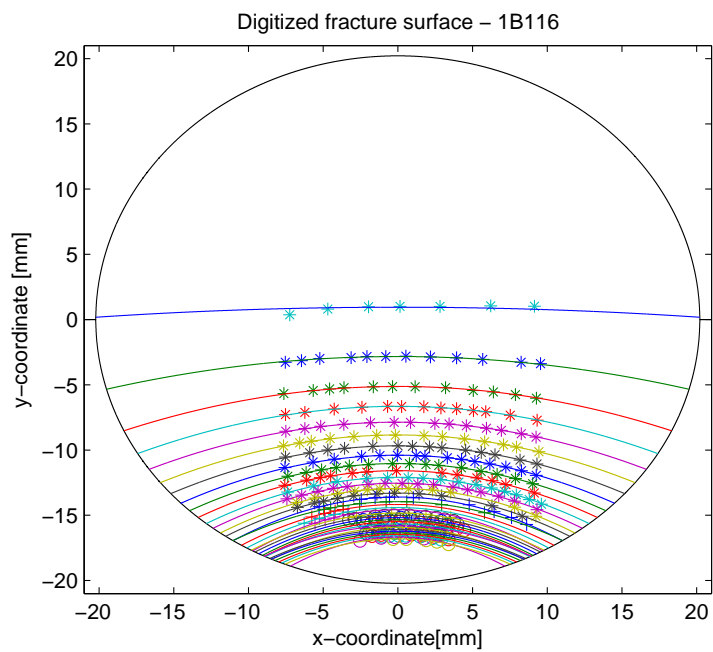


Figure C.16: Plot of the digitized fracture surface of specimen 2B116.

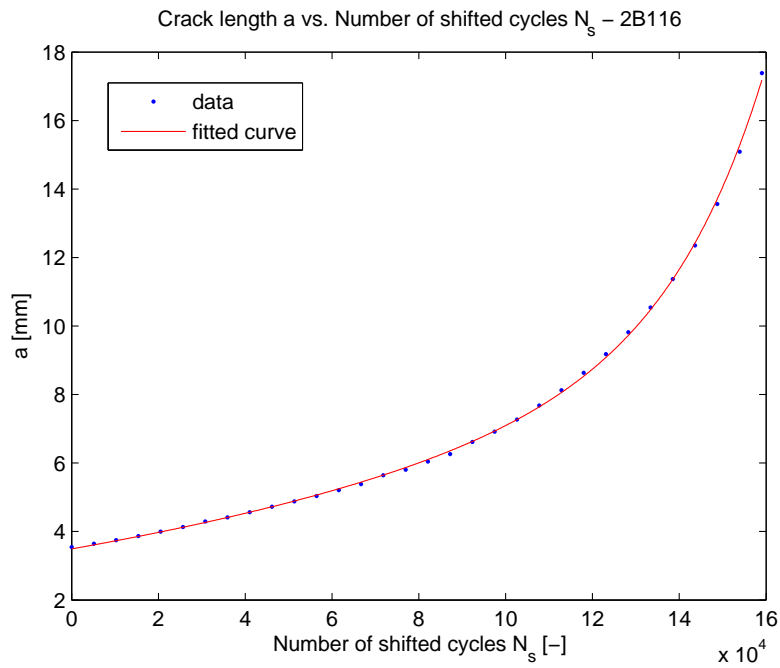


Figure C.17: Crack length a versus the shifted amount of cycles N_s for specimen 2B116.

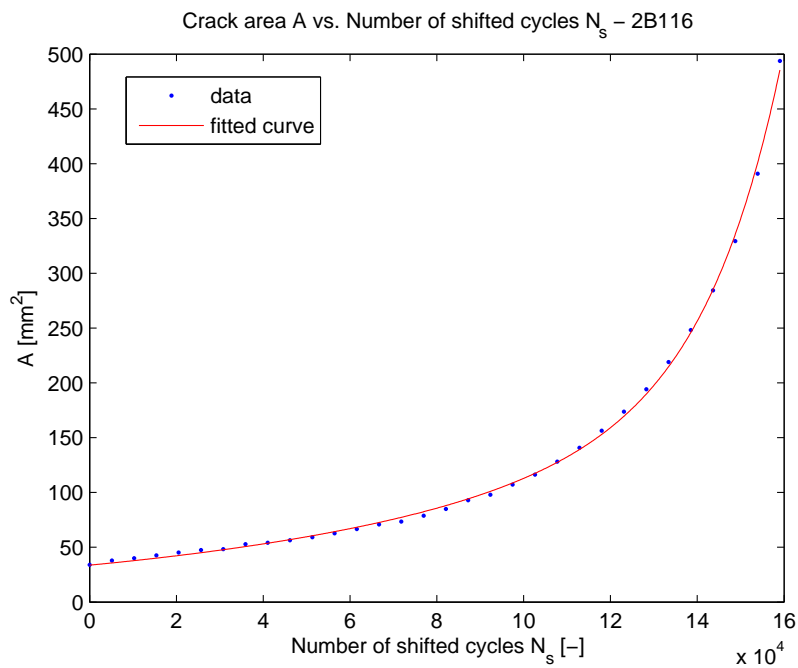


Figure C.18: Crack area A versus the shifted amount of cycles N_s for specimen 2B116.

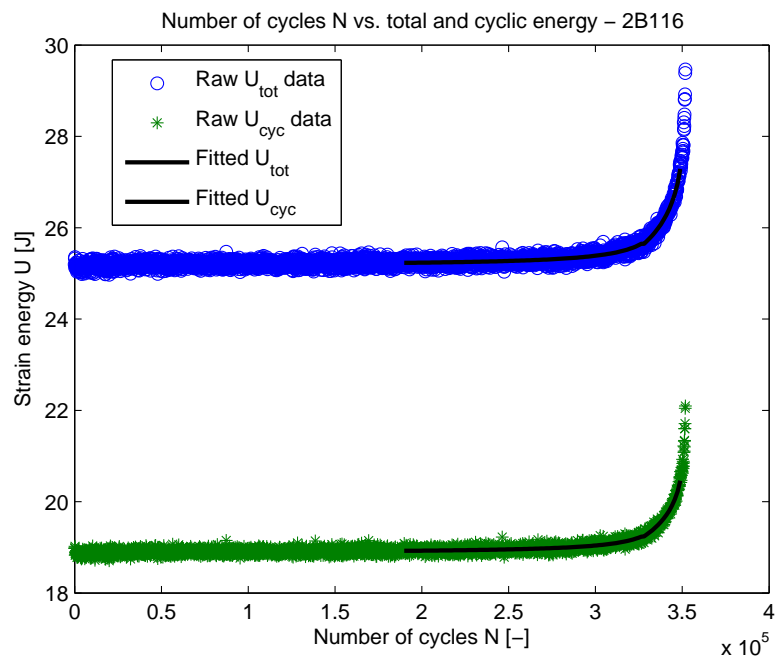


Figure C.19: Energy data for specimen 2B116.

C.3 Specimens with shoulder fillet, $K_t = 2$

C.3.1 Specimen 1B40, $R=0.05$

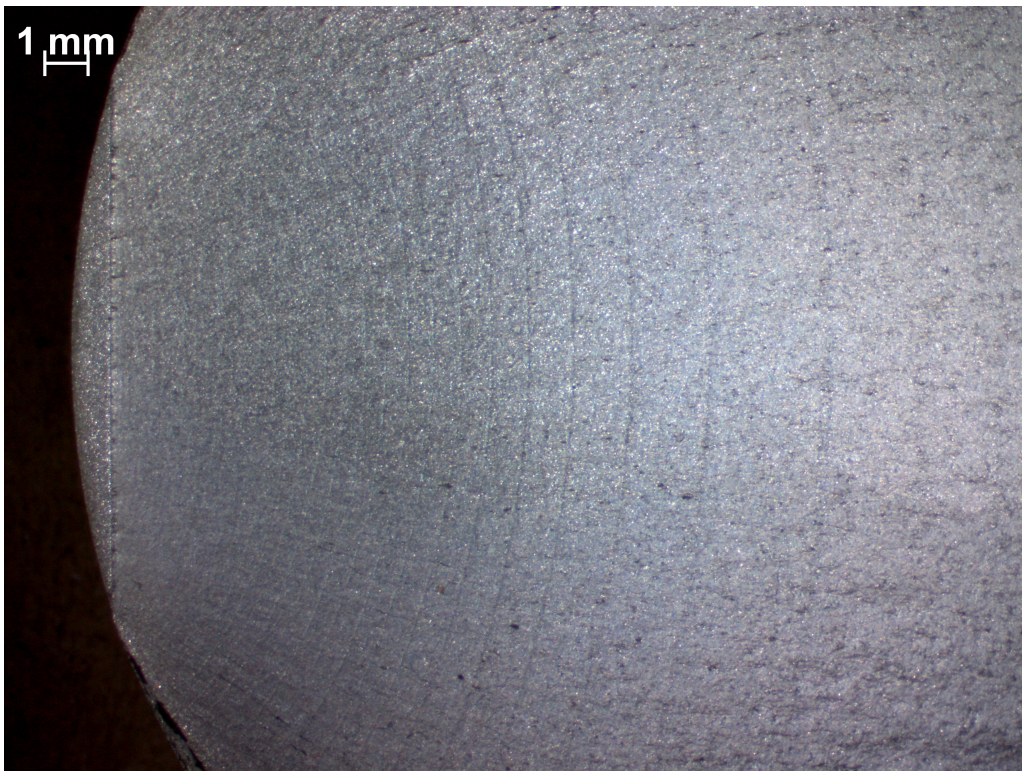


Figure C.20: Picture of the fracture surface of specimen 1B40.

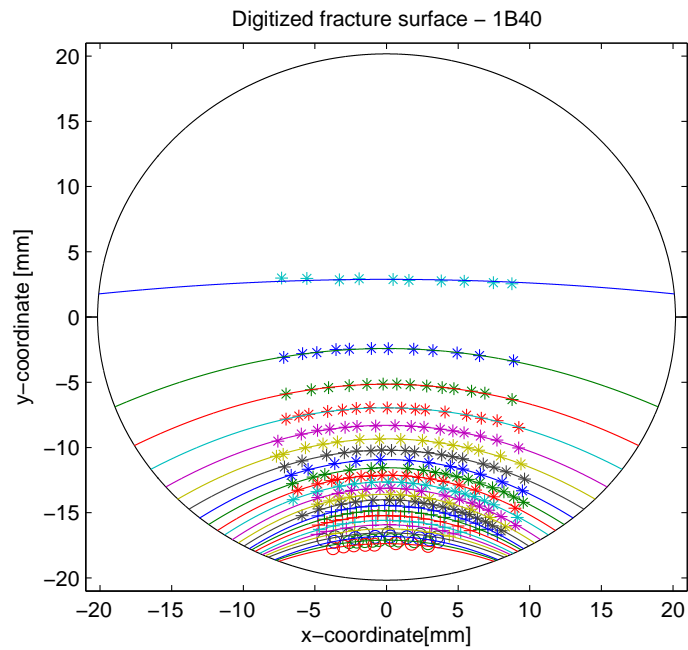


Figure C.21: Plot of the digitized fracture surface of specimen 1B40.

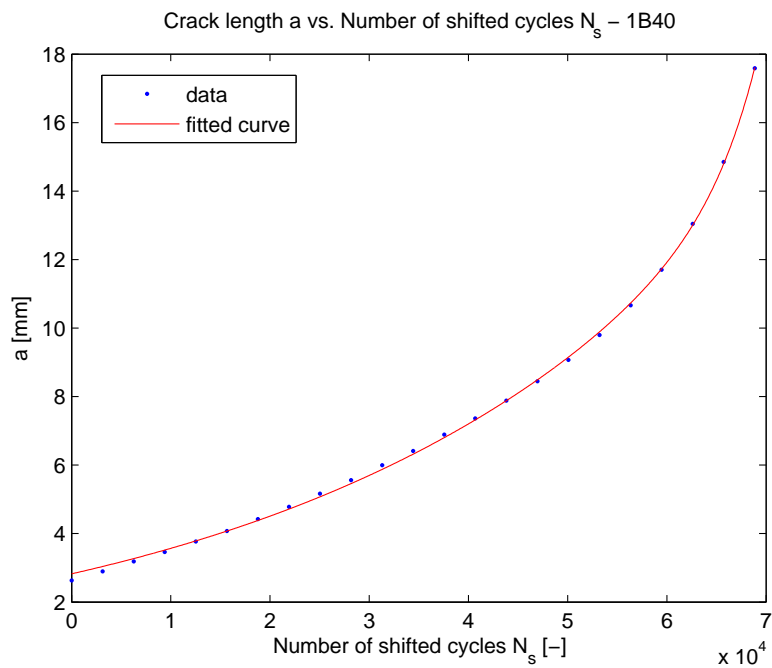


Figure C.22: Crack length a versus the shifted amount of cycles N_s for specimen 1B40.

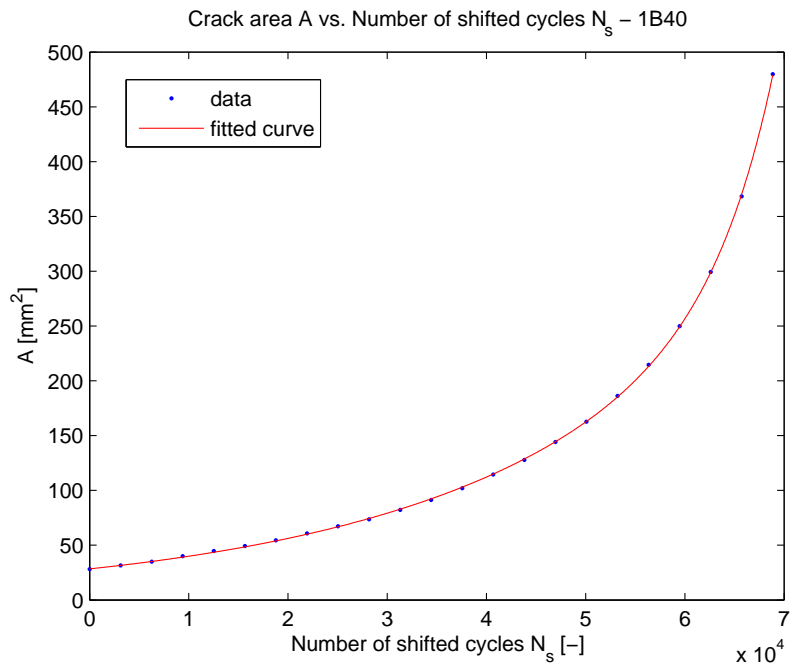


Figure C.23: Crack area A versus the shifted amount of cycles N_s for specimen 1B40.

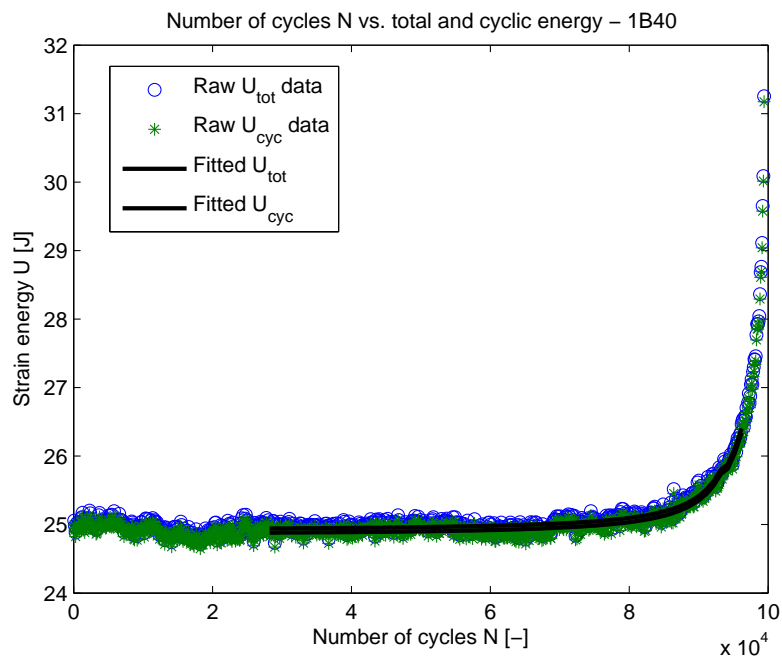


Figure C.24: Energy data for specimen 1B40.

C.3.2 Specimen 2B40, R=0.5

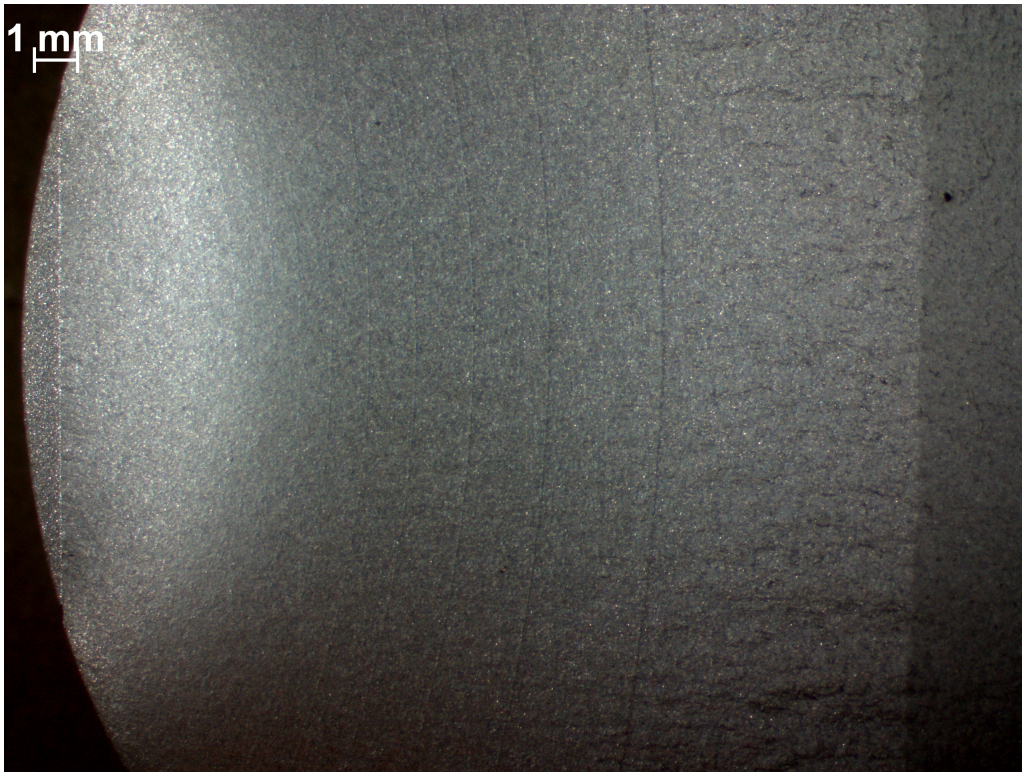


Figure C.25: Picture of the fracture surface of specimen 2B40.

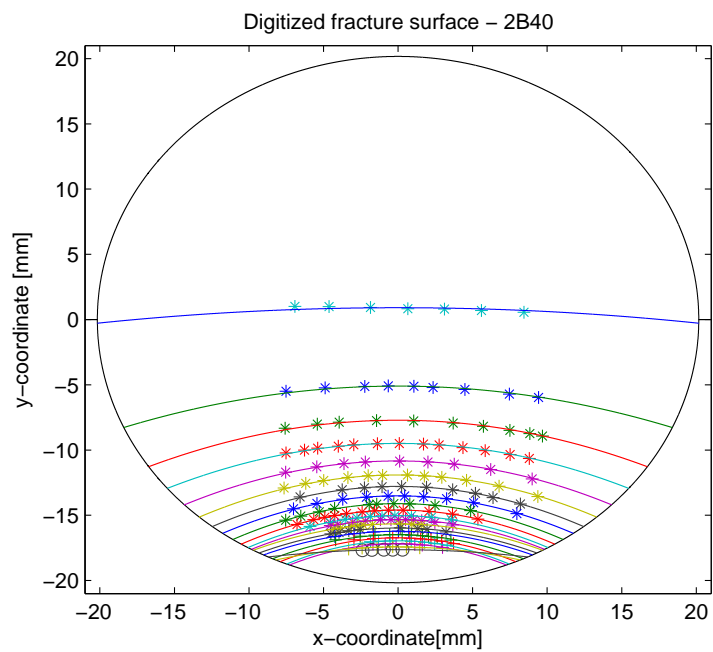


Figure C.26: Plot of the digitized fracture surface of specimen 2B40.

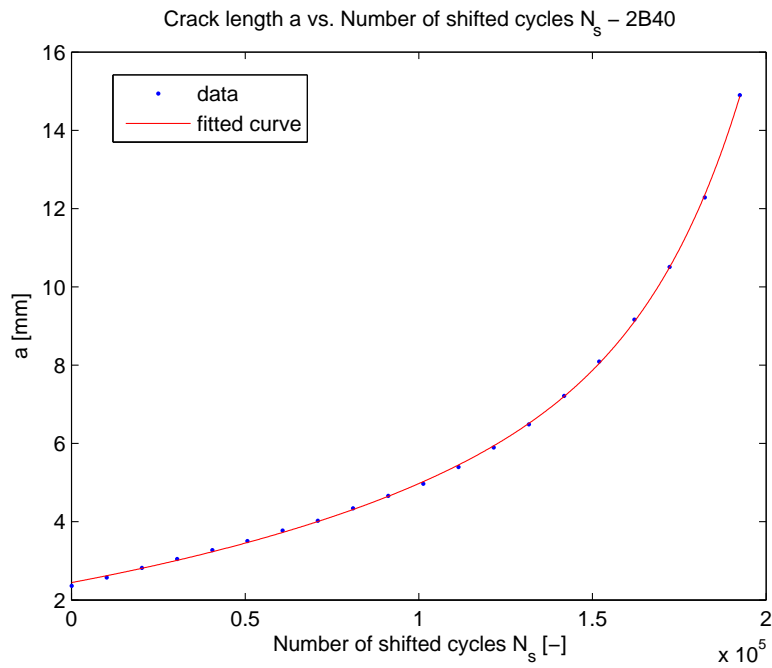


Figure C.27: Crack length a versus the shifted amount of cycles N_s for specimen 2B40.

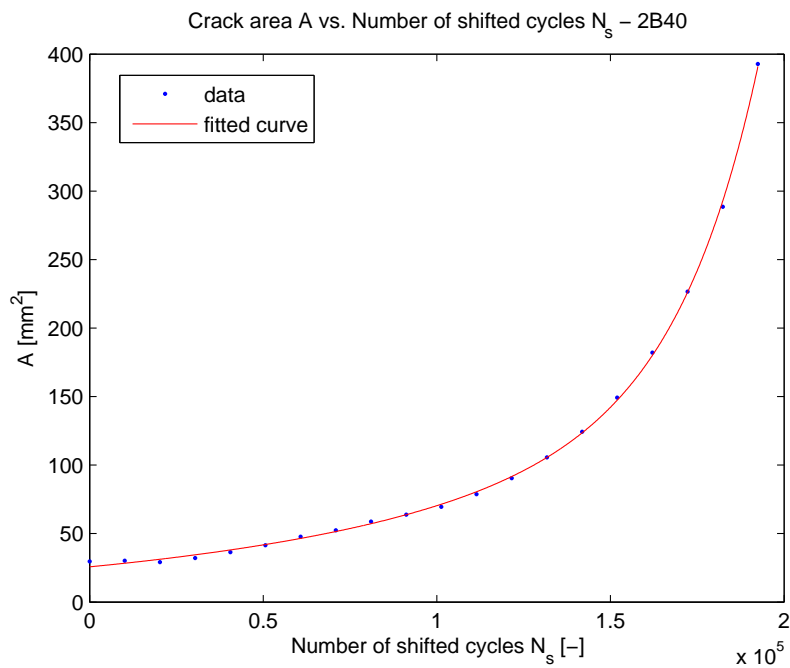


Figure C.28: Crack area A versus the shifted amount of cycles N_s for specimen 2B40.

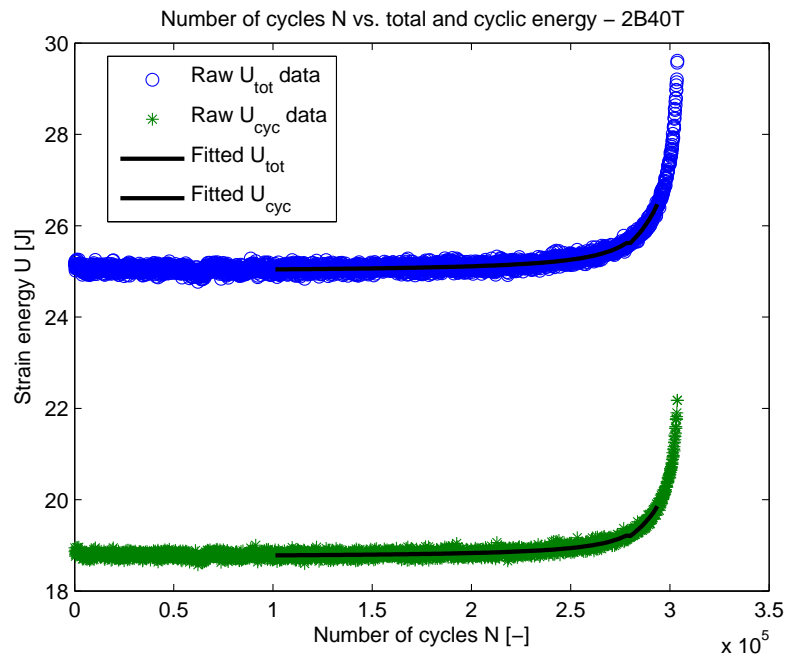


Figure C.29: Energy data for specimen 2B40.

C.4 Specimens with shoulder fillet, $K_t = 3$

C.4.1 Specimen 1Z13, R=0.05

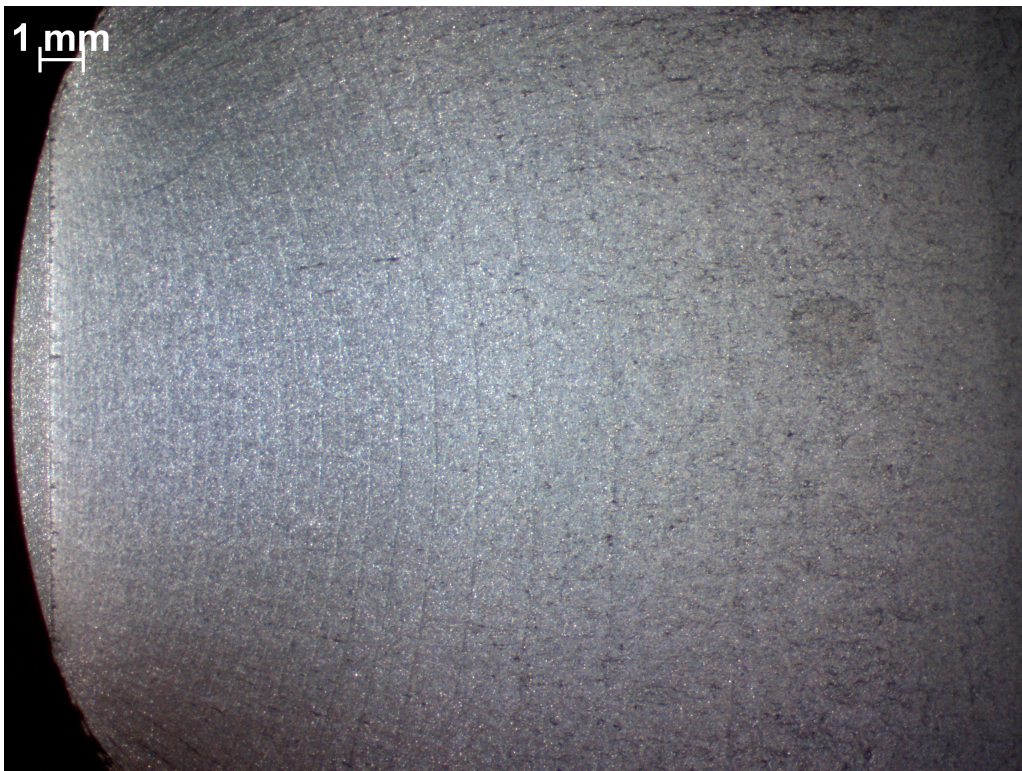


Figure C.30: Picture of the fracture surface of specimen 1Z13.

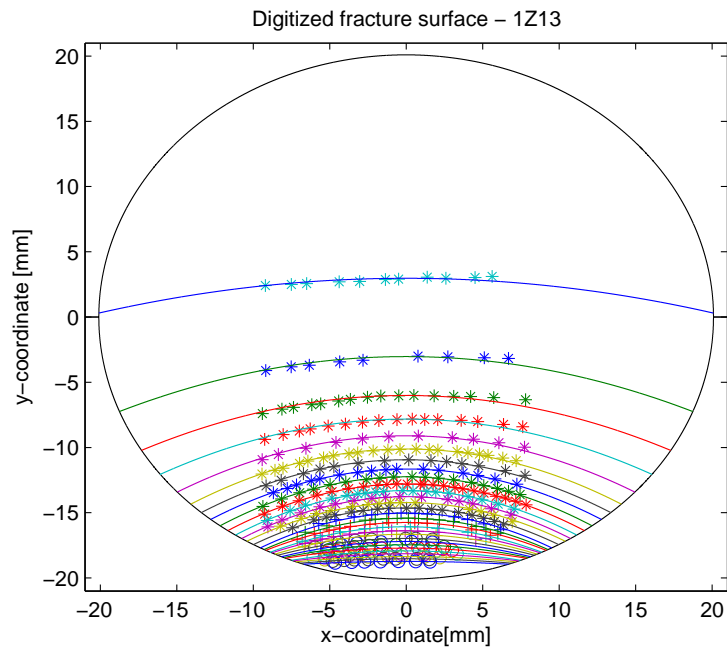


Figure C.31: Plot of the digitized fracture surface of specimen 1Z13.

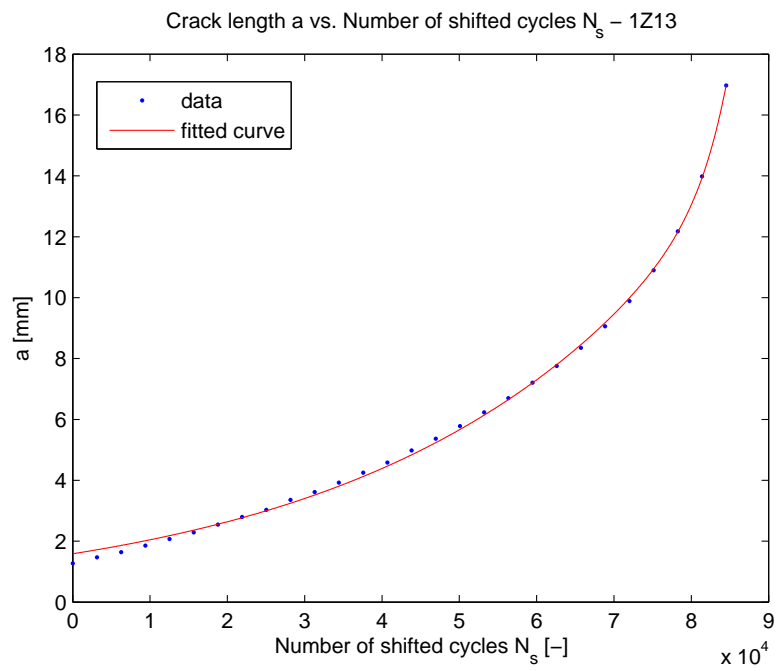


Figure C.32: Crack length a versus the shifted amount of cycles N_s for specimen 1Z13.

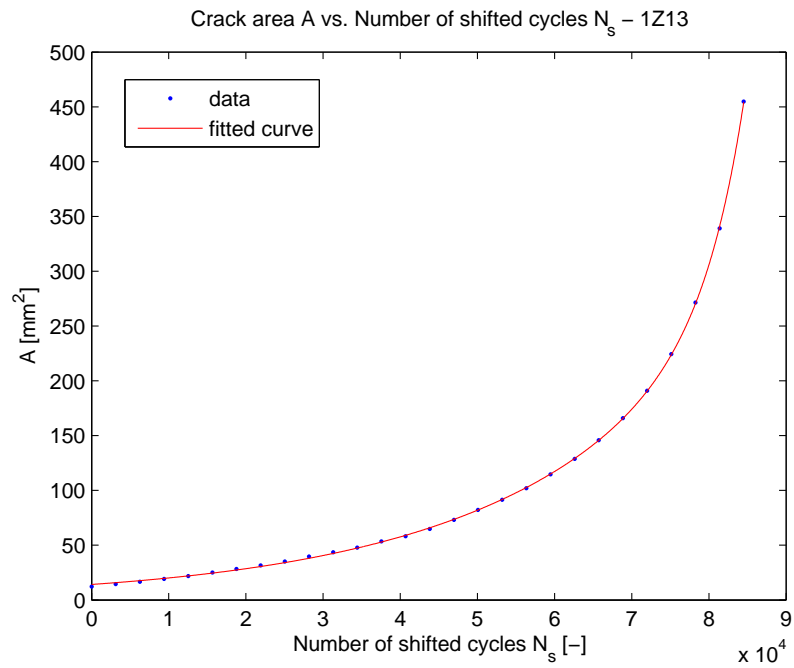


Figure C.33: Crack area A versus the shifted amount of cycles N_s for specimen 1Z13.

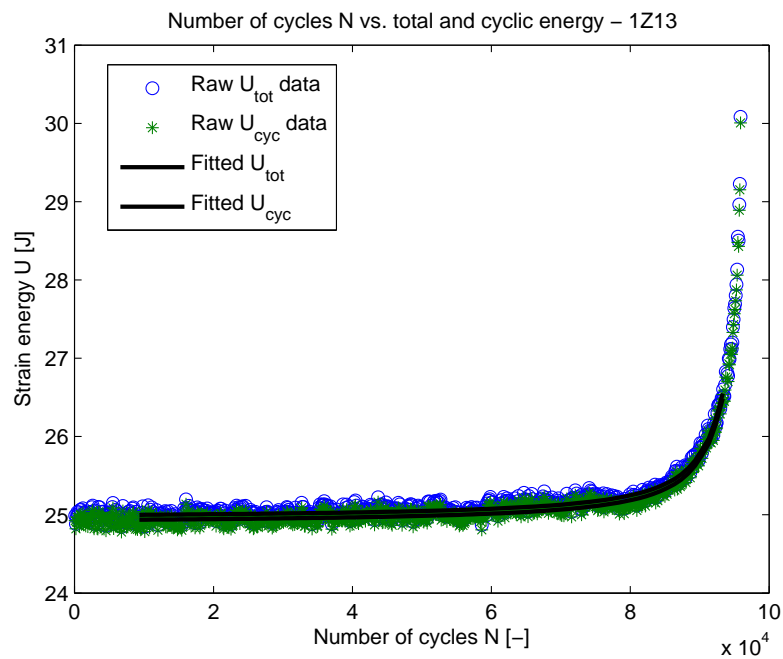


Figure C.34: Energy data for specimen 1Z13.

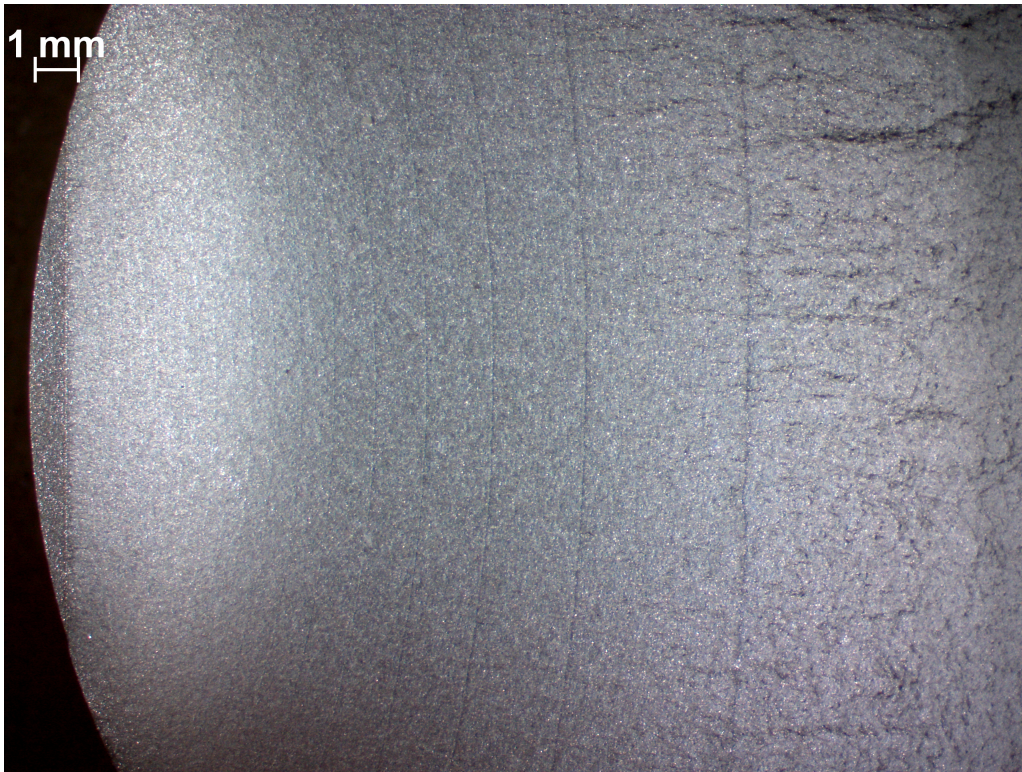
C.4.2 Specimen 2Z13, $R=0.5$ 

Figure C.35: Picture of the fracture surface of specimen 2Z13.

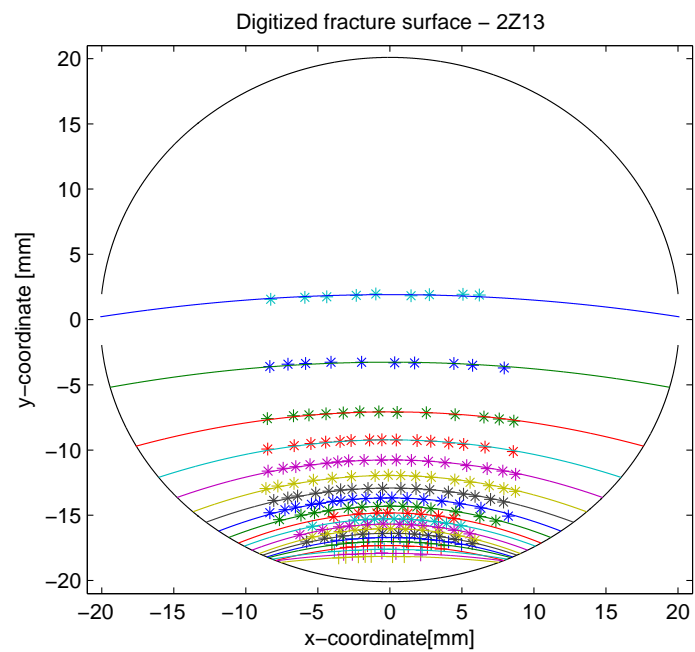


Figure C.36: Plot of the digitized fracture surface of specimen 2Z13.

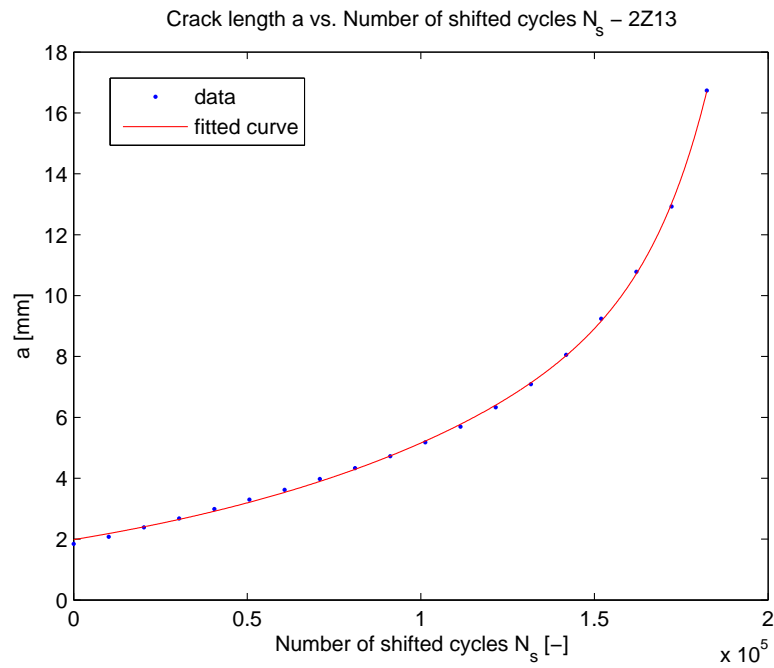


Figure C.37: Crack length a versus the shifted amount of cycles N_s for specimen 2Z13.

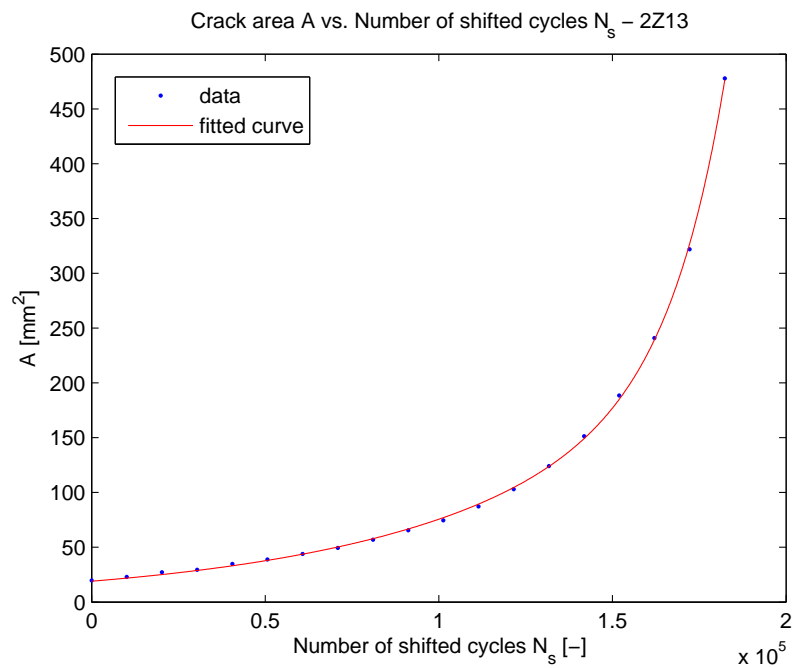


Figure C.38: Crack area A versus the shifted amount of cycles N_s for specimen 2Z13.

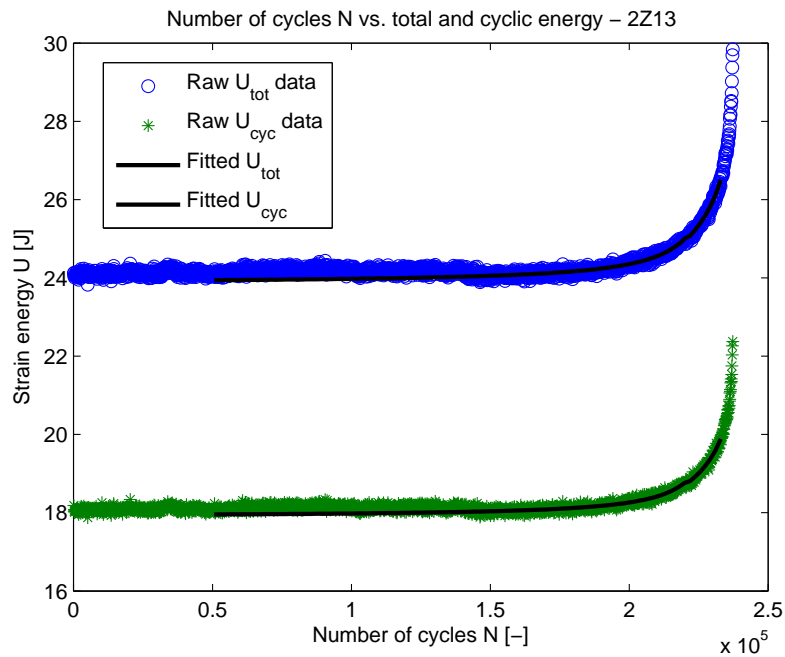


Figure C.39: Energy data for specimen 2Z13.

C.5 Specimens with shoulder fillet, $K_t = 4.1$

C.5.1 Specimen 1Z06, $R=0.05$

No measurements done due to multiple fatigue crack initiation sites as can be seen on the picture of the fracture surface:

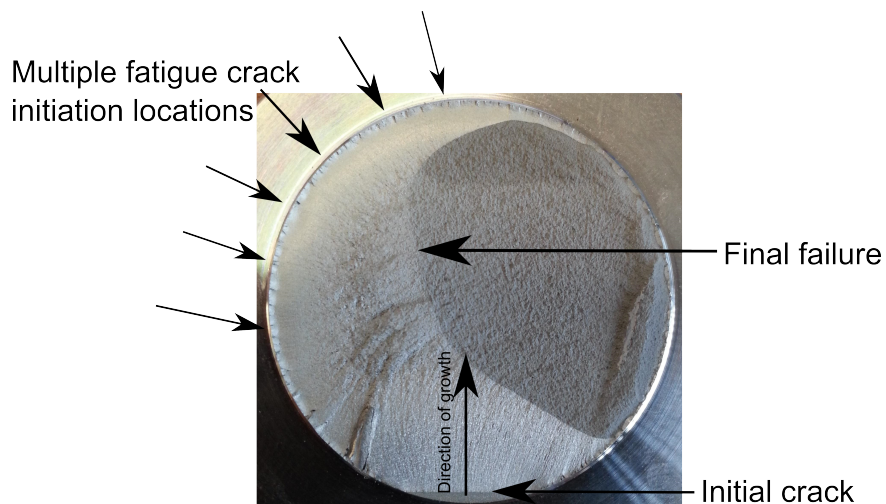


Figure C.40: Picture of the fracture surface of specimen 1Z06.

C.5.2 Specimen 2Z06, R=0.5

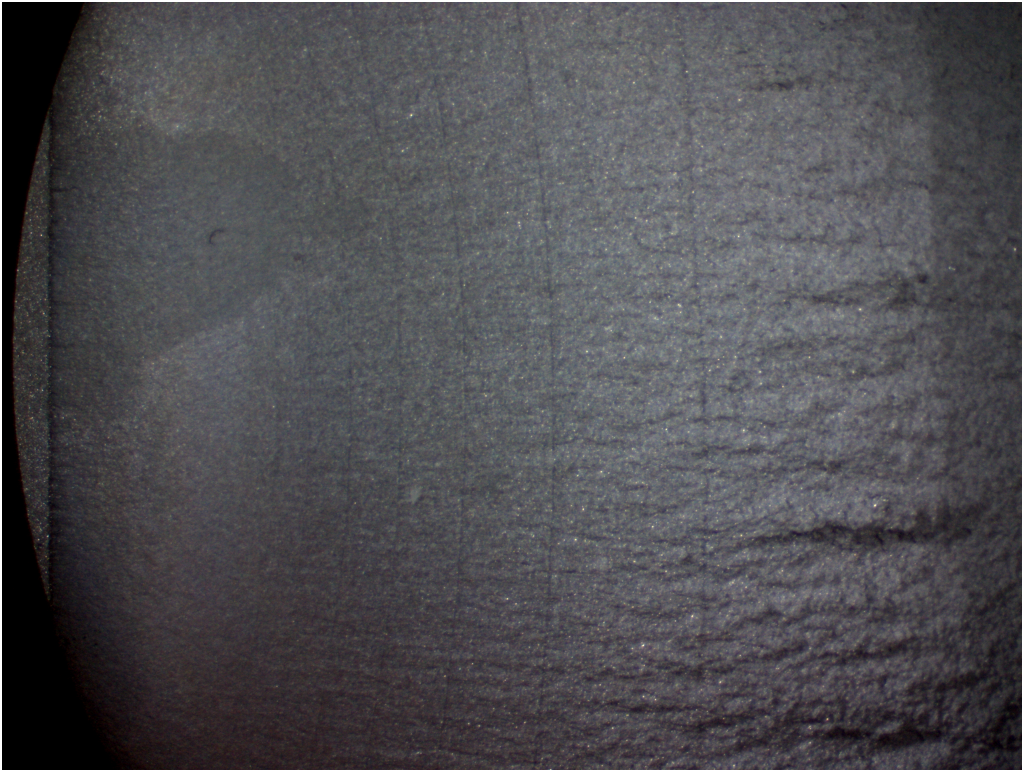


Figure C.41: Picture of the fracture surface of specimen 2Z06.

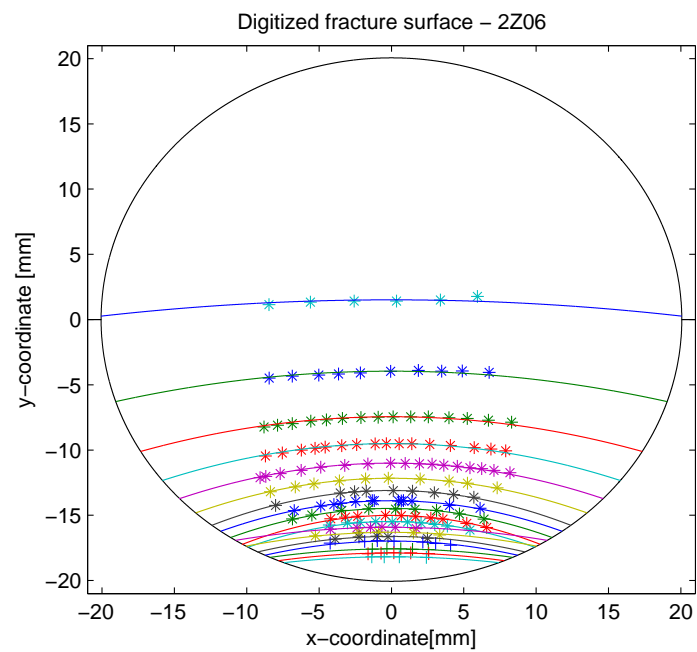


Figure C.42: Plot of the digitized fracture surface of specimen 2Z06.

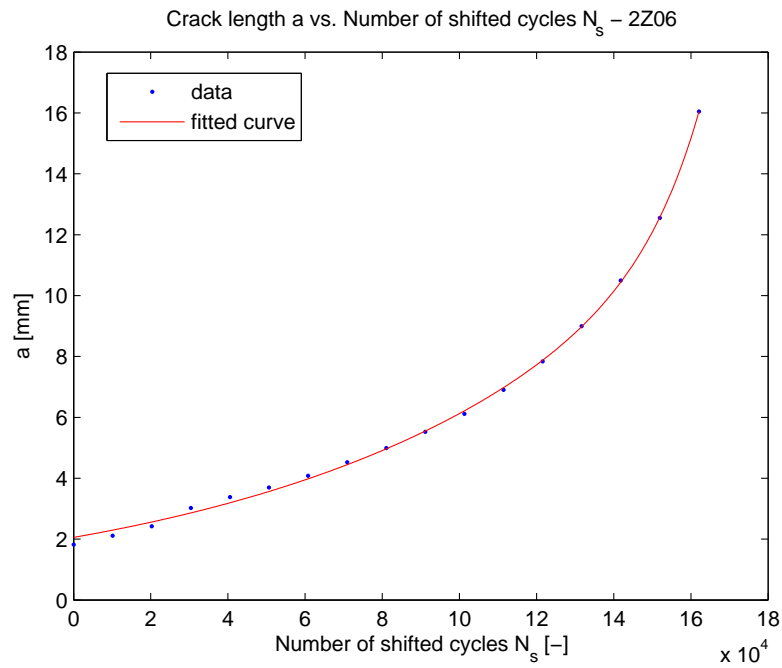


Figure C.43: Crack length a versus the shifted amount of cycles N_s for specimen 2Z06.

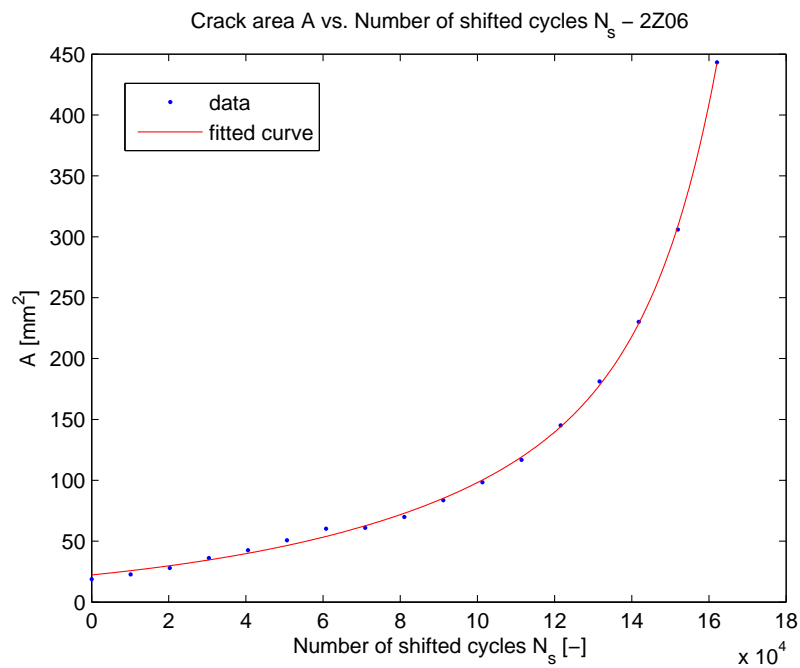


Figure C.44: Crack area A versus the shifted amount of cycles N_s for specimen 2Z06.

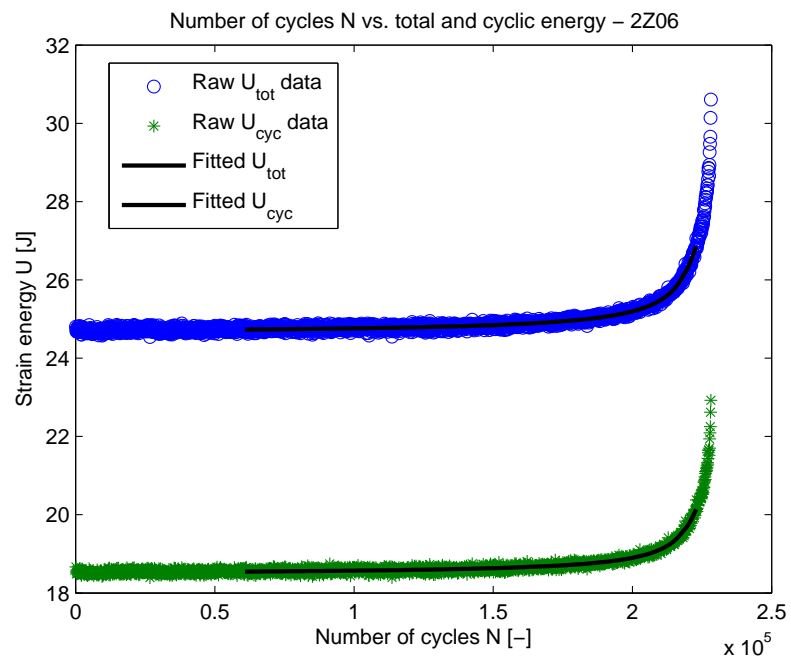


Figure C.45: Energy data for specimen 2Z06.